Robert Bains

On the Usage of Parasitic Antenna Elements in Wireless Communication Systems

Thesis for the degree philosophiae doctor

Trondheim, May 2008

Norwegian University of Science and Technology
Faculty of Information Technology, Mathematics
and Electrical Engineering
Department of Electronics and Telecommunications

NTNU

NTNU
Norwegian University of Science and Technology

Thesis for the degree philosophiae doctor

Faculty of Information Technology, Mathematics and Electrical Engineering
Department of Electronics and Telecommunications

ISBN 978-82-471-9211-5 (printed version)
ISBN 978-82-471-9225-2 (electronic version)
ISSN 1503-8181

Doctoral theses at NTNU, 2008:156

Printed by NTNU-trykk

Abstract

Multiple-Input-Multiple-Output (MIMO) is a technology that uses multiple antennas at both the transmitter and the receiver to be able to enhance the spectral efficiency. This technology gained a high popularity among researchers, which shows off in the high number of publications on the area. There are however some drawbacks when it comes to how many antennas may be put inside a small volume, when it is required that each additional antenna should give a substantial increase in the obtained spectral efficiency. This dissertation considers an alternative approach for achieving higher capacities.

Part I of the thesis explores the concept of a virtually fast rotating directional receive antenna, which rotates once or several times during a symbol interval. The antenna rotation is obtained by using a single active antenna element and multiple parasitic elements. This concept has some similarities with MIMO technology, but also many differences. The rotating antenna consists of multiple antennas which also MIMO receivers do. In addition, the antenna rotation results in spatial multiplexing, which is also obtained by MIMO receivers. It is shown in the thesis that the rotating receiver antenna provides a much higher capacity than a single receiver antenna. But at the same time, it looses in terms of capacity performance when comparing with multiple antennas that occupy the same volume as the rotating antenna.

Part II of the thesis considers a novel compact transmitter that consists of a single active antenna element and multiple parasitic elements. The parasitic elements are used for creating directive antenna patterns. The directive antenna patterns are not used for achieving high signal-to-noise ratio (SNR) at the receiver as in beamforming, but rather the choice of antenna pattern itself represents information. The transmitter encodes information both by the choice of antenna pattern (chooses possibly a different antenna pattern on each symbol interval) and the choice of symbol to be transmitted with the antenna pattern. The spectral efficiency obtained by this scheme is demonstrated to be comparable to the performance of widely spaced an-

tennas.

The similarity between Part *I* and *II* of the thesis is that in both cases a single active antenna element and multiple parasitic elements are considered. In addition, the parasitic elements are used for creating antenna patterns, which means that the mutual coupling between the antenna elements is taken advantage of.

Preface

This dissertation is submitted in partial fulfilment of the requirements for the degree of *Philosophiae Doctor* (PhD) at the Department of Electronics and Telecommunications, Norwegian University of Science and Technology (NTNU). Ralf R. Müller and John Anders Aas have been my main and co-supervisor, respectively. Both are with the Department of Electronics and Telecommunications, NTNU.

The studies have been carried out in the period from January 2004 to March 2008. I initially started out with a different research topic (Cross-talk models for twisted pair cables) and supervisor (Nils Holte), but in April 2005 I decided to change to the present topic. The work includes the equivalent of half a year of full-time course studies and approximately one year of teaching assistance in various graduate classes.

I have spent most of the time at NTNU, except for 3 months abroad (January through March 2007) at Athens Information Technology (AIT).

The work included in this thesis has been funded by the Co-optimized Ubiquitous Broadband Access Networks (CUBAN) project and by the Department of Electronics and Telecommunications, NTNU. The teaching assistantship has been funded by the Department of Electronics and Telecommunications, NTNU.

Acknowledgements

Finally, I would like to thank my supervisors Ralf R. Müller and John Anders Aas for their help and support during my research period. I would especially like to thank Ralf for his guidance, and I have to say that I am truly amazed of his ability to understand almost every technical and scientific matter. I also appreciate the cooperation I had with Nils Holte during my initial research topic. Nils is the professor I have had most contact with socially, and I will always remember the funny stories he told during our coffebreaks late in the evenings. During my research stay in Athens I was

lucky to be able to cooperate with Antonis Kalis. I would like to express my gratitude to Antonis for his Greek hospitality. There are several people I would like to thank among the PhD-students, but I choose not to mention any by names, since mentioning only a few of them will ultimately lead to someone feeling they have been left out. I appreciate the sometimes technical discussions I have had with some of the PhD-students, but mostly I would like to thank them for the non-technical activities.

At last I would also like to thank my parents, my brother and the most important one when it comes to my life, my fiancee.

Contents

List of Figures

List of Tables

Notations and Symbols

r^*	Complex conjugate.
$\mathbf{r}^T$	Transpose.
$\mathbf{r}^H$	Hermitian (conjugate transpose).
$\mathbf{R}^{-1}$	Inverse.
$\|\mathbf{R}\|$	Determinant.
$\|r\|$	Absolute value.
$\mathbf{r}_k$	Either element number k in the vector **r** or the vector **r** at discrete time index k.
Γ	Reflection coefficient.
$\delta(t)$	Dirac delta function.
η	Intrinsic impedance of the propagation medium (air).
θ	Zenith angle.
λ	Wavelength.
σ_n^2	Noise variance.
ϕ	Azimuth angle.
ω	Rotation speed in rad/s.
Ω	Either angular frequency in rad/s or unit of impedance. The angular frequency is given by $\Omega = 2\pi f$, where f is the frequency.
Ω_t	Solid angle in 3-dimensional space.
a_l	The l'th Fourier component of the antenna pattern.
$\mathbf{A}$	Pattern coefficient matrix.
$A_p(\Omega)$	Spectrum of antenna pattern.
A_t	Normalized electric field correlation matrix.

$AF(\phi)$	Array factor.
$\mathbf{b}_k$	Transmit symbol vector at discrete time k.
E_θ	Electric far-field component in the direction of unit vector θ.
$\mathbb{E}\{\}$	Expectation operator.
$\mathbf{E_t}(\Omega_t)$	Electric field matrix. Expresses the electric far-field at solid angle Ω_t.
f_c	Carrier frequency in Hz.
Δf	Bandwidth in Hz.
$\mathbb{F}\{\}$	Fourier transform.
$g(t)$	Pulse-shaping filter.
$g(\phi_r, \phi_t)$	The channel coefficient for a signal transmitted from angle ϕ_t and received from angle ϕ_r.
$g_p(t)$	Sampled antenna pattern function.
$\mathbf{H}$	Channel matrix.
i_1, i_2	Current on antenna 1 and 2 respectively.
$\mathbf{i}$	Antenna currents.
$\Im()$	Operator that takes the imaginary part of a number.
j	Imaginary unit.
$\mathrm{J}_l()$	Bessel function of the first kind and order l.
$\mathbf{K}_n$	Noise correlation matrix.
$\mathbf{K}_{v_{oc}}$	Open-circuit voltage correlation matrix.
L	$2L + 1$ is the number of Fourier components of the antenna pattern.
$L()$	The Lagrangian.
$\mathbf{n}$	Noise vector.
$\hat{\mathbf{n}}$	Noise on the output of a matched filter.
n_r	Number of receive antennas.
n_t	Number of transmit antennas.
N_0	Noise power spectral density in J/s/Hz.

N_l	Interference power spectral density in the l'th subband.
$\mathbf{P}$	Matrix with elements from the sinc-function. This matrix takes care of the extra bandwidth expansion due to antenna rotation with discrete steps.
$\hat{\mathbf{P}}$	Matrix with elements from the sinc-function. But with a different structure than $\mathbf{P}$.
$P_n(\phi)$	Angular noise power distribution.
P_T	Average transmit power constraint.
P_R	Average received power.
$\mathbf{q}$	Adjacent channel interference.
Q	Quality factor.
Q_t	Quality factor of the antenna array.
Q_e	Quality factor of an antenna element.
$r(t)$	Signal received by the rotating antenna.
$\mathbf{r}(t)$	Signal received by the rotating antenna. Each component of the vector corresponds to a signal in a separate subband.
$\hat{\mathbf{r}}_k$	Received signal on the output of a matched filter at discrete time k.
$\Re()$	Operator that takes the real part of a number.
s_p	Signal that approaches the antenna from azimuth angle ϕ_p.
t	Time in seconds.
T	Symbol interval in seconds.
T_c	Sample interval in seconds.
$\mathrm{tr}()$	Trace operator.
$\mathbf{V}$	An operator that makes linear combinations of the approaching waves and outputs these linear combinations in each of the $2L+1$ subbands.
v_{oc}	Open-circuit voltage.
v_t	Voltage signal source.
$\mathbf{v}_t$	Voltage signal source.

$\mathbf{x}(t)$	Transmitted signal.
x	Reactive impedance.
Z_{11}	Self impedance.
Z_{12}	Mutual coupling impedance between antenna 1 and 2.
Z_L	Termination impedance.
$\mathbf{Z}$	Mutual coupling impedance.

List of Abbreviations

2-D	2-dimensional
AWGN	Additive White Gaussian Noise
i.i.d	independent identically distributed
MIMO	Multiple-Input Multiple-Output
MISO	Multiple-Input Single-Output
PDF	Probability Density Function
PIN	Positive Intrinsic Negative
SIR	Signal-to-Interference Ratio
SINR	Signal-to-Interference-Noise Ratio
SNR	Signal-to-Noise Ratio

Chapter 1

Introduction

Wireless communication has become important in most peoples lives in one way or another. Cellular phones are perhaps the best example of a technology that many people have become dependent on. But also for industrial usage it seems that wireless communication has become more and more dominant. However, wireless communication has a disadvantage compared to wired communication when it comes to the channel itself through which information is transmitted. The wireless channel usually suffers due to fading and shadowing, and in addition only a limited frequency bandwidth is in most cases available. These three factors used to mean that only low bit rates were achievable.

In the 90's a new technology was discovered that enabled higher bitrates on the wireless channel than before. Telatar [1999]; Foschini and Gans [1998] proposed Multiple-Input Multiple-Output (MIMO) which is a technology that uses multiple antennas at both the transmitter and receiver side. These large capacity gains, promised by MIMO systems, satisfy the demands of many applications. But there are some drawbacks with MIMO that prevent it from being widely implemented in small mobile terminals. The higher bitrate comes at the expense of both larger space requirements since multiple antennas are utilized, and higher costs since multiple RF-frontends are required. These drawbacks became the motivation behind this thesis, and the goal was to construct and analyze an antenna system which is both compact and cheap, which at the same time offers some of the capacity achievements of regular MIMO systems.

Since this thesis seeks to overcome some of the drawbacks of MIMO, a brief introduction on the research on MIMO is in place. Telatar [1999]; Foschini and Gans [1998] showed that the capacity scales linearly with the minimum number of receive and transmit antennas when the channel co-

efficients are independent identically distributed (i.i.d) complex Gaussian random variables. This assumption about the channel coefficients may not hold in a practical scenario due to various reasons. Shiu, Foschini, Gans, and Kahn [2000] claim that putting too many antennas inside a small terminal leads to high spatial correlation due to spatial oversampling. However, there are other effects as well, which come into play when antennas are closely spaced. Mutual coupling, which is the electromagnetic interaction between the antennas, become more dominant for small antenna spacings. There have been some conflicting views on the consequence of mutual coupling. Some have claimed that mutual coupling leads to higher capacity while others claim the opposite. Svantesson and Ranheim [2001]; Chiurtu, Rimoldi, Telatar, and Pauli [2003]; Andersen and Lau [2006] showed that mutual coupling may decorrelate the signals at the antenna connectors in some cases, and therefore Svantesson and Ranheim [2001] conclude that a higher capacity can be achieved than first expected. Janaswamy [2002] considers putting an increasing number of antenna elements within a fixed length array. He concludes that by including the effect of the mutual coupling the capacity increases slightly by putting 7 or less antenna elements within an fixed array length of 5λ (λ is the carrier wave-length). The capacity is believed to increase because of the decorrelating effect of mutual coupling. But for a higher number of antenna elements within the fixed array length, the capacity is shown to drop because of a reduced signal-to-noise ratio (SNR) which is caused by mutual coupling.

The effect of mutual coupling between the antennas can be most easily be seen by considering two dipole antennas that are closely spaced. Fig. 1.1 shows the element antenna pattern for a dipole antenna when its neighbour antenna is placed at a distance $\lambda/16$ apart from it. Because of the mutual coupling the antenna pattern is not completely omni-directional anymore. The antenna pattern has a slightly larger directivity towards 180 degrees in the azimuth plane, whereas the element antenna pattern for the second antenna has a larger directivity towards 0 degrees. This results in a decoupling effect of the received signals, and the signals become less correlated than predicted by Jakes model (Jakes [1974]). Jakes model, which uses the zeroth order Bessel function to describe the antenna correlation, was widely used in the first publications on MIMO. The model is only accurate for a rich scattering scenario, where the multipath arrivals are uniformly distributed in angle, and for widely spaced antennas (since mutual coupling is neglected). An additional effect of mutual coupling is that it changes the antenna impedance, which may lead to impedance mismatch if no matching network is used. Several authors, Kildal and Rosengren [2003]; Wallace and Jensen [2004b]; Kildal and Rosengren [2004]; Wal-

lace and Jensen [2004a]; Morris and Jensen [2005], have considered this effect. The effect of impedance mismatch at the receiver is that not all of the available power is absorbed by the receiver termination. Impedance mismatch is especially deleterious when the dominant signal impairment is receiver/amplifier noise. Impedance mismatch yields lower received signal power and therefore reduces receiver SNR. From (Wallace and Jensen [2004a]) it is clear that the antenna impedance matching network also has an impact on the correlation of the received signals. It is stated in the paper by Wallace and Jensen [2004a] that with the optimal antenna impedance match the radiation patterns for two closely spaced dipole antennas become orthogonal over $[0, 2\pi]$ in the azimuth plane.

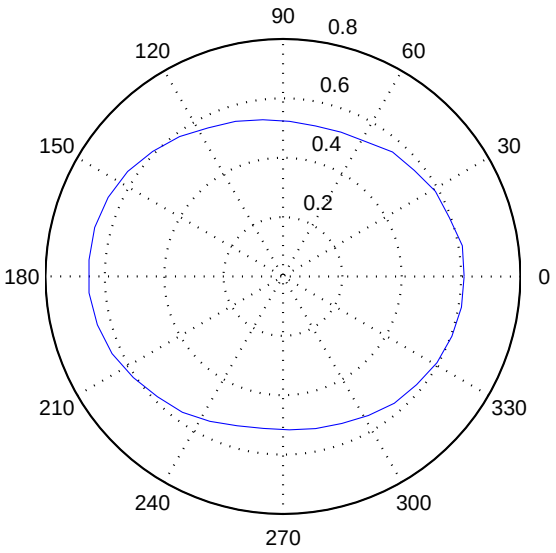

FIGURE 1.1: Antenna pattern for an active antenna element when a neighbour antenna element is placed at a distance $\lambda/16$ away from it. Both antenna elements are terminated with 50 Ω.

There are other authors that, instead of focusing on mutual coupling, have described the number of degrees of freedom of the electromagnetic field. Poon, Brodersen, and Tse [2005]; Poon, Tse, and Brodersen [2006] have expressed the degrees of freedom by the wavevector-aperture product, $\mathcal{A}|\Omega|$. The symbol $\mathcal{A}$ represents the effective aperture which relates to the geometrical size of the transmitter/receiver, and $|\Omega|$ is the angular

spread of the scatterers. In a similar way, Pollock, Williams, and Abhayapala [2005] express the number of significant eigenvalues of the correlation matrix of a uniform circular array in a two dimensional isotropic diffuse field as $\lceil \pi er/\lambda \rceil$, with r being the radius of the antenna array. This expression indicates that there is no point in using a higher number of antenna elements than the number of significant eigenvalues of the correlation matrix. Migliore [2006] relates in a slightly different way the effective number of degrees of freedom of the field on a given observation curve, surface or volume to the number of (spatial) Nyquist intervals the observation curve encompasses. The number of singular values of the electromagnetic field and their relative strengths then give the possibilities for finding capacity expressions. However these capacity expressions are only approximations. Different results may be obtained when the measurement devices (antennas) are included. The antennas themselves, simply by being conductive material, affect the electromagnetic field.

The goal of this thesis is to investigate a compact and cost-effective antenna solution that offers spectral efficiencies comparable to what is obtainable with regular MIMO systems. The thesis is divided into two parts.

Part I explores a concept for a MIMO receiver which is quite different from previous research on MIMO. Instead of sampling values of the electromagnetic field with antennas at discrete spatial points, it is proposed to over-sample values of the field at the same physical location. A time-variant receiver is suggested which makes sure that the antenna pattern is time varying during a symbol period. More specificially, a directive antenna pattern is created which is rotated once or several times during a symbol period. It will be shown that spatial multiplexing can be converted into frequency multiplexing. As a result of this, different sub-channels are created in the frequency domain. These sub-channels have the same effect as multiple receive antennas in traditional MIMO systems.

Part II investigates a new concept for a transmitter which was first proposed by Kalis and Carras [2005]; Kalis, Kanatas, Carras, and Constantinides [2006]. Instead of changing the antenna pattern during the symbol period, as the receiver does, a different antenna pattern may be chosen on each symbol period. The idea behind this transmission scheme is that not only the symbol transmitted with a certain antenna pattern but also the choice of antenna pattern represents information to the receiver.

It should be noted that even though this dissertation only considers dipole antenna elements, the results presented here may easily be extended to other antenna structures, such as for example patch antennas (Ngamjanyaporn and Krairiksh [2002]).

The focus of this thesis is on a mobile unit, and hence when the down-

link and uplink is spoken of, it refers to the view point of the mobile unit. Downlink refers then to the transmission from the basestation to the mobile unit, and the uplink refers to transmission in the opposite direction.

The implementation of the two schemes presented in Part I and II is realized by the usage of parasitic antenna elements and hence the title of the thesis.

1.1 Related work

There are some papers by other researchers as well, that are relevant for this thesis and therefore should be mentioned. Wennstrom and Svantesson [2001] considered using parasitic elements at the receiver for over-sampling the electromagnetic field at various angular directions within a symbol period, which is the same as the idea that is presented in Part I of the thesis. This paper was unknown to us before starting the work presented here. It seems that the authors of the mentioned paper only discovered the basic idea, i.e. oversampling the electromagnetic field within a symbol period. It does not seem that they have recognized the bandwidth expansion and the increased adjacent channel interference. These two effects, which will be presented in Part I, are some of the consequences of over-sampling the field within a symbol period.

A second paper, (Migliore, Pinchera, and Schettino [2006]), also uses parasitic elements, but the results are less related to the work in this thesis than the paper mentioned above. The authors consider multiple active antenna elements and multiple parasitic elements. The parasitic elements are used for improving the antenna patterns of the active elements for each channel realization, in order to maximize the MIMO capacity. The disadvantage of their approach, is that it requires that the channel is estimated several times, since each new configuration of the parasitic elements results in a different channel for the active antenna elements.

1.2 Outline of the thesis

The thesis is organized as follows:

- *Chapter* 2: The basic concept of the rotating receive antenna is explained. It is shown how parasitic antenna elements may be used to create a directive antenna pattern which may be rotated once or several times within the duration of a symbol period. The capacity of this scheme is evaluated by simulations. Numerical results show that

this receiver structure achieves a higher capacity than a single receive antennna.

- *Chapter* 3: This chapter deals with signal power, noise power and sampling issues. The antenna pattern rotation leads to an expanded frequency bandwidth of the received signal. The effect of the bandwidth expansion on the received signal and noise power is investigated. The reduction in capacity because of increased adjacent channel intereference, which is a consequence of the antenna pattern rotation, is also evaluated by simulations. Equations that describe the discrete rotation of the antenna pattern, instead of continuous rotation, are presented.

- *Chapter* 4: A brief discussion on the antenna efficiency, broadband properties of the antenna, and transient effects of the antenna pattern rotation follows. These issues are connected to a practical implementation of the antenna, and due to time limitation and interests the emphasis of the thesis is not put on these themes.

- *Chapter* 5: The capacity of the rotating antenna is compared with the capacity obtained by using multiple active antenna elements. Previous chapters have only compared the capacity of the rotating antenna with a single omni-directional receive antenna.

- *Chapter* 6: An introductory chapter to the second part of the thesis. Results done by other researchers on this field are briefly mentioned. Chapters 2-5 consider the downlink capacity, whereas Chapters 6 and 7 consider the uplink spectral efficiency.

- *Chapter* 7: The spectral efficiency of a novel compact transmitter, that codes information by both the choice of antenna pattern and by the choice of symbol to be transmitted with the antenna pattern, is evaluated.

- *Chapter* 8: Gives concluding remarks and suggestions for further research.

- *Appendix* A: Derives an expression for the radiated power from a two element antenna array.

- *Appendix* B: Gives the proof of the concavity of equation (3.56) with respect to τ.

Part I

Parasitic Elements for Implementing the Receiver

Chapter 2

Rotating receive antenna-Basic concept and practical implementation

This chapter deals with both the theoretical aspects of a rotating receive antenna and the practical realization of such an antenna. In Section 2.1 the concept of a rotating receiver antenna is explained. This new concept presents an alternative to MIMO for achieving increased spectral efficiencies. It becomes obvious that a direct implementation of the rotating antenna is not possible. Therefore an approximate realization of the rotating antenna is searched for in Section 2.2. It is shown that in order to obtain high spectral efficiencies it is necessary for the antenna pattern to satisfy certain properties. In Section 2.3 a more advanced practical implementation of the rotating antenna, that achieves patterns with higher directivity than Section 2.2, is presented. The capacities of all the proposed practical implementations are finally analyzed in Section 2.4.

Parts of the material in this chapter are presented in (Müller, Bains, and Aas [2005]; Bains and Müller [2006a, c]).

2.1 Rotating antenna

Imagine a directive receiver antenna that rotates 360°around periodically. A directive antenna means that signals coming from different angular directions are weighted differently. Since the antenna is rotating periodically it means that a signal from a certain angular direction is given a different weight by the antenna as time moves on. A pictorial description of the antenna pattern rotation is shown in Fig. 2.1. In the analysis of this thesis a

geometrical channel model is assumed. Scatterers are distributed at random positions within a two dimensional plane. This choice is justified by the fact that most of the energy received by the antenna is localized over the azimuth directions (Correia [2001]). Consider P different signals that approach the antenna. Let $s_p(t)$ denote a signal heading towards the antenna from azimuth angle ϕ_p. Assume that the incoming signal $s_p(t)$ is weighted according to the antenna pattern function $a(\phi_p)$.

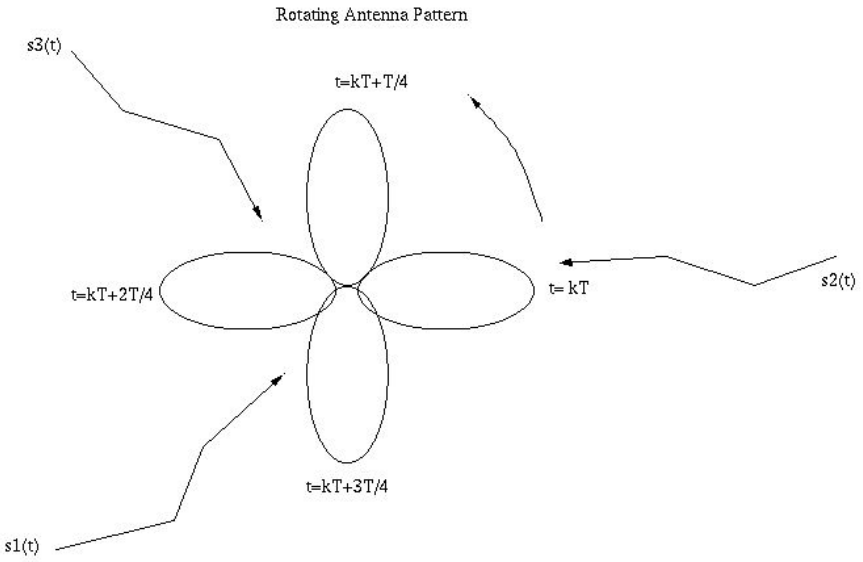

FIGURE 2.1: Rotating antenna pattern. The direction of the antenna beam is shown for $t = kT,\ kT + T/4,\ kT + 2T/4,\ kT + 3T/4$. For each of the antenna beam directions the incoming signals $s_1(t), s_2(t), s_3(t)$ are weighted in a different way.

Consider now that the antenna rotates with an angular speed ω rad/s, thus $r(t)$ which is the received signal can then be described by

$$r(t) = \sum_{p=1}^{P} a(\omega t + \phi_p) s_p(t). \tag{2.1}$$

The antenna pattern function $a(\omega t + \phi)$ is now time-dependent because of the rotation.

We need a certain requirement on the rotation speed

$$\frac{1}{T} \leq \frac{\omega}{2\pi} \ll f_c, \tag{2.2}$$

where T is the symbol time and f_c is the carrier frequency. This requirement must hold in order to avoid aliasing. The necessity of (2.2) will be explained later in this section.

Since the antenna pattern function is a periodic function, we note that it can be Fourier expanded

$$a(\omega t) = \sum_{l=-L}^{+L} a_l e^{jl\omega t}, \tag{2.3}$$

where we have assumed the antenna pattern function to be bandlimited, with a total of $2L+1$ frequency components. The l-th frequency component is given by a_l. There is one component a_0 at the fundamental frequency and $2L$ harmonics. By inserting (2.3) into (2.1) we obtain

$$r(t) = \sum_{l=-L}^{+L} e^{jl\omega t} \underbrace{a_l \sum_{p=1}^{P} e^{jl\phi_p} s_p(t)}_{r_l(t)}. \tag{2.4}$$

From this expression we see that the physical rotation of the antenna results in frequency-shifts of the received signal. If the signal $s_p(t)$ is centered around carrier frequency Ω_c the multiplication with $e^{jl\omega t}$ results in the signal being frequency-shifted to $\Omega_c + l\omega$. Note that frequency Ω_c is defined by $\Omega_c = 2\pi f_c$. Each frequency-shift corresponds to a sub-band. Fig. 2.2 shows how the signal bandwidth is expanded. Going back to inequality (2.2), we see that the lower bound needs to be fulfilled in order to avoid spectral aliasing between the subbands. The rotation speed ω can be exactly equal to $\frac{2\pi}{T}$ if the signals $s_p(t),\ p = 1....P$ have a bandwidth $\leq \frac{1}{T}$. In many cases the bandwidth is larger due to pulse shaping and therefore a larger rotation speed is needed. In order to separate the sub-band components a filter bank of band-pass filters may be employed. The sub-band components can be expressed in vector notation as

$$\underbrace{\begin{bmatrix} r_{-L}(t) \\ \vdots \\ r_{+L}(t) \end{bmatrix}}_{\mathbf{r}(t)} = \underbrace{\begin{bmatrix} a_{-L} & 0 & 0 \\ 0 & \ddots & 0 \\ 0 & 0 & a_{+L} \end{bmatrix}}_{\mathbf{A}} \cdot \underbrace{\begin{bmatrix} e^{-jL\phi_1} & \dots & e^{-jL\phi_P} \\ \vdots & \ddots & \vdots \\ e^{+jL\phi_1} & \dots & e^{+jL\phi_P} \end{bmatrix}}_{\mathbf{V}} \underbrace{\begin{bmatrix} s_1(t) \\ \vdots \\ s_P(t) \end{bmatrix}}_{\mathbf{s}(t)}, \tag{2.5}$$

where $r_{-l}(t)$ is the sub-band around center frequency $f_c - \frac{l\omega}{2\pi}$. The matrix $\mathbf{A}$ consists of the Fourier components of the antenna pattern and will from now on be named the pattern coefficient matrix. The components of

the pattern coefficient matrix also indicate the strengths of each sub-band signal. The matrix $\mathbf{V}$ is an operator that makes linear combinations of the incoming signals, given by $\mathbf{s}(t)$, and outputs these linear combinations in each of the $2L+1$ sub-bands. Each sub-band can be interpreted as having the same effect as a separate antenna in regular MIMO-systems. This holds because in regular MIMO each antenna would pick up different linear combinations of the incoming waves.

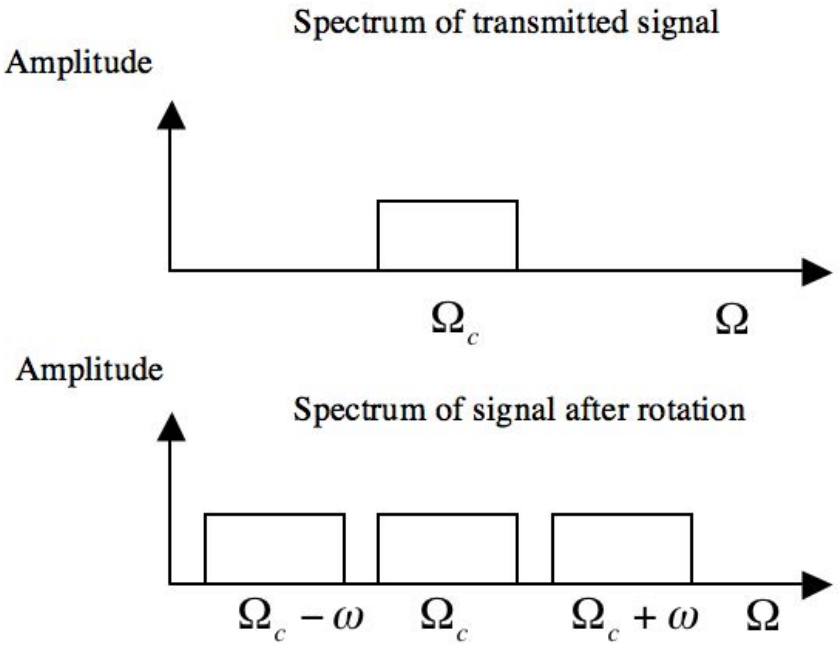

FIGURE 2.2: The spectrum of a signal transmitted at carrier frequency Ω_c is shown. Assuming an antenna rotation of ω rad/s and an antenna pattern with three frequency components the signal gets expanded in frequency, with spectral copies centered at $\Omega_c - \omega$ and $\Omega_c + \omega$.

The capacity of a MIMO system is dependent on the eigenvalue spread of the channel matrix, and the same holds for the system described by (2.5). To achieve high capacity the eigenvalue spread of the channel needs to be small. The pattern coefficient matrix and $\mathbf{V}$ both have an influence on the eigenvalue spread of the channel matrix. The channel matrix is formed by a multiplication of matrices, including the pattern coefficient matrix and $\mathbf{V}$. The elements of $\mathbf{V}$ are dependent on the angles of the incoming sig-

nals. Müller [2002] showed that rich scattering makes $\mathbf{V}$ look like an i.i.d matrix, and thus it has rows with random directions and Marcenko-Pastur distributed eigenvalues (Marcenko and Pastur [1967]). For a rich scattering channel the bottle neck for achieving high capacity is therefore not matrix $\mathbf{V}$, but it is rather more likely that the pattern coefficient matrix becomes the limiting factor.

Most of the simulations in this thesis are done by a rich scattering assumption. The effect of limited scattering, i.e the signals arrive from an interval $[0, \theta]$ where $\theta < 2\pi$, is investigated in Section 3.5.

The link between the number of subband components of the proposed receiver and the number of receive antennas in regular MIMO has already been mentioned. In that respect it is advantageous to increase the number of components of the pattern coefficient matrix. But in addition it is best if the components of the pattern coefficient matrix are equal in magnitude. Unequal magnitude of the elements of this matrix generally increases the eigenvalue spread of the channel matrix and therefore leads to lower capacity.

Since the rotation of the antenna pattern expands the frequency bandwidth this scheme can obviously not be used at transmission. If used at transmission the antenna rotation would expand the bandwidth of the transmitted signal and therefore violate the spectrum regulations. One could argue that it is possible to initially use a smaller bandwidth such that the bandwidth of the transmitted signal falls within the frequency band specified by the spectrum regulators. But this does not lead to a capacity increase since the two effects, increasing the number of channel eigenmodes and using a smaller initial bandwidth, cancel out. Note that the antenna rotation at the receiver does not create problems with the spectrum regulators. The expanded bandwidth is just seen by the rotating antennas that fullfill (2.2) and not by other non-rotating antenna systems or slowly rotating systems that fullfill

$$\frac{\omega}{2\pi} \ll \frac{1}{T}. \tag{2.6}$$

There are some references that have considered a somewhat similar concept. Zekavat and Nassar [2002] have suggested using oscillating antenna patterns for time-diversity. They let the antenna pattern fluctuate around a main beam angle, and hence their scheme differs from ours. Their goals and our goals are also different, since we are interested in spatial multiplexing gain, whereas they are interested in diversity.

2.2 Practical implementation - Sampled rotating antenna

The implementation of the physically rotating antenna is not practical. Imagine that we have a directive antenna that can be rotated mechanically. The requirement of the rotation speed as given by (2.2), in order to avoid aliasing, makes this an almost impossible choice. A mechanical rotation would lead to heat dissipation, and the components of the antenna would very likely be worn out after some usage. As an example consider a mechanical rotation of $2\pi \cdot 1000$ rad/s. This would lead to a data rate of only a few kbits/s. Hence the mechanical rotation becomes a poor alternative for achieving an increased spectral efficiency.

This section considers a practical implementation of the rotating antenna by the usage of parasitic antenna elements. Several references (Vaughan [1999]; Gyoda and Ohira [2000]; Schaer, Rambabu, Borneman, and Vahldieck [2005]; Scott, Leonard-Taylor, and Vaughan [1999]; Nakane, Noguchi, and Kuwahara [2005]) have considered using parasitic elements for creating directive antenna patterns. But their goal is to achieve diversity gain and not spatial multiplexing gain which is the goal in our case. In addition these references do not consider fast rotation of the antenna pattern as defined by (2.2).

First a definition of a parasitic element is in place. Consider two dipole antennas as pictured in Fig 2.3. Let one of the antennas be attached to a voltage source (active antenna), while the other antenna is not attached to any source. Note that the reciprocity theorem states that the same antenna pattern holds for transmission and reception (Balanis [1997],Section 3.8.2). Therefore the analysis here, which assumes that the antenna functions as a transmitter, also holds for reception. The antenna which does not have a source attached to it is called a parasitic element. Current will still run on the parasitic antenna element due to the electromagnetic coupling between the two antennas. The parasitic element acts as a parasite on the electric field supplied by the active antenna and hence the name.

The radiaten pattern for this antenna system is a sum of the radiation patterns of the active and the parasitic element. A single dipole antenna has a omnidirectional pattern in the azimuth plane. By the usage of a parasitic element in close vincinity to the active antenna, the antenna pattern will be altered due to the electromagnetic coupling between the antennas. Assume now that the two dipole antennas are half-wave dipoles, i.e their lengths are equal to half the carrier-wavelength. If the parasitic element is not terminated, which means it is equivalent to one piece of metal of length

$\lambda/2$, it functions as a reflector. This means that the antenna pattern becomes directive towards one direction. The antenna pattern of such a two-antenna system is shown in Fig 2.4. The inter-element distance in this case is $\lambda/64$. It should be noted that all the antenna pattern plots in this dissertation show the magnitude of the antenna patterns and not the phase. If the parasitic element is terminated with a very high impedance value, the parasitic element becomes equivalent to two pieces of dipole antennas with half the dipole lengths. The electromagnetic field is not resonant with dipole antennas of length $\lambda/4$, and the antenna pattern becomes almost omnidirectional in the azimuth plane. If we use electronic switches in the middle of the parasitic element, such as for example Positive Intrinsic Negative (PIN) diodes (Schlub, Thiel, and Lu [2000]), we can switch between a short-circuit and open-circuit state. When the switch is closed the parasitic element acts as one piece of length $\lambda/2$. When the switch is open the antenna acts as two pieces of lengths $\lambda/4$. The advantage of using electronic switches is that the switching operation can be done quite fast. By using PIN diodes switching delays on the order of nanoseconds may be obtained (Packard [1999]). Assume for example that symbols are sent at rate 1 Msymb/s and that the receiver oversamples by a factor of 3. A switching rate of 3 MHz and switching delay of 3 nanoseconds would lead to a total delay of roughly 1 percent relative to the symbol period.

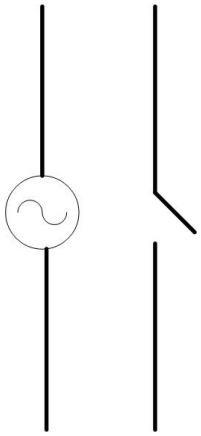

FIGURE 2.3: One active and one parasitic dipole antenna in close vincinity to each other.

Consider now one active antenna and four parasitic elements placed uniformly on a circle around the active antenna. Let one of the parasitic elements be short-circuited while the other three parasitic elements are open circuited. The antenna pattern will be directed towards one direction.

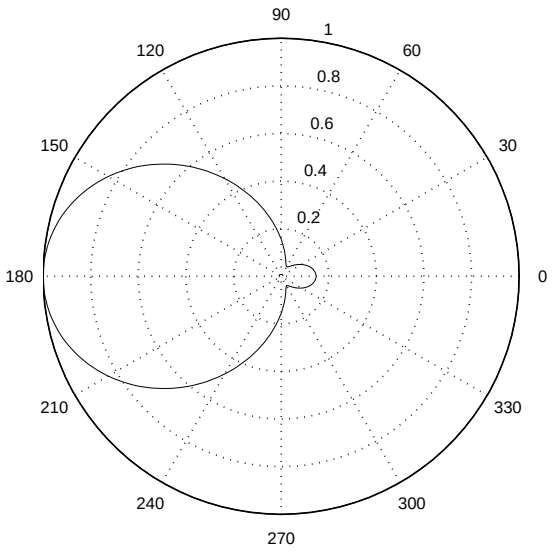

FIGURE 2.4: An antenna pattern obtained by short-circuiting one parasitic element. The parasitic element is placed at distance $\lambda/64$ to the active element. The antenna pattern is normalized and drawn in linear scale, and is found by using an antenna simulation software (Kolundž *et al.* [2000]).

The antenna pattern may be rotated 90° in the azimuth plane by letting the neighbour parasitic element be short-circuited and all the others open-circuited. Proceeding this way the antenna beam may point towards angles 0°,90°,180° and 270°. Hence an approximation to the continuous rotation in Section 2.1 is possible. The difference is that instead of a continuous rotation, a rotation with discrete steps is achieved.

The number of parasitic elements needed, which corresponds to the number of directions the antenna beam points towards, is dependent on the number of Fourier components of the antenna pattern function. An antenna pattern function with $2L+1$ Fourier components needs to be sampled with $2L+1$ samples per rotation in order to avoid aliasing. More details on sampling issues are covered in chapter 3.

Assume that the antenna pattern, when one parasitic element is short-circuited, has $2L+1$ Fourier components. The implementation of the discrete rotation is possible by placing the parasitic elements on the following

angles

$$\phi_i = \frac{2\pi i}{2L+1} \quad i = -L...L. \tag{2.7}$$

This placement of the parasitic elements corresponds to uniform sampling in the angular domain.

The antenna pattern shown in Fig. 2.4 was calculated by using a commerical software (Kolundž *et al.* [2000]). This software, which is based on the method-of-moments, enables us to calculate the electromagnetic field numerically. The next step is to derive analytical expressions for the antenna pattern. Due to reciprocity the antenna pattern on receive and transmit will be the same. Consider one active element and one parasitic element. Let the active element be placed at the center of a coordinate system and directed along the z-axis. The electrical far field component at a point in space due to the active element can be expressed as (Balanis [1997],Equation (4-62a))

$$E_\theta \approx j\eta \frac{i_1 e^{-j\frac{2\pi}{\lambda}r}}{2\pi r}\left[\frac{\cos(\frac{\pi l}{\lambda}\cos(\theta)) - \cos(\frac{\pi l}{\lambda})}{\sin(\theta)}\right], \tag{2.8}$$

where E_θ is one of the three orthogonal components that the electric field can be decomposed into. The angle θ is the zenith angle from the positive z-axis, l is the length of the antenna, r is the radius from the origin of the coordinate system to the point in space, η is the intrinsic impedance of the propagation medium (air) and λ is the carrier-wavelength. Note that since the antenna is placed along the z-axis, the electric field will be symmetric around the z-axis. Hence the electric field has no dependency on the azimuth angle ϕ. It is assumed in the derivation of (2.8) that the current on the antenna has a sinusoidal distribution, with i_1 being the maximum value of the current on the active antenna. Note that the two other orthogonal components of the electric field ,i.e. E_ϕ and E_r, are equal to zero.

We are interested in evaluating the electric field in the azimuth plane which corresponds to $\theta = \frac{\pi}{2}$. We define the antenna pattern in the azimuth plane as

$$a(\phi) = rE_{\theta,1}(\phi) + rE_{\theta,2}(\phi) = \frac{j\eta}{2\pi}\left(i_1 + i_2 \cdot e^{j\cdot\frac{2\pi}{\lambda}\cdot d\cos(\phi)}\right), \tag{2.9}$$

where ϕ is the azimuth angle, $E_{\theta,1}(\phi)$ and $E_{\theta,2}(\phi)$ are the electric field contributions from the active and parasitic antenna respectively, i_1 is the current on the active antenna, i_2 is the current on the parasitic antenna, and d is the inter-element distance.

The currents on the antenna elements can be expressed by taking into account the mutual coupling (Balanis [1997], Equation (8-63))

$$\begin{aligned} i_1 &= \frac{Z_{11} \cdot v_T}{Z_{11}(Z_{11} + Z_L) - Z_{12}^2} \\ i_2 &= -\frac{Z_{12} v_T}{Z_{11}(Z_{11} + Z_L) - Z_{12}^2} = -\frac{Z_{12}}{Z_{11}} \cdot i_1, \end{aligned} \tag{2.10}$$

where Z_{11} is the self-impedance of the active and parasitic element, Z_{12} is the mutual coupling impedance between the active and parasitic element, Z_L is the termination impedance of the active antenna and v_T is the voltage source attached to the active antenna.

The Fourier components of the antenna pattern can be found by combining (2.9) and (2.10) and by taking the Fourier transform. The Fourier components become

$$\begin{aligned} a_0 &= \frac{j\eta}{2\pi}\left(i_1 + i_2 \cdot \mathrm{J}_0\left(\frac{2\pi}{\lambda} \cdot d\right)\right) = \frac{j\eta \cdot i_1}{2\pi} \cdot \left(1 - \frac{Z_{12}}{Z_{11}} \cdot \mathrm{J}_0\left(\frac{2\pi}{\lambda} \cdot d\right)\right) \\ a_l &= -\frac{\eta \cdot i_2}{2\pi} \cdot \mathrm{J}_l\left(\frac{2\pi}{\lambda} \cdot d\right) = \frac{\eta \cdot i_1}{2\pi} \cdot \frac{Z_{12}}{Z_{11}} \cdot \mathrm{J}_l\left(\frac{2\pi}{\lambda} \cdot d\right) \quad , l = -L....L,\ l \neq 0, \end{aligned} \tag{2.11}$$

where a_l is the l-th Fourier component and $\mathrm{J}_l(\cdot)$ is the Bessel function of the first kind and of order l. Higher order Bessel functions are almost zero valued when the argument of the function is small, which means that small inter-element distances, i.e. small arguments of $\mathrm{J}_l(\cdot)$, lead to to Fourier components with small amplitudes. As a result of this, small inter-element distances generally lead to antenna patterns with 3 main Fourier components. As an example consider an inter-element spacing of $\lambda/64$. According to (2.11) the antenna pattern consists of 3 Fourier components with equal strengths. By increasing the inter-element distance to $\lambda/4$, we also increase the number of Fourier components of the antenna pattern. The Fourier coefficients found by using (2.11) seems to be in full agreement with the results obtained by using the antenna simulation software (Kolundž *et al.* [2000]).

The fact that small inter-element distances give larger mutual-coupling than larger distances, and that the values of the Bessel functions become lower for smaller inter-element distances suggests that there should be an optimum inter-element distance.

2.3 Advanced practical implementation

From (2.5) it is clear that the number of eigenmodes of the channel matrix is dependent on the number of Fourier components of the antenna pattern. Since the number and the strength of the eigenmodes determine the capacity, antenna patterns with many Fourier components should be searched for. Directive antenna patterns imply antenna patterns with many Fourier components, and thus directive antenna patterns will be sought after. An analogue to a directive antenna pattern can be made with a signal in the time domain: A peaky signal in the time domain, for example the Dirac delta function $\delta(t)$, represents a signal with large bandwidth in the frequency domain.

In a paper by Harrington [1978] an expression for the antenna gain function, which takes into account both the mutual coupling parameters and the termination of the antennas, can be found. The antenna gain function is given by

$$G = \frac{k^2\eta}{4\pi} \frac{|\mathbf{v}_{oc}^T[\mathbf{Z} + \mathbf{Z}_L]^{-1}\mathbf{v}_T|^2}{\mathbf{i}^H \Re\{\mathbf{Z} + \mathbf{Z}_L\}\mathbf{i}}, \tag{2.12}$$

where G is the gain, $\mathbf{Z}$ is the mutual coupling impedance matrix, $\mathbf{Z}_L$ is a diagonal matrix with the termination impedances of the antennas on the diagonal, $\mathbf{v}_T$ is the voltage excitation vector and $\mathbf{v}_{oc}$ is the open-circuit port voltage of the antenna system when excited by a plane wave from the direction of gain evaluation. The gain function as defined here is the ratio of the radiation intensity in a given direction to the radiation intensity that would be obtained if the power accepted by the antenna were radiated isotropically. Harrington [1978] considers terminating the parasitic elements with reactive loads. Reactive loads imply imaginary valued loads, which represents either capacitive or inductive loads. In this way the magnitude and the phase of the currents that run on the parasitic elements can be controlled to some extent. Since the parasitic elements are loaded with reactive impedances they do not consume energy. However in practise the parasitic elements will have some resistance, and therefore they consume some portion of the energy.

Consider one active antenna and several parasitic elements placed uniformly on a circle around the active antenna. Let the parasitic elements be loaded with reactive impedances. We now seek to maximize the gain given by (2.12) in a certain direction with respect to the reactive impedances. The direction of the gain-function is chosen by $\mathbf{v}_{oc}$. Vector $\mathbf{v}_{oc}$ expresses the magnitude and phase difference of the open circuit voltage at the terminals of all the antenna elements due to different spatial locations. Note

that the gain function in (2.12) is non-convex with respect to the reactive impedances. By employing a numerical algorithm to maximize the gain-function we do not know if the solution we obtain is a local or global maximum. The only way to be sure if it is a global maximum or not is to try out all the possible combinations of the reactive impedances.

The maximization of the gain-function was done by using the simulated annealing algorithm (Kirkpatrick, Gelatt, and Vecchi [1983]; Thiel and Smith [2002]). Six parasitic elements were placed on a circle around the active antenna with a $\lambda/8$ distance to the active antenna element. The antenna pattern that resulted from this maximization is shown in Fig. 3.12. Because of the symmetry a total number of four different reactive impedances are needed for the six parasitic elements.

The antenna pattern rotation when using reactive impedances becomes more complex than in Section 2.2. To be able to rotate the antenna beam the parasitic elements need to be loaded with new reactive impedances. Varactor diodes might be used for that purpose. A varactor diode can represent different reactive impedances by changing an input control voltage to the varactor diode (Gyoda and Ohira [2000]).

The Fourier coefficients of the antenna pattern when using reactive loads are shown in Fig 2.5. Since there are 5 strong Fourier components, the number of relevant eigenmodes is also 5. The received signal is expanded in bandwidth by a factor 5, and in each subband there is a different linear combination of signals received from various angular directions.

There is also an alternative way of achieving directive antenna patterns without terminating the parasitic elements. If the parasitic elements have a slightly longer or shorter length than $\lambda/2$ the mutual coupling between the elements becomes different. This can be realized in practise by placing switches not only in the middle of the parasitic elements but also in other positions of the parasitic elements. By using various combinations of the open/close state of the switches different antenna element lenghts may be realized. The same gain-function as in (2.12) may be used to find the parasitic element lengths that maximize the gain. In addition the impedance values of the parasitic elements must be set to zero. To be able to maximize the gain function, an expression for the mutual coupling parameters as a function of antenna length is needed. Expressions for the mutual coupling parameters may be found in (Balanis [1997],Section 8.5.2, Section 8.6.2). An alternative way of finding the mutual coupling impedances for various antenna lengths is to use the matlab software package available at (Orfanidis. [Orfanidis.]). The latter approach was followed in our case. The simulated annealing algorithm was used to maximize the gain function. One important difference between the realization of parasitic elements with variable

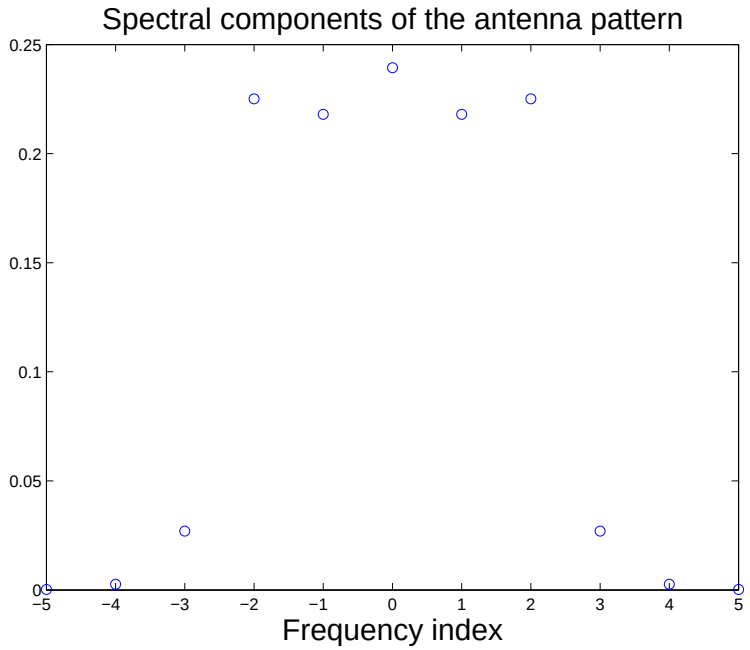

FIGURE 2.5: Fourier components of the antenna pattern which was created by loading the parasitic elements with reactive impedances.

lengths and parasitics with reactive loads is the electronic switches that are needed. The parasitic elements with variable lengths only need switches that represents an open- and short-circuit state which may be achieved with relatively cheap PIN diodes. Loading the parasitic with variable reactive impedances may be accomplished with varactor diodes.

The antenna pattern obtained by maximizing the gain-function with respect to the lengths of the parasitic elements is shown in Fig. 3.12. Note that in theory, a fixed aperture size can achieve any desired directivity value (Hansen [1981]). There are however practical problems with antennas, within a small aperture size, that have very high directivity (superdirective). Some of the drawbacks are low antenna efficiency, sensitive excitation and position tolerances and narrow bandwidth.

2.4 Capacity simulations

So far three different ways of implementing a sampled rotating antenna have been mentioned: Open/short circuiting the parasitic elements, terminating the parasitic elements with reactive impedances and using para-

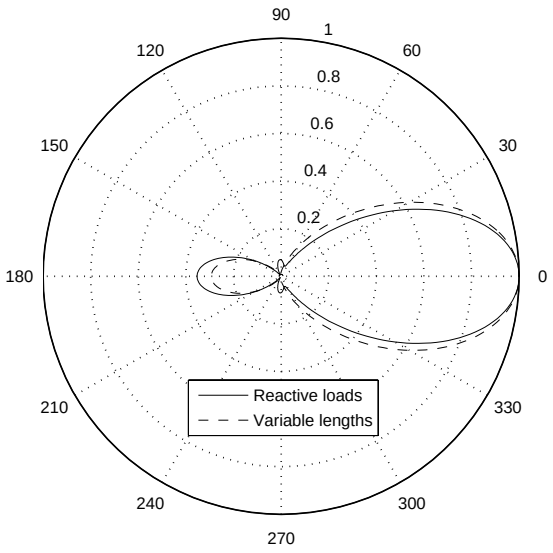

FIGURE 2.6: Antenna patterns obtained by reactively loading 6 parasitic elements (solid line) and employing parasitic elements with variable lengths (dashed line) respectively. Distance $\lambda/8$ between the parasitic elements and the active antenna. The antenna patterns are drawn in linear scale. Each of the antenna patterns is normalized independently. The patterns were found by using an antenna simulation software (Kolundž *et al.* [2000]).

sitic elements with different lengths. But the spectral efficiencies of these schemes are yet to be analyzed. In this section, simulation results are presented that reveal the capacities of the proposed schemes.

2.4.1 Channel model

The channel model used is a geometrical rich scattering channel model with 120 scatterers placed at random positions. The relatively high number of scatterers is chosen in order to avoid statistical dependencies in the channel matrix (Müller [2002]). To study solely the effect of the receiver on the capacity, we choose the transmitters to be a linear array of 20 widely spaced antennna elements. The linear scaling of mutual information with the number of degrees of freedom is best observed at high SNR. Therefore, the noise is chosen to be AWGN 20 dB below the received signal power. Note that the noise is assumed predominantly to be channel noise, and

therefore the antenna efficiency is not considered to be important. A low antenna efficiency would mean that less power is extracted from the incoming waves. But since the same would happen to the channel noise, the receiver SNR would not change significantly.

Let the received signal be described by the following equation

$$\mathbf{r} = \mathbf{AVHx} + \mathbf{n}, \tag{2.13}$$

where $\mathbf{x}$ is the transmitted signal vector, $\mathbf{r}$, $\mathbf{A}$, and $\mathbf{V}$ are defined the same way as in (2.5). Vector $\mathbf{n}$ is the circularly complex additive white Gaussian noise (AWGN) vector, and matrix $\mathbf{H}$ describes the propagation path from the transmit antennas to a certain angular direction at the receiver. Note that equation (2.13) is in discrete time whereas the equations in Section 2.1 are given in continuous time. Details around the transition between continuous and discrete time are given in Section 3.1.

In this thesis, it is mainly the ergodic capacity which is considered. The definition of ergodic capacity is as follows

$$C = \max_{P_{\mathbf{x}}} \mathbb{E}\{I(\mathbf{r};\mathbf{x}|\mathbf{H})\}, \tag{2.14}$$

where C is the ergodic capacity, $I(\mathbf{r};\mathbf{x}|\mathbf{H})$ is the mutual information for a certain channel realization, and $P_{\mathbf{x}}$ is the probability density function (PDF) of the transmitted signal vector. The ergodic capacity is found by maximizing the average mutual information with respect to the PDF of the transmitted signal. For all the calculations in this thesis the channel is assumed to be ergodic, which implies that the channel statistics do not change with time.

2.4.2 Short/open circuiting the parasitic elements

The receiver is assumed to have full channel state information (CSI), whereas to the transmitter the channel is unknown. Figure 2.7 shows the ergodic capacity when short circuiting one parasitic element at a time, as in Section 2.2. The capacity is calculated for various numbers of parasitic elements and for different distances between the active and the parasitic element. The number of parasitic elements equals the number of samples per rotation. For example, 4 parasitic elements implies that the antenna-beam can point towards 4 different angles. The capacity curve shows that 3 samples per rotation are sufficient when the inter-element distance is less than $\lambda/32$. Fig. 2.8 helps in explaining this. The plot shows the Fourier coefficients of the antenna pattern for different distances between the active and the parasitic elements. Since the antenna pattern consists of 3 main Fourier

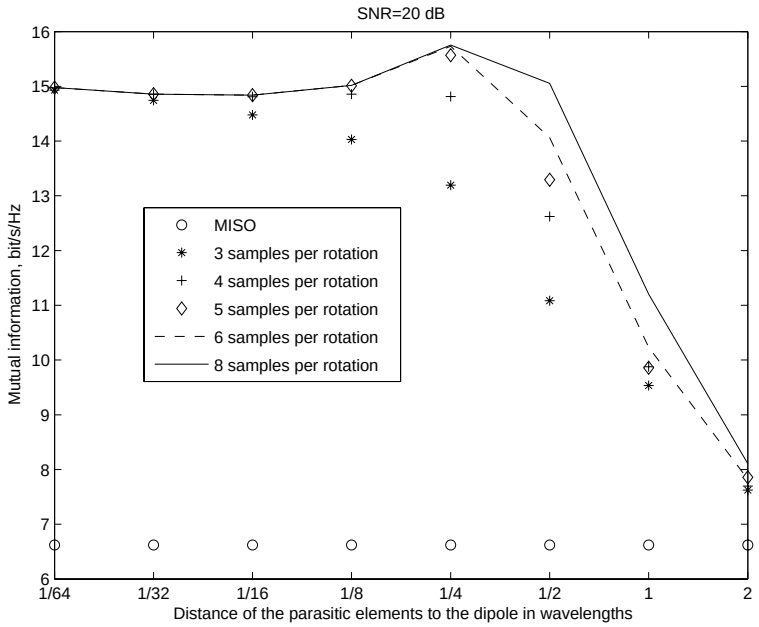

FIGURE 2.7: Mutual information as a function of the distance between the parasitic elements and the active antenna. The number of parasitic elements corresponds to the number of samples per rotation.

components for inter-element distances below $\lambda/32$ there is no point in sampling the antenna pattern by more than 3 samples per rotation. Note that for a larger inter-element distance than $\lambda/8$ the capacity increases by increasing the number of samples per rotation. The reason for this is that the number of Fourier components with significant strength is larger than 3. By sampling 3 time per rotation, the antenna pattern is actually under-sampled. The additional degrees of freedom can therefore not be exploited due to the aliasing effect.

For an inter-element distance equal to $\lambda/4$ it seems that there are 5 significant Fourier components according to Fig. 2.8. This shows off in Fig. 2.7 as well, since 5 samples per rotation are sufficient. Note however that the magnitude of the extra Fourier components, i.e a_{-2} and a_2, are quite weak compared to the strongest Fourier component a_0. Whether the weak Fourier components contribute much to capacity or not is dependent on the SNR. For high SNR the weak Fourier components, which correspond to weak eigenmodes, contribute to capacity. But for low SNR the weak components contribute less. This holds also for regular MIMO systems as

well. Therefore the number of samples per rotation which is necessary for each inter-element distance is actually dependent on the SNR. More details on sampling issues are covered in Chapter 3.

Note from Fig. 2.7 that the rotating antenna achieves 2.3 times higher capacity than a single receiver antenna even for an inter-element distance as low as $\lambda/64$.

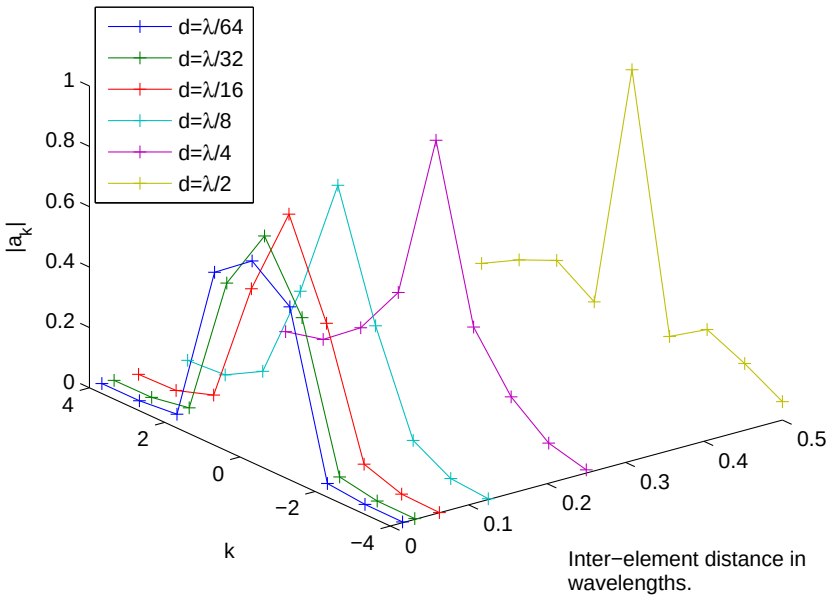

FIGURE 2.8: Antenne pattern Fourier components for various inter-element distances.

2.4.3 Reactive loading and parasitic elements with variable lengths

By using reactive impedances as termination of the parasitic elements or by using parasitic elements with variable lengths, even more directive antenna patterns are achieved. In these cases, the capacity is expected to be higher than the open/short circuit implementation.

In order to evaluate the broadband properties of the antenna patterns, the ergodic capacity is evaluated for different frequencies. In that respect, only the variation of the antenna patterns with frequency is considered. Perfect impedance match is assumed at all frequencies. To get a more real-

istic picture practical impedance matching solutions might be considered. But there are multiple ways of matching an antenna, and each matching technique has different broadband properties. Therefore, as a first step, we only consider how the antenna patterns vary with frequency.

For the capacity simulations, the same channel model is assumed as in the preceeding section: 120 scatterers at random positions, 20 transmitter antennas and AWGN 20 dB below the received signal power level.

The ergodic capacity as a function of frequency is shown in Fig. 2.9. The capacity, when loading the parasitic elements with reactive loads, is shown to be 3.2 times higher than the Multiple-Input-Multiple-Output (MISO) capacity. In comparison, the capacity of the short/open-circuit scheme was 2.3 times higher than the MISO capacity.

Note that the capacity when using parasitic elements with variable lengths shows a larger frequency variation than when loading the parasitic elements with reactive impedances.

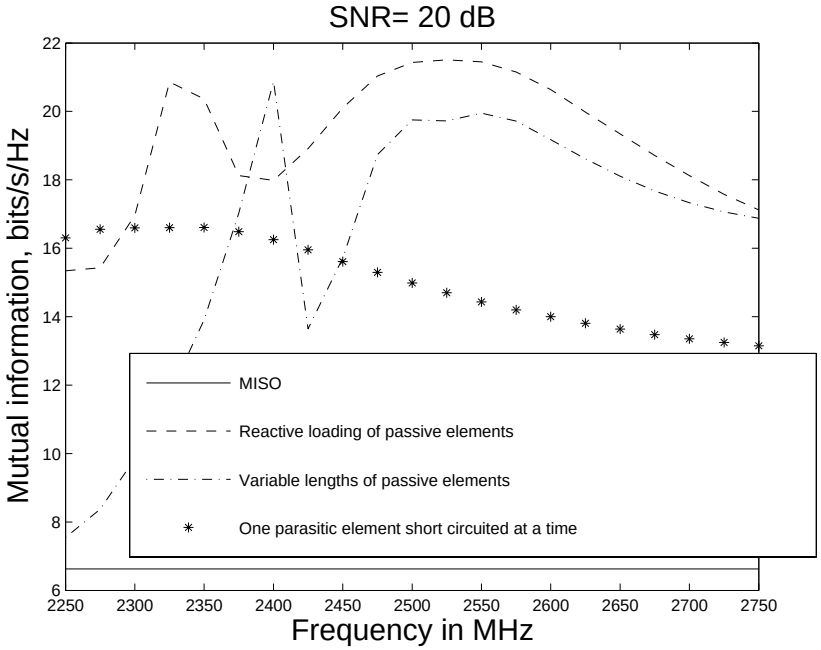

FIGURE 2.9: Mutual information over different frequencies. Distance $\lambda/8$ between the parasitic elements and the active antenna. 6 parasitic elements are used.

Chapter 3

Signal power, noise power and sampling issues

Rotating the antenna pattern of the receiver antenna expands the bandwidth of the received signal. But the bandwidth expansion also happens to adjacent channel signals. The result is that signals from different frequency bands get mixed up with each other. This chapter investigates the signal and noise power issues related to the receiver antenna. Section 3.1 presents an analysis of the receiver SNR when the noise source is considered to be AWGN. In Section 3.2, a discussion on the adjacent-channel interference is presented. The capacity is evaluated in Section 3.3 by including adjacent channel interference and by varying various parameters regarding the antenna pattern and the adjacent channel interference. Equations that describe the discrete rotation of the antenna pattern are given in Section 3.4. The importance of rich scattering on the performance of the rotating antenna is analyzed in Section 3.5. Finally, Section 3.6 finds how long the antenna beam should point towards a certain angular direction before rotating to the next discrete angular direction. The optimal time to stay on each angular direction is found by maximizing the mutual information.

Parts of the material in this chapter are presented in (Bains and Müller [2006b, c,a]).

3.1 Bandwidth expansion, signal and noise power

From (2.5) it is clear that the bandwidth of the received signal is expanded. Then it becomes natural to consider what happens to the SNR. In this section we assume that the only noise source present is channel noise, which we represent as AWGN. No adjacent channel interference is assumed. For

this purpose we compare the SNR when the antenna is a conventional non-rotating antenna to a rotating antenna. The signal of interest which is accessed by the conventional and the rotating antenna is denoted by $r_{conv}(t)$ and $r(t)$ respectively. We assume that the signal has a bandwidth $\frac{1}{T}$, with T being the symbol duration.

The word sampling has a two-fold meaning in this thesis. It may denote the spatial sampling, which is the result of the antenna listening towards different angular directions at different time instants. It may also refer to regular sampling of a signal in the time domain, which is obtained by a sample and hold circuit. Note that the spatial sampling is also temporal sampling since the spatial samples are taken at different time instants. Which ever of these two sampling strategies is spoken of will become clear from the context.

Before comparing the received power of a conventional non-rotating antenna to a rotating antenna, an appropriate normalization of the antenna pattern function is needed. The antenna pattern function $a(\phi)$ is normalized according to

$$\frac{1}{2\pi}\int_0^{2\pi} |a(\phi)|^2 d\phi = 1. \tag{3.1}$$

This equation states that no matter what shape the antenna pattern has, the received power should be the same when the arriving waves are uniformly distributed in the angular directions and uncorrelated with each other. Section 4.1 shows that if the receiving antenna has a perfect antenna-impedance match then this requirement holds. The implication of the normalization in (3.1) is that

$$\sum_{l=-L}^{L} |a_l|^2 = 1. \tag{3.2}$$

Let us define the signal received by a conventional omni-directional antenna as

$$r_{conv}(t) = \mathbf{1}^T \cdot \mathbf{H} \cdot \mathbf{x}(t) + n(t), \tag{3.3}$$

where $\mathbf{1}$ is a vector with dimension $(P \times 1)$ which consists of ones. This operator describes an omni-directional antenna that weights each wave with equal phase and amplitude. The constant P is the number of waves approaching the antenna. Matrix $\mathbf{H}$ is a $(P \times n_t)$ dimensional matrix that describes the channel propagation paths from the n_t transmit antennas to a certain angular direction at the receiver. Vector $n(t)$ is AWGN with noise

spectral density N_0 (J/s/Hz), and $\mathbf{x}(t)$ is the transmit signal vector with dimension $(n_t \times 1)$. The channel matrix is normalized according to

$$\mathbf{1}^H \mathbb{E}\{\mathbf{H} \cdot \mathbf{H}^H\}\mathbf{1} = n_t. \tag{3.4}$$

The transmit signal vector may be expressed as

$$\mathbf{x}(t) = \sum_{k=-\infty}^{\infty} g(t - kT)\mathbf{b_k}, \tag{3.5}$$

where $g(t)$ is the transmit pulse shape and $\mathbf{b_k}$ is the transmitted symbol vector at time instant $k \cdot T$. The energy of the pulse shape is given by

$$\int_0^T |g(t)|^2 dt = 1. \tag{3.6}$$

The average power of the transmitted symbols becomes

$$\mathbb{E}\{\mathbf{b}_k^H \mathbf{b}_k\} = P_T, \tag{3.7}$$

with P_T being the average transmit power constraint.

By assuming a flat fading channel the convolution between the transmitted signal and the channel becomes a multiplication. Consider the convolution between the flat fading channel impulse response $h(t) = h \cdot \delta(t)$ and transmit signal $x(t)$. The convolution becomes

$$h(t) * x(t) = h \cdot \delta(t) * \sum_{k=-\infty}^{\infty} g(t - kT)b_k = h \cdot \sum_{k=-\infty}^{\infty} g(t - k \cdot T)b_k, \tag{3.8}$$

with h being the complex path gain. By using a matched filter at the receiver and by sampling the filtered signal every T seconds, the sampled signal $\hat{r}_{conv}(k \cdot T)$ may be expressed as

$$\begin{aligned}\hat{r}_{conv}(k \cdot T) &= \mathbf{1}^T \mathbf{H} \cdot \mathbf{b}_k \cdot \int_{-T/2}^{T/2} |g(t)|^2 dt + \int_{k \cdot T - T/2}^{k \cdot T + T/2} n(\tau) \cdot g(\tau - k \cdot T) d\tau \\ &= \mathbf{1}^T \mathbf{H} \cdot \mathbf{b}_k + \int_{k \cdot T - T/2}^{k \cdot T + T/2} n(\tau) \cdot g(\tau - k \cdot T) d\tau. \end{aligned} \tag{3.9}$$

The average signal power of sample $\hat{r}_{conv}(k \cdot T)$ may be calculated by taking into consideration the normalizations in (3.4) and (3.7)

$$\mathbb{E}\{|\hat{r}_{conv}(k \cdot T)|^2\} = P_T + N_0. \tag{3.10}$$

The power received by the rotating antenna may be expressed in a similar way. Let the signal received by the rotating antenna be written as

$$\mathbf{r}(t) = \mathbf{AVHx}(t) + \mathbf{n}(t), \tag{3.11}$$

where $\mathbf{r}$, $\mathbf{A}$ and $\mathbf{V}$ are defined in (2.5), $\mathbf{x}(t)$ is defined in (3.5), and $\mathbf{H}$ is the same channel matrix as in (3.3). Note that the statistics and the power of the noise does not change as a result of the antenna rotation. The noise as described by $\mathbf{n}(t)$ will therefore be AWGN with variance N_0 for each component of the vector. The question now is what kind of filter should be applied to the received signal. One possible approach is to apply each of the subband signals to a matched filter. Consider the l'th subband signal r_l

$$r_l(t) = a_l \cdot \mathbf{v}_l^H \mathbf{H}\mathbf{x}(t) + n(t), \tag{3.12}$$

where $\mathbf{v}_l^H$ is the l'th row of matrix $\mathbf{V}$. If $r_l(t)$ is processed by a matched filter and sampled at time instant $k \cdot T$, the sampled signal $\hat{r}_l(k \cdot T)$ may be expressed as

$$\begin{aligned}\hat{r}_l(k \cdot T) &= a_l \cdot \mathbf{v}_l^H \mathbf{H} \cdot \mathbf{b}_k \cdot \int_{-T/2}^{T/2} |g(t)|^2 dt + \int_{k \cdot T - T/2}^{k \cdot T + T/2} n(\tau) \cdot g(\tau - k \cdot T) d\tau \\ &= a_l \cdot \mathbf{v}_l^H \mathbf{H} \cdot \mathbf{b}_k + \int_{k \cdot T - T/2}^{k \cdot T + T/2} n(\tau) \cdot g(\tau - k \cdot T) d\tau. \end{aligned} \tag{3.13}$$

By making some assumptions about the scatterers, as explained in Section 3.5, the received power in the l-th sub-band becomes

$$\mathbb{E}\{|\hat{r}_l(k \cdot T)|^2\} = |a_l|^2 \cdot P_T + N_0. \tag{3.14}$$

Note that summing the signal powers from all $2L + 1$ subbands gives the total power P_T, which means the rotating and the conventional antenna receives the same amount of power. A discrete time equivalent to equation (3.11) may now be found. From now on $\hat{\mathbf{r}}_k$ is used to denote the discrete time equivalent of the received signal. The discrete time signal $\hat{\mathbf{r}}_k$ may be written as

$$\hat{\mathbf{r}}_k = \mathbf{AVH} \cdot \mathbf{b}_k + \hat{\mathbf{n}}_k, \tag{3.15}$$

where $\hat{\mathbf{n}}_k$ is the noise sampled on the output of the matched filter. Note from (3.13) and (3.14) that the noise variance of $\hat{\mathbf{n}}_k$ is equal to N_0. If we assume that the channel is known to the receiver the mutual information becomes

$$I(\hat{\mathbf{r}}_k; \mathbf{b}_k) = \log_2 \left(\left| \mathbf{I} + \frac{P_T}{N_0 \cdot n_t} \mathbf{AVHH}^H \mathbf{V}^H \mathbf{A}^H \right| \right) = \sum_{l=1}^{2L+1} \log_2 \left(1 + \frac{P_T}{N_0} \sigma_l^2 \right), \tag{3.16}$$

where σ_l is l-th singular value of $1/n_t \cdot \mathbf{AVH}$. By assuming high SNR, an approximate expression for the average mutual information can be found

$$\mathbb{E}\{I(\hat{\mathbf{r}}_k; \mathbf{b}_k)\} \approx (2L+1) \cdot \log_2 \left(\frac{P_T}{(2L+1) \cdot N_0} \right) + \mathbb{E}\left\{ \sum_{l=1}^{2L+1} \log_2 \left((2L+1)\sigma_l^2 \right) \right\}. \tag{3.17}$$

The high SNR approximation is valid when $\frac{P_T}{N_0} \gg \max_l \frac{1}{\sigma_l^2}$ holds. Let us assume rich scattering and that the Fourier components of the antenna pattern are equally strong. By exploiting the concavity of the $\log()$ function an upper bound on the average mutual information may be found as given by

$$\begin{aligned} &\mathbb{E}\{I(\hat{\mathbf{r}}_k; \mathbf{b}_k)\} \approx (2L+1) \cdot \log_2 \left(\frac{P_T}{(2L+1) \cdot N_0} \right) \\ &+ \mathbb{E}\left\{ \sum_{l=1}^{2L+1} \log_2 \left((2L+1)\sigma_l^2 \right) \right\} \\ &\leq (2L+1) \cdot \log_2 \left(\frac{P_T}{(2L+1) \cdot N_0} \right) + \sum_{l=1}^{2L+1} \log_2 \left((2L+1)\mathbb{E}\{\sigma_l^2\} \right) \\ &= (2L+1) \cdot \log_2 \left(\frac{P_T}{(2L+1) \cdot N_0} \right). \end{aligned} \tag{3.18}$$

The last step of the equation follows from the fact that $\mathbb{E}\{\sigma_l^2\} = 1/(2L+1)$.

Let us see what the spatial multiplexing gain of this scheme is. The spatial multiplexing gain can be defined as the ratio of the mutual information for the rotating antenna and the mutual information for a Multiple-Input-Single-Output (MISO) system. The spatial multiplexing gain becomes then

$$\frac{(2L+1)\log_2(\frac{P_T}{(2L+1)\cdot N_0})}{\log_2(\frac{P_T}{N_0})} = (2L+1)\left(1 - \frac{\log_2(2L+1)}{\log_2(\frac{P_T}{N_0})}\right), \tag{3.19}$$

where $\log_2(\frac{P_T}{N_0})$ represents the average mutual information for a MISO-system. As we see from the equation, we do not get a multiplexing gain equal to the number of frequency components of the antenna pattern. Since there is a decrease in the effective SNR the multiplexing gain is reduced. Note that the reduction of the multiplexing gain vanishes for high SNR, although only logarithmically.

Next we wish to examine a somewhat artificial case. Assume that the antenna pattern has an infinite number of Fourier components with equal

magnitudes. Assume further an infinite number of transmit antennas and a full rank rich scattering channel. An upper bound on the capacity may then be found, and it is given by

$$\begin{aligned}
&\lim_{L\to\infty} \mathbb{E}\{I(\mathbf{r}_k;\mathbf{b}_k)\} = \lim_{L\to\infty} \mathbb{E}\left\{\sum_{l=1}^{2L+1} \log_2\left(1+\frac{P_T}{N_0}\sigma_l^2\right)\right\} \\
&\leq \lim_{L\to\infty} \sum_{l=1}^{2L+1} \log_2\left(1+\frac{P_T}{N_0}\mathbb{E}\{\sigma_l^2\}\right) = \lim_{L\to\infty} \sum_{l=1}^{2L+1} \log_2\left(1+\frac{P_T}{N_0}\frac{1}{2L+1}\right) \\
&= \frac{P_T}{N_0}\frac{1}{\log(2)}.
\end{aligned} \tag{3.20}$$

The last step was obtained by using L'Hospital's rule (Edwards and Penney [1998], Section 8.3). Equation (3.20) shows that the capacity scales linearly with $\frac{P_T}{N_0}$ when the assumptions above are fulfilled.

3.2 Adjacent channel interference

So far we have only considered the SNR that results from AWGN. If signals are transmitted in adjacent frequency bands, these signals will be expanded in bandwidth too. The result will be that the frequency bandwidth of our signal of interest will overlap with the frequency bands of interfering signals. The received signal in the l-th sub-band may be written as

$$r_l(t) = a_l \sum_{p=1}^{P} e^{j\phi_p l} s_p(t) + \sum_{i\neq 0} a_{l-i} \sum_{p=1}^{P} e^{j(l-i)\beta_{p,i}} q_{p,i}(t), \tag{3.21}$$

where $q_{p,i}(t)$ is an adjacent channel interference signal originating from frequency band $f_c - \frac{\omega i}{2\pi}$. The subscript p denotes that the signal is arriving at angle $\beta_{p,i}$. The signals $s_p(t)$, $p = 1...P$, are our desired signals. The effect that this interference has on our receiver depends on the nature of the interferers. In that respect, we distinguish between two cases, operation in licensed and unlicensed bands. For operation in unlicensed bands the co-channel interference power might be comparable to the adjacent channel interference power. Therefore (3.19) can be a rough estimate of the performance of our system in unlicensed operation. The assumption made in this case is that the interference behaves as AWGN. For operation in licensed bands, signals that are transmitted in adjacent bands are expected to have higher power than co-channel interference. Whether we can gain something from the rotating antenna system compared to MISO for operation in licensed bands will be investigated in the next section.

3.3 Capacity simulations

The capacity simulations presented in chapter 2 were done for SNR = 20 dB. In Section 3.2 it was shown that the expression for the multiplexing gain has a penalty term. Since this penalty term is more pronounced for low SNR, it is of high interest to see the performance of the ergodic capacity as a function of the receiver SNR.

We wish to evaluate the capacity when adjacent channel interference is present. The received signal when adjacent channel interference is included may be expressed as

$$\hat{\mathbf{r}}_k = \mathbf{AVHb}_k + \sum_{i=-2L}^{2L} \hat{\mathbf{q}}_{i,k} + \hat{\mathbf{n}}_k, \tag{3.22}$$

where $\hat{\mathbf{q}}_{i,k}$ is the interfering signal originating from frequency band $f_c - \frac{\omega \cdot i}{2\pi}$, and k is the discrete time index. To make the analysis simpler all adjacent channel interferers are assumed to transmit in non-overlapping frequency bands. The matrices $\mathbf{A}, \mathbf{V}$ and $\mathbf{H}$ are defined as before. The interfering signal may be expressed as

$$\hat{\mathbf{q}}_{i,k} = \mathbf{A}_i \mathbf{V}_i \mathbf{H}_i \mathbf{q}_{i,k}, \tag{3.23}$$

where $\mathbf{A}_i$ and $\mathbf{V}_i$ are matrices that describe the frequency bandwidth expansion of the interfering signal in a similar manner to equation (3.21), and $\mathbf{H}_i$ describes the propagation from the transmitter antennas to a certain angular direction at the receiver. The interference vector $\mathbf{q}_{i,k}$ is the transmit signal of the i-th interfering user. The structure of the matrices $\mathbf{A}_i$ and $\mathbf{V}_i$ is dependent on the index i. For $i = -1$ and for an antenna pattern that consists of 3 Fourier components the matrices become

$$\mathbf{A}_{-1} = \begin{bmatrix} a_0 & 0 & 0 \\ 0 & a_1 & 0 \\ 0 & 0 & 0 \end{bmatrix}$$
$$\mathbf{V}_{-1} = \begin{bmatrix} 1 & \dots & 1 \\ e^{j\beta_{1,-1}} & \dots & e^{j\beta_{P,-1}} \\ 0 & \dots & 0 \end{bmatrix} \tag{3.24}$$

Note that the dimension of the interference vector $\mathbf{q}_{i,k}$, i.e. the number of antennas of the interfering user, has an impact on the capacity achieved by the rotating antenna. If the interference consists of single antenna users the i-th interfering signal is described by

$$\hat{\mathbf{q}}_{i,k} = \mathbf{A}_i \mathbf{V}_i \mathbf{h}_i q_{i,k}. \tag{3.25}$$

Since each interfering user has only one antenna, $q_{i,k}$ becomes a scalar and $\mathbf{h}_i$ a vector. Multiple antenna interferers span a larger signal space at the receiver than single antenna interferers, which means that a lower capacity is expected with multi-antenna interferers than single antenna interferers.

The capacity of the rotating antenna will be considered for 3 different scenarios in the following sections.

3.3.1 Capacity as a function of the number of Fourier components of the antenna pattern

In this section the capacity is evaluated as a function of the number of Fourier components of the antenna pattern. We assume that all Fourier components have the same magnitude. The transmitter is chosen to be a 10 element antenna array with $\lambda/2$ spacing between the antennas. The adjacent channel interference is represented by one interfering user in each adjacent channel and it is assumed that no AWGN is present. All interfering users are assumed to be single antenna users.

The interference power in sub-channel i is denoted by N_i. The interference power received by a standard omni-directional antenna becomes

$$\mathbb{E}\{|\mathbf{1}^T\mathbf{h}_i \cdot q_{i,k}|^2\} = N_i \tag{3.26}$$

In this section the interference power within each sub-channel is held at the same level, i.e. $N_i = N_j$ for all i, j.

The capacity of the rotating antenna is shown in Fig. 3.1 as a function of signal-to-interference ratio (SIR) and number of Fourier components of the antenna pattern. The SIR is defined as follows

$$SIR = \frac{P_T}{N_i}. \tag{3.27}$$

The SIR is defined as the SIR that a regular omni-directional antenna would experience. The power of the signal of interest is given by P_T.

As expected, the plot shows that the capacity increases for an increasing number of Fourier components of the antenna pattern. For comparison the capacity when the receiver has a single omni-directional antenna is also included. The capacity of the rotating antenna is higher than the capacity of the single antenna receiver for all SIRs.

3.3.2 Capacity with different power levels on co- and adjacent channel interference

When the power levels on the adjacent channel interference and the co-channel interference are the same there is a obviously a capacity gain by

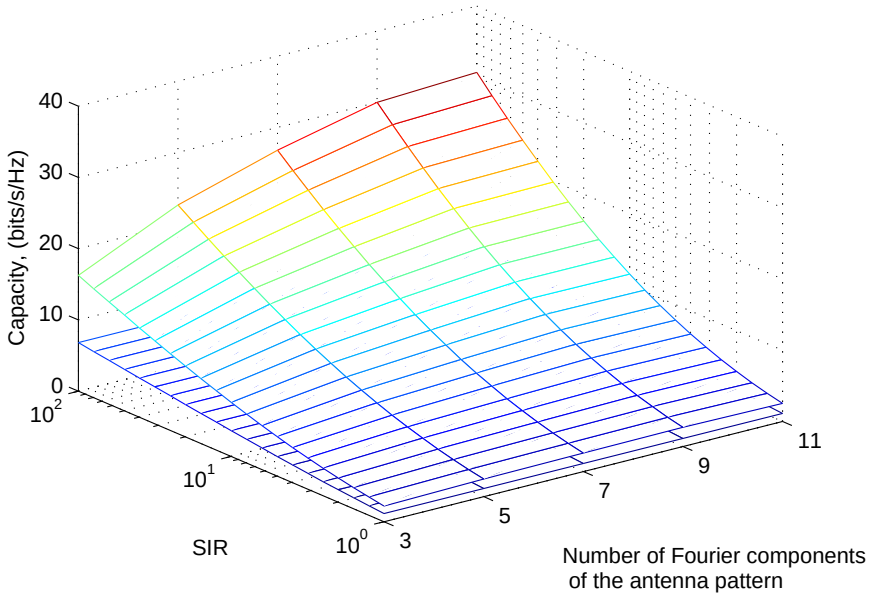

FIGURE 3.1: Capacity as a function of SIR and antenna pattern Fourier components. The upper plot represents the rotating antenna, the lower plot represents a single omni-directional receive antenna.

using the rotating antenna when comparing against the capacity of a single omni-directional antenna. As already mentioned, the equal power case may be a valid assumption for operation in unlicensed frequency bands. For licensed frequency bands the power level of the adjacent channel interference is expected to be much higher than the co-channel interference. Therefore, the aim of this section is to evaluate the capacity when the level of the adjacent channel interference is higher than the level of the co-channel interference.

Let N_0 and N_{int} denote the power of the co-channel and adjacent channel interference respectively. Thus the power level of the adjacent channel interference from all sub-channels are the same. The transmit power level of the signal of interest is denoted by P_T.

Fig. 3.2 shows the capacity as a function of the co-channel SIR, $\frac{P_T}{N_0}$, and the ratio $\frac{N_{int}}{N_0}$. The antenna pattern is assumed to consist of 3 equally strong Fourier components. The co- and adjacent channel interference are caused by single antenna interferers, and only one interfering user is transmitting in each sub-channel. The capacity plot shows that the capacity of the rotating antenna decreases rapidly as the ratio $\frac{N_{int}}{N_0}$ increases.

An important question that arises in the context of different levels of co-channel and adjacent channel interference is: When is it possible to obtain capacity gains by the rotating antenna relative to the capacity achieved by a single omni-directional receiver antenna? The area below the curve in Fig. 3.3 marks the area for which the capacity of the rotating antenna exceeds the capacity of an omni-directional antenna. The co- and adjacent channel interference in this case are caused by multi-antenna interferers, 5 antennas at each interferer, and only one interfering user is transmitting in each sub-channel. Fig. 3.3 shows that at low co-channel SIR, i.e. low $\frac{P_T}{N_0}$, only a small increase in the adjacent channel interference level relative to co-channel level is tolerated, before the capacity of the rotating antenna drops below the capacity of a single antenna. At high co-channel SIR, for example $\frac{P_T}{N_0} = 20$ dB, the rotating antenna outperforms the single omni-directional antenna as long as the adjacent power level is less than 12 times higher than the co-channel power level.

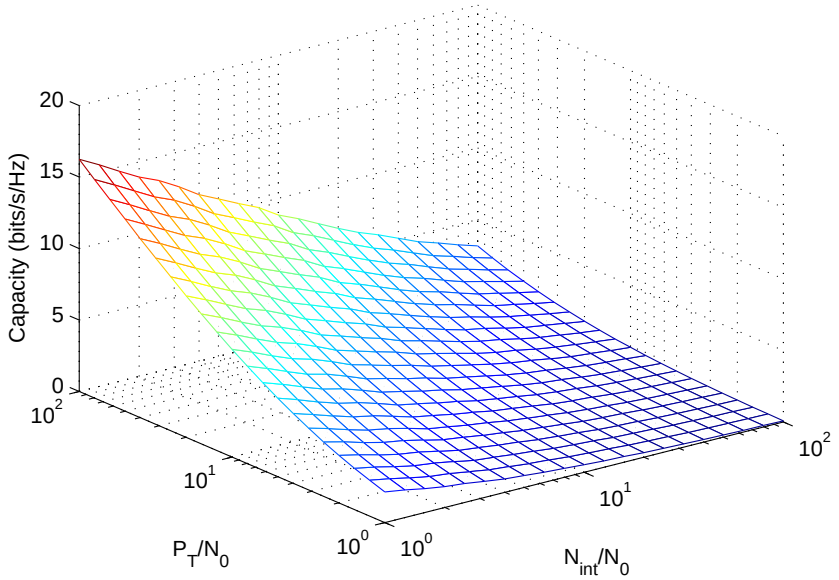

FIGURE 3.2: Capacity as a function of co-channel SIR and the ratio of adjacent channel interference power to the co-channel interference power level. The antenna pattern of the rotating antenna consists of 3 Fourier components of equal magnitude.

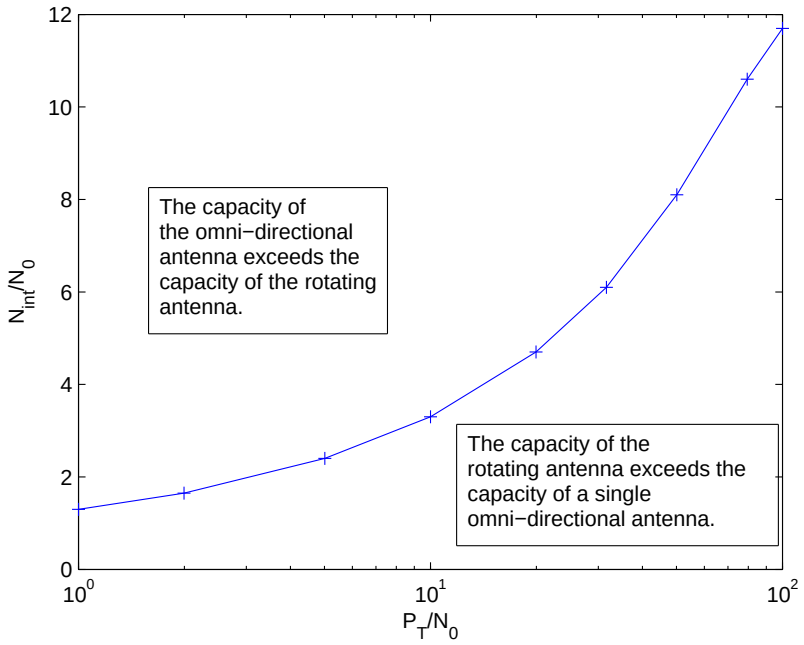

FIGURE 3.3: The plot shows the area for which the rotating antenna obtains a higher capacity than an omni-directional antenna.

3.3.3 Capacity as a function of the number of antenna elements of interfering users

In Section 3.3.1 the interferers were single antenna users. If the interferers are multi-antenna users the interference described by $\sum_{i=-2L}^{2L} \hat{\mathbf{q}}_{i,k}$ in equation (3.22) is expected to span a larger signal space.

The capacity as a function of SIR and number of antennas at the interfering users is depicted in Fig. 3.4. The antenna pattern of the rotating antenna is assumed to consist of 3 equally strong Fourier components. The capacity plot shows that the capacity decreases as the number of antennas increases. This result confirms that multiple antenna interferers span a larger signal space than single antenna interferers.

3.4 Sampling issues

Until now we have not gone deep into the sampling issues of the antenna pattern. The present section seeks to describe the sampling of the antenna pattern mathematically. Let us assume that the antenna pattern is sampled

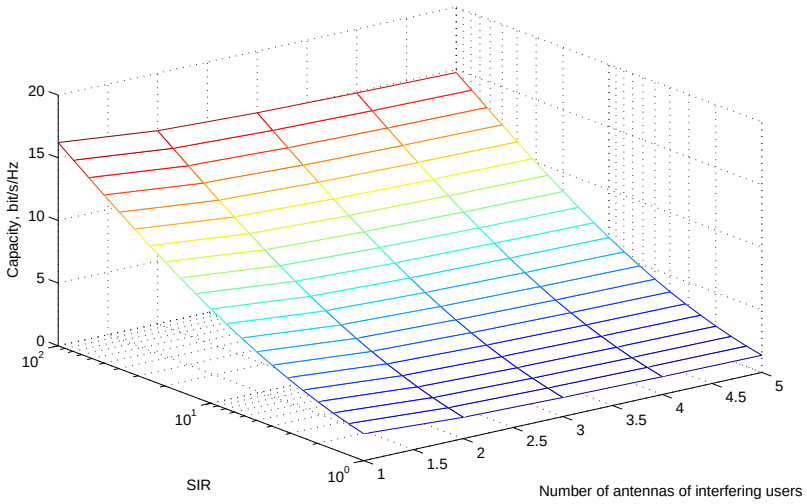

FIGURE 3.4: Capacity as a function of both the number of antennas that are used by each interfering user and the SIR. The antenna pattern of the rotating antenna consists of 3 Fourier components of equal magnitude.

every T_c seconds, then we obtain

$$g_p(t) = \sum_{n=-\infty}^{\infty} a(\omega t + \phi_p)\delta(t - nT_c). \tag{3.28}$$

This function consists of Dirac delta pulses, but in reality the antenna pattern function should hold a constant value for T_c seconds before it changes value. This can be obtained by folding $g_p(t)$ with a rectangular pulse $p(t)$. The rectangular pulse should have the duration of T_c seconds. Let $p(t)$ be defined as

$$p(t) = \text{rect}\left(\frac{t}{T_c}\right), \tag{3.29}$$

where rect() is defined as follows

$$\text{rect}(t) = \begin{cases} 1 & \text{for} \quad -1/2 \leq t \leq 1/2 \\ 0 & \text{otherwise} \end{cases}. \tag{3.30}$$

Let us now define the sampled antenna pattern function as

$$a_{s,p}(t) = g_p(t) * p(t) = \sum_{n=-\infty}^{\infty} \int_{\tau=-\infty}^{\infty} p(\tau) a(\omega(t-\tau)+\phi_p)\delta(t-nT_c-\tau)d\tau$$
$$= \sum_{n=-\infty}^{\infty} p(t-nT_c)a(\omega nT_c+\phi_p). \tag{3.31}$$

More insight is obtained by viewing this operation in the frequency domain. We note that a folding operation in the time domain is equivalent to multiplication in the frequency domain. The following therefore holds

$$g_p(t) * p(t) \Leftrightarrow G_p(\Omega) \cdot P(\Omega). \tag{3.32}$$

Where Ω is the angular frequency. In order to express $G_p(\Omega)$ we first need to find the spectrum of the continuous antenna pattern function $a(\omega t + \phi_p)$

$$A_p(\Omega) = \mathbb{F}\{a(\omega t+\phi_p)\} = \sum_{l=-L}^{L} a_l \delta(l\omega - \Omega)e^{jl\phi_p}, \tag{3.33}$$

where $\mathbb{F}\{\cdot\}$ denotes the Fourier transform. $G_p(\Omega)$ will consist of spectral copies of $A_p(\Omega)$ due to sampling

$$G_p(\Omega) = \sum_{k=-\infty}^{\infty} A_p\left(\Omega + \frac{2\pi k}{T_c}\right) = \sum_{k=-\infty}^{\infty}\sum_{l=-L}^{L} a_l \delta\left(l\omega - \Omega + \frac{2\pi k}{T_c}\right)e^{jl\phi_p}. \tag{3.34}$$

The sampled antenna pattern will therefore be given by

$$A_{s,p}(\Omega) = \sqrt{T_c}\text{sinc}\left(\Omega\frac{T_c}{2\pi}\right)\sum_{k=-\infty}^{\infty}\sum_{l=-L}^{L} a_l\delta\left(l\omega-\Omega+\frac{2\pi k}{T_c}\right)e^{jl\phi_p}. \tag{3.35}$$

Equation (3.35) shows that the sampled antenna pattern function consists of weighted spectral copies. The weighting is done by the sinc function $P(\Omega)$, where $P(\Omega)$ is just the Fourier transform of $p(t)$ in (3.29). The separation between each spectral copy is $\frac{2\pi}{T_c}$, which means it is determined by the sampling interval. An example will better illustrate the sampling issues of the antenna pattern. Assume an antenna pattern function that has 3 Fourier components. Fig. 3.5 shows $G_p(\Omega)$ and $P(\Omega)$ for the case when the antenna pattern function is sampled with frequency $\Omega_s = 3\omega$. The result of sampling the antenna pattern function is shown in Fig. 3.6. Note that a lower sampling frequency than 3ω gives overlap between the

spectral copies and therefore results in aliasing. When comparing the number of harmonics of the continuously rotating antenna function $A_p(\Omega)$ with $A_{s,p}(\Omega)$, we see that the sampled antenna pattern function has several more harmonics than the continuously rotating antenna. This means that the spectrum of the received signal will be expanded even more in frequency with the sampled antenna pattern than with the continuous rotating antenna pattern. This might lead us to the erroneous belief that the degrees of freedom for the sampled antenna pattern is even higher than when the antenna rotates continuously. We can see from (3.35) that the signal in the extra sub-bands have the same linear combinations of the incoming waves as the original sub-bands. The same $e^{j\phi_1 l}$, ..., $e^{j\phi_p l}$ factors are used to weight the incoming waves. Therefore there will be no new information in these extra sub-bands.

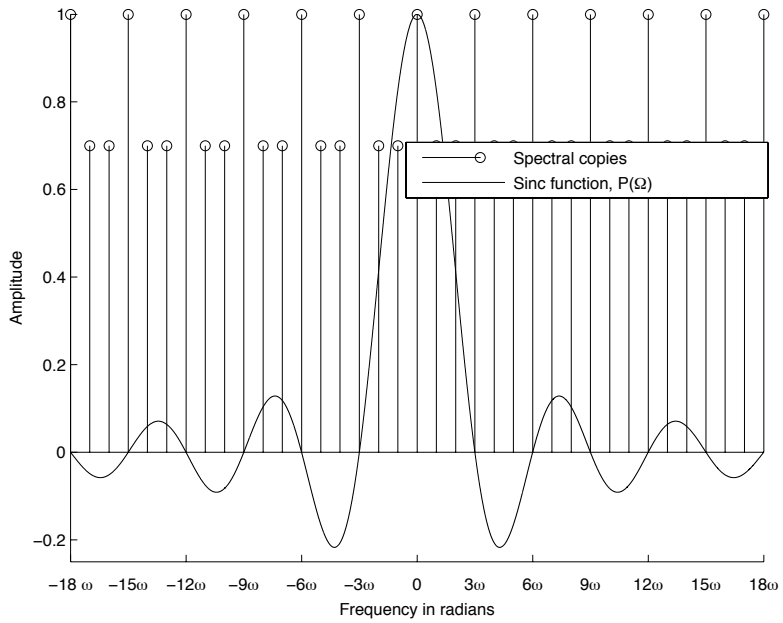

FIGURE 3.5: Plots of $G_p(\Omega)$, the repeated spectral copies of the antenna pattern due to sampling, and $P(\Omega)$ which represents the hold operation. The continuously rotating antenna pattern consists of 3 frequency components. The antenna pattern is sampled at frequency 3ω, i.e. at the lowest sampling frequency that avoids aliasing.

These extra sub-bands can still be of use. Let us assume that there are no adjacent channel signals present, just AWGN. We have seen that

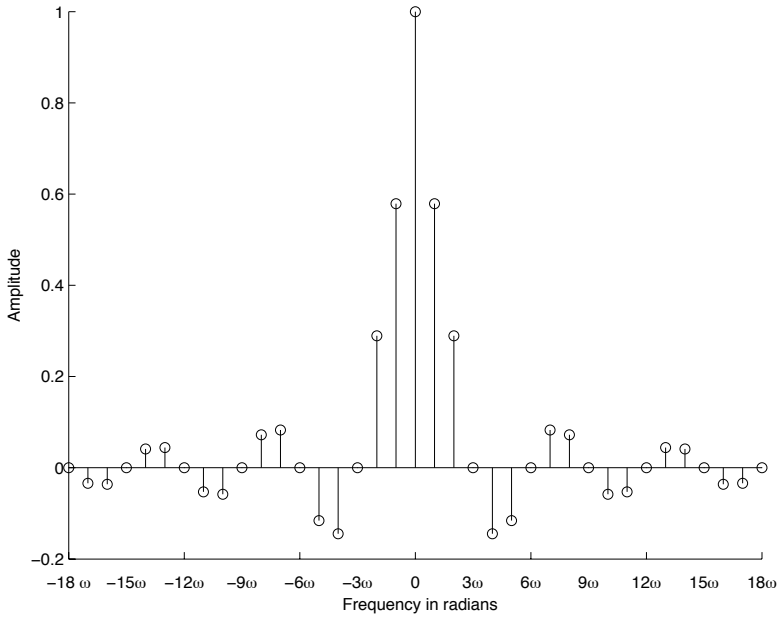

FIGURE 3.6: The sampled antenna pattern function, which results from sampling at frequency 3ω. The corresponding continuously rotating pattern consists of 3 frequency components.

the sampled rotating antenna spreads the signal bandwidth even more than the continuously rotating antenna. A wider signal bandwidth implies a higher noise bandwidth. However, the sampled rotating antenna does not loose in terms of performance compared to the continuous rotating antenna. This holds under the assumption that the antenna pattern is sampled sufficiently. Consider a signal $\tilde{r}_l(t)$ in the l-th frequency sub-band and a spectral copy $\tilde{r}_{l+2L+1}(t)$ due to the discrete rotation in the $(l+2L+1)$-th sub-band. From (3.35) we see that $\tilde{r}_{l+2L+1}(t)$ will be a scaled and phase-shifted version of $\tilde{r}_l(t)$. Let us assume that the SNR in the l-th and $(l+2L+1)$-th sub-band is given by

$$\mathrm{SNR}_l = \frac{E_l}{N_0} \tag{3.36}$$

$$\mathrm{SNR}_{l+2L+1} = \frac{E_l \cdot |a|^2}{N_0}, \tag{3.37}$$

where the complex constant a indicates the scaling and phase-shift of the signal in the $(l+2L+1)$-th sub-band. The energy of the signal of interest

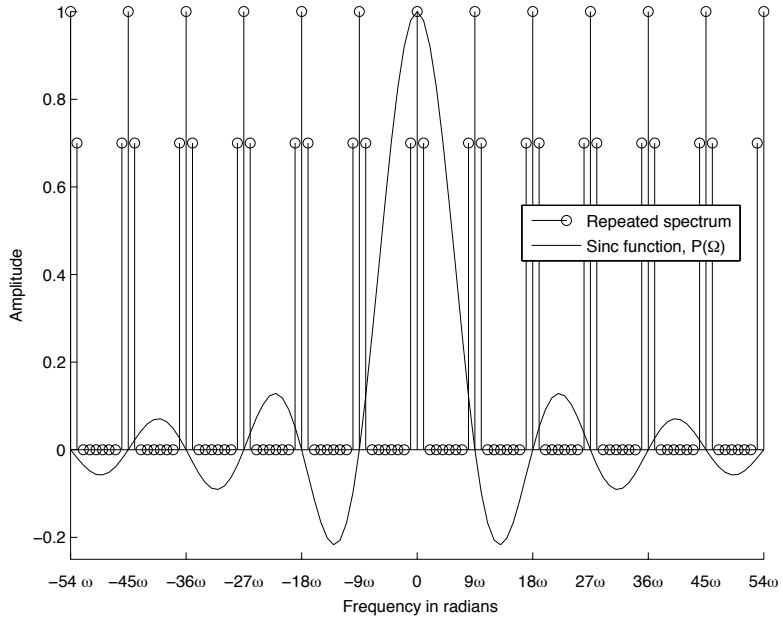

FIGURE 3.7: Plots of $G_p(\Omega)$, the repeated spectral copies of the antenna pattern due to sampling, and $P(\Omega)$ which represents the hold operation. The continuously rotating antenna pattern consists of 3 frequency components. The antenna pattern is sampled at frequency 9ω, i.e. 3 times higher than the lowest sampling frequency that avoids aliasing.

in l-th sub-band is given by E_l. By coherently combining the signal in the l-th and $(l + 2L + 1)$-th sub-band we obtain a signal with SNR equal to $\frac{E_l \cdot (1+|a|^2)}{N_0}$. If we coherently combine all the extra sub-bands due to discrete rotation we will achieve the same SNR as the continuous rotating antenna.

We proceed by finding a matrix expression similar to (2.5) for the received signal

$$\tilde{\mathbf{r}}(t) = \begin{bmatrix} \tilde{r}_{-K(2L+1)-L}(t) \\ \vdots \\ \tilde{r}_{+K(2L+1)+L}(t) \end{bmatrix} = \mathbf{PAVs}(t) + \mathbf{n}. \tag{3.38}$$

Vector $\tilde{\mathbf{r}}(t)$ is the received signal of the sampled rotating antenna. The dimension of $\tilde{\mathbf{r}}(t)$ is much higher than the dimension of $\mathbf{r}(t)$ from (2.5), because the sampled rotating antenna spreads the signal even more. The number of Fourier components of the continuously rotating antenna is denoted by $2L + 1$, whereas K is an integer that describes the extra bandwidth

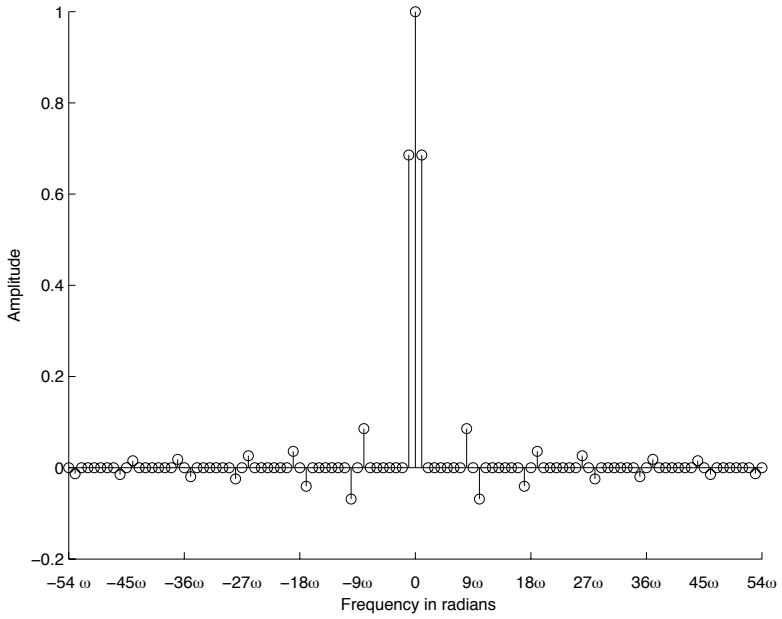

FIGURE 3.8: The sampled antenna pattern function. The original antenna pattern consists of 3 frequency components. The antenna pattern is sampled at frequency 9ω.

expansion. From the matrix expression we see that the sampled antenna rotation is described by a multiplication with matrix **P**. Matrix **P** has elements

that are values from the sinc function. The structure of matrix $\mathbf{P}$ becomes

$$\underbrace{\begin{bmatrix}
\vdots & \vdots & \vdots & \vdots & \vdots \\
P(-\omega L - \Omega_s) & & & & \\
\vdots & \ddots & & & \\
\vdots & & P(-\Omega_s) & & \\
 & & & \ddots & \\
0 & & & & P(\omega L - \Omega_s) \\
P(-\omega L) & 0 & & & \\
 & \ddots & \vdots & & \\
 & & P(\omega \cdot 0) & & \\
 & & & \ddots & \\
 & & & & P(\omega L) \\
P(-\omega L + \Omega_s) & & 0 & & \\
\vdots & \ddots & & & \\
\vdots & & P(\Omega_s) & & \\
 & & & \ddots & \\
 & & & & P(\omega L + \Omega_s) \\
\vdots & \vdots & \vdots & \vdots & \vdots
\end{bmatrix}}_{2L+1}. \tag{3.39}$$

If we assume that the number of rows of P grows large, i.e. $K \to \infty$, and we assume that the antenna pattern is sampled sufficiently, then we get

$$\mathbf{P}^H\mathbf{P} = \mathbf{I}. \tag{3.40}$$

Note that sampling sufficiently means that the number of samples per rotation is not smaller than the number of frequency components of the antenna pattern. We now assume that the received signal can be written as

$$\tilde{\mathbf{r}}(t) = \mathbf{PAVHx}(t) + \mathbf{n}, \tag{3.41}$$

where $\mathbf{H}$ describes the propagation path from the transmitter antennas to a certain angular direction at the receiver, $\mathbf{x}(\mathbf{t})$ is the transmitted signal vector and $\mathbf{n}(t)$ is a AWGN vector. By assuming that the received signal is processed by a matched filter and then sampled on the output of the filter as in Section 3.1, the discrete time signal $\tilde{\mathbf{r}}_k$ may be written as

$$\tilde{\mathbf{r}}_k = \mathbf{PAVHb}_k + \hat{\mathbf{n}}. \tag{3.42}$$

We proceed by finding an expression for mutual information for perfect channel knowledge at the receiver side and a spatially white transmitted signal

$$I(\mathbf{b}_k;\tilde{\mathbf{r}}_k) = \log_2\left|\left(\mathbf{I}+\frac{1}{N_0}\mathbf{PAVHH}^H\mathbf{V}^H\mathbf{A}^H\mathbf{P}^H\right|\right) \tag{3.43}$$

$$= \log_2\left|\left(\mathbf{I}+\frac{1}{N_0}\mathbf{AVHH}^H\mathbf{V}^H\mathbf{A}^H\mathbf{P}^H\mathbf{P}\right|\right) \tag{3.44}$$

$$= \log_2\left|\left(\mathbf{I}+\frac{1}{N_0}\mathbf{AVHH}^H\mathbf{V}^H\mathbf{A}^H\right|\right). \tag{3.45}$$

Equation (3.45) is identical to the expression for the mutual information for a continuously rotating antenna. This shows that mutual information becomes the same for the continuous rotating antenna and the sampled rotating antenna. From (3.43) to (3.44) the determinant principle is used. The principle says that the order of the matrices inside the determinant can be changed as long as the dimension of the identity matrix is also changed. The step from (3.44) to (3.45) assumes that we are including an infinite number of sub-bands, which means $\mathbf{P}^H\mathbf{P} = \mathbf{I}$. When $\mathbf{P}$ contains only a finite number of sub-bands, then $\mathbf{P}^H\mathbf{P} = \mathbf{I}$ does not hold. The effect of this will be a somewhat larger eigenvalue spread of the matrix product $\mathbf{AVHH}^H\mathbf{V}^H\mathbf{A}^H\mathbf{P}^H\mathbf{P}$, and therefore some decrease in the mutual information.

3.4.1 Over-sampling

Since the receiver cannot, because of complexity, use too many subbands for reconstruction, an alternative might be to over-sample. Observe what happens if we over-sample the antenna pattern. Fig. 3.7 and Fig. 3.8 show the case when the sampling frequency is 9ω. This is three times higher than the number of frequency components of the continuously rotating antenna pattern. The effect of over-sampling is that the sampled antenna pattern function gets more similar to the continuously rotating antenna pattern function. This means that the power of the received signal is focused in a narrower frequency band, which is desirable. But there is also an unwanted effect by over-sampling which is caused by non-ideal switches. The more often we perform a switch the more often broadband impulse noise occurs. Since there is a trade-off between these two effects, there will be an optimum oversampling factor in practice.

3.4.2 Under-sampling

Under-sampling relates to sampling the wave-field with fewer samples per rotation than the number of frequency components of the antenna pattern. This case is more of theoretical interest than practical, since we would of course take advantage of all the available degrees of freedom and not "loose" it by under-sampling. To illustrate what happens when we under-sample the wave-field, consider this example: Assume an antenna pattern with $2L+1$ Fourier components which is sampled with $2L$ samples per rotation. This would give spectral aliasing which is reflected in the $\mathbf{P}$ matrix

$$\underbrace{\begin{bmatrix}
\vdots & \vdots & \vdots & \vdots & \vdots \\
P(-3\omega L) & & & & \\
0 & \ddots & 0 & \dots & 0 \\
\vdots & & P(-2\omega L) & & \vdots \\
0 & \dots & 0 & \ddots & 0 \\
P(-\omega L) & 0 & \vdots & 0 & P(-\omega L) \\
0 & \ddots & 0 & 0 & 0 \\
\vdots & & P(\omega \cdot 0) & & \vdots \\
0 & \dots & 0 & \ddots & 0 \\
P(\omega L) & 0 & \vdots & 0 & P(\omega L) \\
0 & \ddots & 0 & 0 & 0 \\
\vdots & & P(2\omega L) & & \vdots \\
0 & \dots & 0 & \ddots & 0 \\
P(3\omega L) & 0 & \dots & 0 & P(3\omega L) \\
\vdots & \vdots & \vdots & \vdots & \vdots
\end{bmatrix}}_{2L+1} . \tag{3.46}$$

When the wave-field was sampled sufficiently, there was only one element different from zero in each row. Under-sampling results in more than one element different from zero in each row. For the above case there are some rows with two elements that are different from zero. Note also that the two elements have the same value. The consequence of this is that the product $\mathbf{P}^H\mathbf{P}$ becomes a matrix which has two equal rows. This has the effect of loosing one eigen-mode from the complete channel matrix and therefore one degree of freedom.

To see the effect on the sampling rate on capacity, the capacity is calculated as a function of the number of samples per rotation. The antenna pattern used for the capacity calculation consists of 5 dominant Fourier components. According to the sampling theorem 5 samples per rotation should be sufficient if all the sub-band components are included at the receiver. Fig. 3.9 shows the capacity when 9 or 400 sub-band components are included at the receiver. The plot shows that undersampling the antenna pattern clearly leads to capacity reduction. By including 400 sub-band components at the receiver a higher capacity is achieved than if only 9 sub-bands are used, since more of the signal energy is captured. A higher sampling rate than 5 samples per rotation also increases capacity, since the signal energy is concentrated in a smaller frequency bandwidth. A larger portion of the signal energy is therefore captured by the 9 or 400 sub-band components.

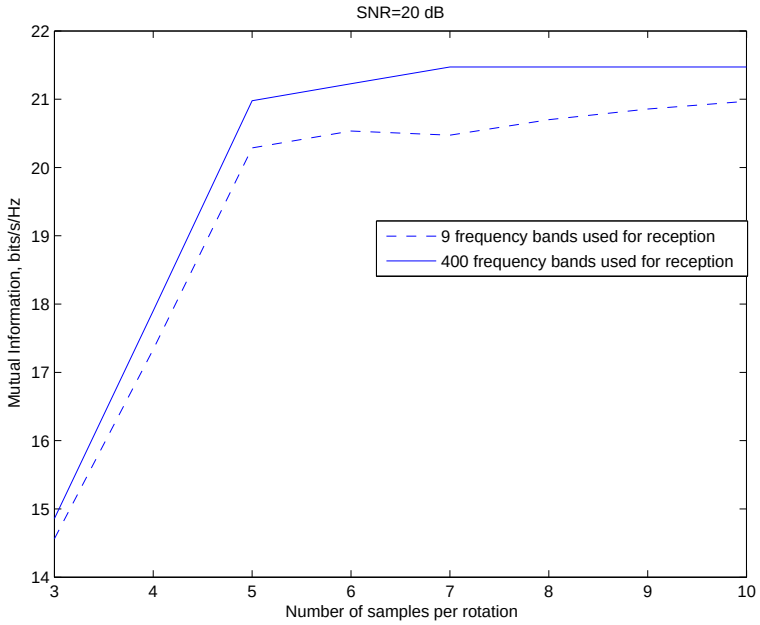

FIGURE 3.9: Capacity versus number of samples per rotation. The antenna pattern consists of 5 main Fourier components.

3.4.3 Adaptive rotation speed

The rotation of the antenna pattern expands the received signal bandwidth. The additional subbands that are created have a high chance of being occupied by other users. Therefore it would be advantageous to select a rotation speed that spreads our signal of interest into subbands that have small or ideally no interfering signals. If our antenna rotates at angular speed ω, the subbands will be spaced ω apart in frequency. If we choose n-fold rotation speed $n\omega$, then the subbands will be spaced $n\omega$ apart. The practical implementation of such an adaptive rotation scheme is simplest if $\frac{T}{T_c}$ is a prime number. The parameters T and T_c denote the symbol and sampling interval respectively. Assume that we have 7 parasitic elements distributed evenly on a circle around the active receiver antenna. This configuration gives the possibility of 3 different rotation speeds. Let us number each of the parasitic element from 1 to 7. The 3 different rotation speeds are enabled by activating the parasitics in the following order

$$\begin{array}{rl} \text{Basic speed} & 1-2-3-4-5-6-7 \\ \text{Double speed} & 1-3-5-7-2-4-6 \\ \text{Triple speed} & 1-4-7-3-6-2-5. \end{array} \tag{3.47}$$

Note that each parasitic stays short-circuited for the same duration for each of these rotation speeds. The only difference between these rotation speeds is in which order the parasitics are short-circuited. Fig. 3.10 shows the frequency domain description of the sampled antenna pattern function for a triple rotation speed. It is assumed that the activation of 1 parasitic element gives an antenna pattern with 3 Fourier components. Triple rotation speed, 3ω, gives a separation of 3ω between each Fourier component of the continuously rotating antenna. A sampling frequency of 7ω, since we are using 7 parasitic elements, yields 7ω separation in frequency between each spectral copy. As a result of the triple rotation, the received signal is mainly modulated into frequency bins $f_c - 4\omega$, $f_c - 3\omega$, f_c, $f_c + 3\omega$, $f_c + 4\omega$, where f_c is the carrier frequency.

3.5 Impact of scattering richness on performance

From regular MIMO systems we know that a high amount of scattering is necessary to achieve high multiplexing gain. It is expected that the rotating antenna system will have the same dependency on the scattering richness as a regular MIMO system. In order to investigate this we perform simulations. We calculate mutual information as a function of angular spread. An

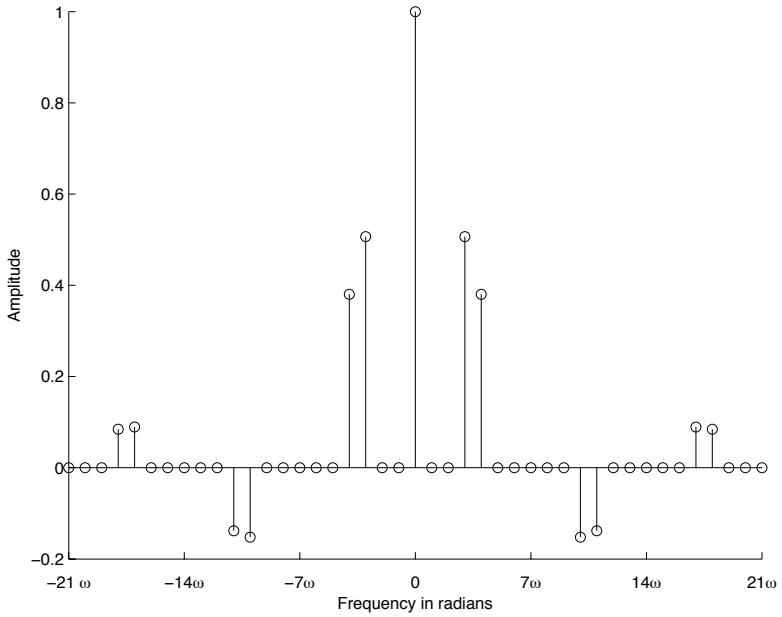

FIGURE 3.10: Sampled antenna pattern obtained by rotation frequency 3ω and sampling frequency 7ω.

angular spread of 45° means that the scatterers are uniformly distributed within an angle of 45° in the azimuth plane.

The channel noise in this section is assumed to be spatially white with uniform power distribution. The correlation between the noise from two different angular directions may be written as

$$\mathbb{E}\{n(\phi_r)n(\psi_r^*)\} = P_n(\phi_r)\delta(\phi_r - \psi_r) = \frac{\sigma_n^2}{2\pi}\delta(\phi_r - \psi_r), \qquad (3.48)$$

with $P_n(\phi_r)$ being the angular power distribution of the noise and ϕ_r and ψ_r are two different receive angles.

Fig 3.11 shows mutual information for an increasing angular spread when a total of 100 scatterers are assumed. The simulations show that the mutual information increases with increasing angular spread. When the angular spread is 360° the reactively loaded antenna achieves 21 bits/s/Hz. For an angular spread of 18 degrees the mutual information drops down to 8 bits/s/Hz, which means it drops by a factor of 2.5. Thus the rotating antenna depends on rich scattering in order to obtain high spectral efficiencies.

It should be noted that even though the angular spread is small, the average received power of the rotating antenna will be the same as the power received by a single omni-directional antenna if certain assumptions about the scatterers are satisfied. To see this, assume for simplicity that only two scatterers are present. Let these scatterers be placed in the far-field of both the transmitter and receiver. If the transmitter consists of two widely spaced antennas, mutual coupling between the transmitter antennas can be neglected, and the channel may then be represented by

$$\mathbf{H} = \begin{bmatrix} g_1 & 0 \\ 0 & g_2 \end{bmatrix} \cdot \begin{bmatrix} 1 & e^{j\frac{2\pi}{\lambda}d\cdot\cos(\phi_{t,1})} \\ 1 & e^{j\frac{2\pi}{\lambda}d\cdot\cos(\phi_{t,2})} \end{bmatrix}, \tag{3.49}$$

where g_1 and g_2 describes the attenuation and phase change of a signal that bounces off scatterer 1 and 2 respectively, $\phi_{t,1}$ and $\phi_{t,2}$ are the transmit angles, d is the antenna inter-element distance, and λ is the wavelength. It is assumed that each propagation path bounces off only a single scatterer. For the rotating antenna, the average received power of the noiseless signal in the l'th subband may be calculated in a similar way to (3.14)

$$\begin{aligned}\mathbb{E}\{|r_l(k\cdot T)|^2\} = P_T\cdot|a_l|^2\cdot\mathbb{E}\{\ |g_1|^2+|g_2|^2+\Re\{g_1g_2^*e^{jl(\phi_{r,1}-\phi_{r,2})}\} \\ +\Re\{g_1g_2^*e^{j\cdot l(\phi_{r,1}-\phi_{r,2})}e^{j\cdot\frac{2\pi}{\lambda}d(\cos(\phi_{t,1})-\cos(\phi_{t,2}))}\}\ \},\end{aligned} \tag{3.50}$$

where $\phi_{r,1}$ and $\phi_{r,2}$ are the receive angles and P_T is the average transmit power. The transmitter is assumed to transmit a spatially white signal, i.e. the covariance matrix of the transmitted signal is $P_T\cdot\mathbf{I}$. We further assume that the propagation coefficients are defined as

$$\begin{aligned} g_1 &= \frac{C}{d_1}e^{-j\frac{2\pi}{\lambda}d_1}e^{j\theta_1} \\ g_2 &= \frac{C}{d_2}e^{-j\frac{2\pi}{\lambda}d_2}e^{j\theta_2}, \end{aligned} \tag{3.51}$$

where C describes the attenuation that each scatterer introduces (same attenuation for each scatterer), d_1 and d_2 are the total distances that propagation path 1 and 2 travel, θ_1 and θ_2 are the phase changes that the scatterers introduce. Note that equation (3.51) describes the propagation according to the free space path loss model, i.e. the electric field decays as $1/d_1$ if d_1 is the distance. Let us now assume that the phases, θ_1 and θ_2, which the scatterers introduce are independent of each other and also independent of the position of the scatterers. If the phase change is uniformly distributed between 0 and 2π, the average received power becomes

$$\mathbb{E}\{|r_l(k\cdot T)|^2\} = P_T\cdot|a_l|^2\cdot\mathbb{E}\{|g_1|^2+|g_2|^2\}. \tag{3.52}$$

By summing the power from all the $2L + 1$ subbands the total received power becomes $P_T \cdot \mathbb{E}\{|g_1|^2 + |g_2|^2\}$. It may be shown that the received power for a single omni-directional antenna becomes the same under the assumptions of independent phases. Note that the received power is independent of the angular spread of the received signals, which means that even though the scatterers are confined to a small angular interval the received power becomes the same. When the antenna rotates, it listens to angular directions with both high and low energy. If the antenna rotates uniformly, which means it spends the same amount of time on each angular direction the received power will be same as for a single omni-directional antenna. However, if the rotating antenna dwells a longer time on the angular directions that has high signal power, the received power will be higher for the rotating antenna than a single omni-directional antenna. If the propagation coefficients g_1 and g_2 are correlated, then the average received power does not necessarily become equal for the rotating antenna and the omni-directional antenna.

Even though the assumption of independent phase change of the scatterers leads to the same average received power no matter how small the angular spread of the scatterers is, the singular value spread of the matrix product **AVH** is dependent on the angular spread. A low angular spread leads to a large singular value spread of the matrix product, which means that the capacity approaches the capacity achieved by a single omni-directional antenna.

3.6 Optimizing the time duration on each antenna pattern

Until now it is assumed that when the antenna rotates with discrete steps, it directs its beam towards each angular direction for the same amount of time. If the receiver has instantaneous channel knowledge it may optimize the time duration on each angular direction. For simplicity assume that the rotating antenna covers the angular space with two angular samples per rotation. The goal is to optimize the time duration on each angular direction. The analysis presented here can easily be extended to a higher number of discrete angular directions. Since the same principle holds in both cases, the simplest case is chosen in order to avoid complicated notation.

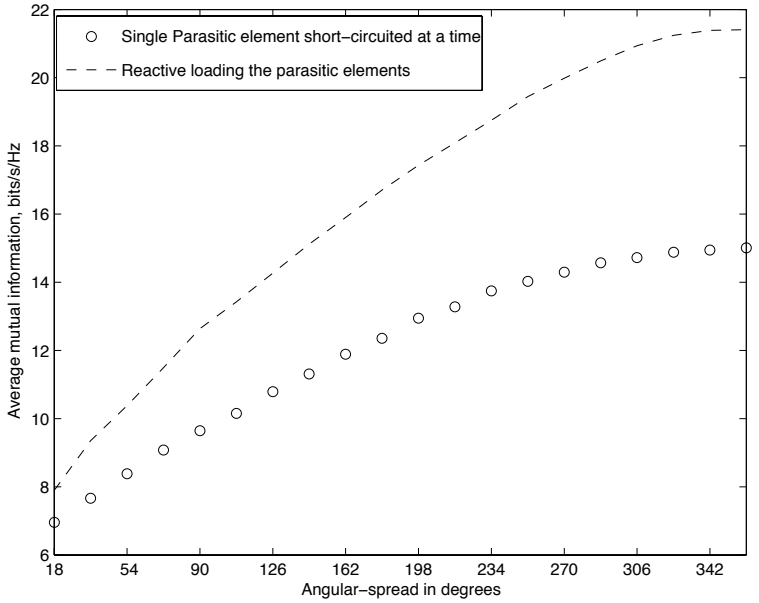

FIGURE 3.11: Mutual information as a function of scattering angular spread. The scatterers are uniformly distributed within the angle.

Let the received signal $\mathbf{r}(t)$ be defined by

$$\begin{aligned}\mathbf{r}(t) = &\sum_{n=-\infty}^{\infty} \text{rect}\left(\frac{t-nT}{\tau}\right) \cdot \sum_{p=1}^{P} a(\phi_p) s_p(t) \\ &+ \sum_{n=-\infty}^{\infty} \text{rect}\left(\frac{t-nT-\tau}{T-\tau}\right) \cdot \sum_{p=1}^{P} a(\phi_p+\theta) s_p(t) \\ &\text{for } \ 0 \geq \tau \geq T, \end{aligned} \tag{3.53}$$

where $s_p(t), \phi_p, a(\phi)$ and P are defined as in Section 2.1, θ describes how much the antenna pattern is rotated in radians, and rect() denotes the rectangular function as defined in (3.30). Note that τ and $T-\tau$ in (3.53) represent the duration of the rectangular pulses, in other words it describes how long the antenna beam points towards the two angular directions. The expression for $\mathbf{r}(t)$ may now be rewritten by taking into account that the rectangular pulse trains $\sum_{n=-\infty}^{\infty} \text{rect}\left(\frac{t-nT}{\tau}\right)$ and $\sum_{n=-\infty}^{\infty} \text{rect}\left(\frac{t-nT-\tau}{T-\tau}\right)$ can be

represented by their Fourier series expansion

$$\begin{aligned}\mathbf{r}(t) = &\sum_{l=-\infty}^{\infty} \frac{\tau}{T}\text{sinc}\left(\frac{l\cdot\tau}{T}\right) e^{j\frac{2\pi\cdot l\cdot t}{T}} \cdot \sum_{p=1}^{P} a(\phi_p)s_p(t) \\ &+ \sum_{l=-\infty}^{\infty} \frac{T-\tau}{T}\text{sinc}\left(\frac{l\cdot(T-\tau)}{T}\right) e^{j\frac{2\pi\cdot l\cdot(t-\tau)}{T}} \cdot \sum_{p=1}^{P} a(\phi_p+\theta)s_p(t) \\ &\text{for } \ 0 \geq \tau \geq T. \end{aligned} \tag{3.54}$$

By applying $\mathbf{r}(t)$ to a matched filter and by sampling the sub-band signals at rate $\frac{1}{T}$ the discrete time equivalent becomes

$$\begin{aligned}\underbrace{\begin{bmatrix} \hat{r}_{-L,k} \\ \vdots \\ \hat{r}_{0,k} \\ \vdots \\ \hat{r}_{+L,k} \end{bmatrix}}_{\hat{\mathbf{r}}_k} = &\underbrace{\begin{bmatrix} \frac{\tau}{T}\cdot\text{sinc}(\frac{-L\tau}{T}) & \frac{T-\tau}{T}\cdot\text{sinc}(\frac{-L(T-\tau)}{T})\cdot e^{-j\frac{2\pi L\cdot\tau}{T}} \\ \vdots & \vdots \\ \frac{\tau}{T} & \frac{T-\tau}{T} \\ \vdots & \vdots \\ \frac{\tau}{T}\cdot\text{sinc}(\frac{L\tau}{T}) & \frac{T-\tau}{T}\cdot\text{sinc}(\frac{L(T-\tau)}{T})\cdot e^{j\frac{2\pi L\cdot\tau}{T}} \end{bmatrix}}_{\hat{\mathbf{P}}} \\ &\cdot \underbrace{\begin{bmatrix} a(\phi_1) & \dots & a(\phi_P) \\ a(\phi_1+\theta) & \dots & a(\phi_P+\theta) \end{bmatrix}}_{\hat{\mathbf{A}}} \cdot \mathbf{H}\cdot\mathbf{b}_k + \mathbf{n}, \end{aligned} \tag{3.55}$$

with $\hat{r}_{l,k}$ being the filtered and sampled signal from the l'th sub-band at discrete time index k, $\mathbf{H}$ and $\mathbf{b}_k$ are defined the same way as in Section 3.1. The noise which is given by vector $\mathbf{n}$ is assumed to satisfy equation (3.48), which means that the noise has a uniform power distribution in the angular domain and that the noise from different angles are uncorrelated. The implication of this property of the noise is that the statistics and noise power in each subchannel become independent of how long the antenna listens towards each angular direction. Therefore, when we optimize the parameter τ, we only need to consider how the optimization affects the transmitted signal of interest.

Note that because of the rectangular pulses in (3.53) the signal frequency bandwidth goes to infinity. In the further analysis it assumed that $L \to \infty$, which means that an infinite number of sub-bands are included at the receiver. In order to find the optimum value of τ an expression for the mutual

information is needed. The mutual information $I(\hat{\mathbf{r}}_k; \mathbf{b}_k)$ is described by

$$\begin{aligned} I(\hat{\mathbf{r}}_k; \mathbf{b}_k) &= \log_2 \left(\left| \mathbf{I} + \frac{P_T}{N_0 \cdot n_t} \hat{\mathbf{P}} \hat{\mathbf{A}} \mathbf{H} \mathbf{H}^H \hat{\mathbf{A}}^H \hat{\mathbf{P}}^H \right| \right) \\ &= \log_2 \left(\left| \mathbf{I} + \frac{P_T}{N_0 \cdot n_t} \hat{\mathbf{A}} \mathbf{H} \mathbf{H}^H \hat{\mathbf{A}}^H \hat{\mathbf{P}}^H \hat{\mathbf{P}} \right| \right). \end{aligned} \tag{3.56}$$

The matrix product $\hat{\mathbf{P}}^H \hat{\mathbf{P}}$ becomes a diagonal matrix because of the orthogonal columns of matrix $\hat{\mathbf{P}}$. Each column of $\hat{\mathbf{P}}$ is the Fourier transform of a pulse train of rectangular pulses. Rectangular pulses that correspond to two different columns of $\hat{\mathbf{P}}$ are non-overlapping in the time domain and therefore orthogonal in the time domain. The Fourier transform is an orthogonal transform, which means that orthogonality in the time domain implies orthogonality in the frequency domain. The columns of $\hat{\mathbf{P}}$ are therefore orthogonal.

To simplify notation the following matrix is defined

$$\mathbf{K} = \frac{1}{n_t} \hat{\mathbf{A}} \mathbf{H} \mathbf{H}^H \hat{\mathbf{A}}^H. \tag{3.57}$$

The mutual information $I(\hat{\mathbf{r}}_k; \mathbf{b}_k)$ may now be presented as a function of parameter τ

$$I(\hat{\mathbf{r}}_k; \mathbf{b}_k) = \log \left(\left(1 + \frac{P_T}{N_0} \tau K_{11} \right) \cdot \left(1 + \frac{P_T}{N_0} (T - \tau) K_{22} \right) - \frac{P_T}{N_0} |K_{12}|^2 (T - \tau) \right), \tag{3.58}$$

where $K_{i,j}$ is the element on the i-th row and j'th column of matrix $\mathbf{K}$. The maximization of the mutual information may be performed by first defining the Lagrangian. The Lagrangian is defined by

$$\begin{aligned} &L(\tau, \lambda_1, \lambda_2) \\ &= \log \left(\left(1 + \frac{P_T}{N_0} \tau K_{11} \right) \cdot \left(1 + \frac{P_T}{N_0} (T - \tau) K_{22} \right) - \frac{P_T}{N_0} |K_{12}|^2 (T - \tau) \right) \\ &- \lambda_1 \cdot \tau + \lambda_2 \cdot (T - \tau), \end{aligned} \tag{3.59}$$

with λ_1 and λ_2 being the Lagrange multipliers. The optimal value of τ may be obtained by finding the values of τ that satisfies the Karush-Kuhn-

Tucker conditions (Boyd and Vandenberghe [2004])

$$\begin{aligned}
&\nabla_\tau L(\tau, \lambda_1, \lambda_2) + \lambda_1 - \lambda_2 = 0 \\
&\tau \geq 0 \\
&T - \tau \geq 0 \\
&\lambda_1 \geq 0 \\
&\lambda_2 \geq 0 \\
&\lambda_1 \tau = 0 \\
&\lambda_2 \tau = 0.
\end{aligned} \tag{3.60}$$

The mutual information $I(\hat{\mathbf{r}}_k; \mathbf{b}_k)$ is a concave function of the variable τ and hence the solution which is found by solving (3.60) gives the global maximum. The proof of the concavity of $I(\hat{\mathbf{r}}_k; \mathbf{b}_k)$ as a function of τ is given in Appendix B.

In order to analyze the capacity achievements obtained by doing the optimization on the dwell time on each angular direction, we perform simulations. The antenna pattern shown in Fig. 3.12, which is obtained by reactively loading the parasitic elements, is used in the simulations, and it is assumed that the antenna pattern may point towards 6 different angular directions (6 parasitic elements). The capacity calculations are performed for three different channel models. The first channel model assumes that scatterers are uniformly distributed between 0 and 2π in the angular domain. The second channel model assumes the scatterers are uniformly distributed between 0 and π. The third channel model assumes that the scatterers are placed within two clusters. Each cluster has an angular spread equal to $\pi/8$, and the mid-angle of each cluster are uniformly distributed between 0 and 2π. The capacity is compared against the capacity when the antenna pattern stays the same amount of time on each angular direction, and also compared against the capacity of a single omni-directional antenna. The number of transmitter antennas and scatterers are set to 10 and 100 respectively. The capacities plotted in Fig. 3.12 and 3.14 show that the optimization is mostly useful when the scatterers are not uniformly distributed between 0 and 2π in the angular domain. For the last two channel models there is obviously a capacity gain by performing the optimization. It might seem a bit surprising that the capacity of the mentioned two channel models are higher than the rich scattering channel model for low SNR. In that case, it should be mentioned that the SNR refers to the SNR experienced by a single omni-directional antenna. When the channel model is clustered and the SNR is low, it is optimal to direct the antenna beam towards these clusters. The effect of this is that the received SNR obtained by

the beam-forming scheme actually is higher than the SNR achieved by the single omni-directional antenna.

When the scatterers are uniformly distributed between 0 and 2π, there seems to be a small gain in capacity for the low SNR-region by doing the optimization. This can be explained by the fact that we are using a finite number of scatterers. The empirical distribution of the scatterers for each channel realization will in that case not be exactly equal to the uniform distribution. If we assume a higher number of scatterers, the empirical distribution will approach the uniform distribution. For an infinite number of scatterers, the optimum solution will be a uniform antenna rotation, i.e. to dwell the same amount of time on each angular direction.

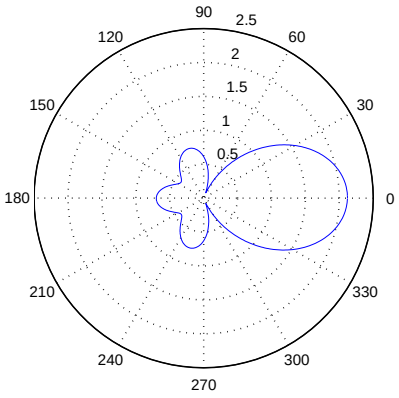

FIGURE 3.12: Antenna pattern obtained by reactively loading 6 parasitic antenna elements. The parasitic elements are placed uniformly on a circle, with radius $\lambda/8$, around the active element.

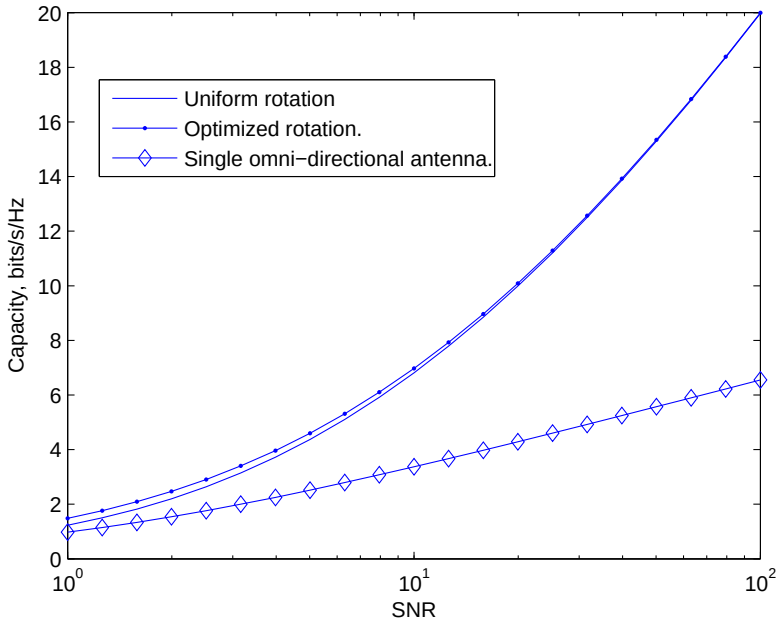

FIGURE 3.13: Capacity for a rich scattering channel. Scatterers are uniformly distributed between 0 and 2π in the angular domain.

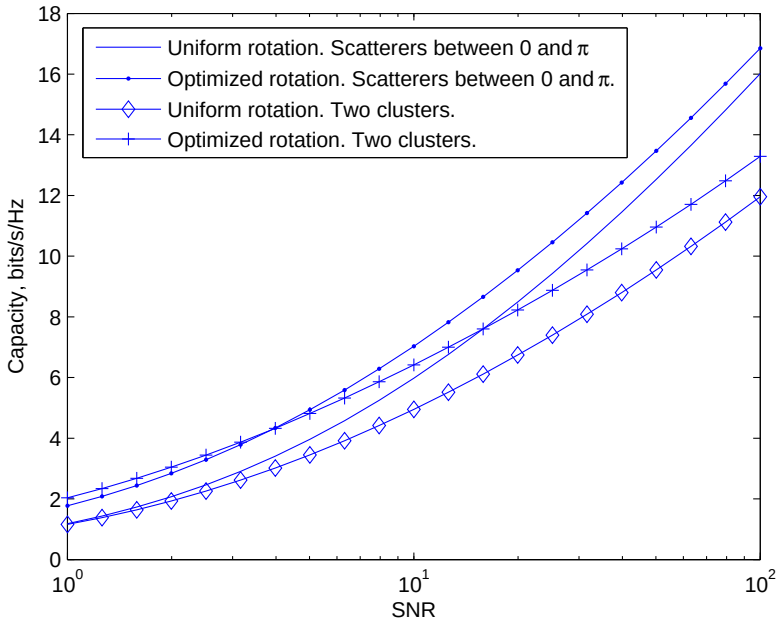

FIGURE 3.14: Capacity for two different channel models.

Chapter 4

Antenna efficiency, broadband properties and transient effects of the rotating antenna

The focus of this thesis is not on the detailed practical implementation of the rotating antenna. There are however multiple issues to consider when implementing the rotating antenna. Some of these issues will be discussed in the following sections.

4.1 Antenna matching

Each of the antenna configurations presented until now represents widely different antenna impedances. For the practical implementation, the antenna impedance is of high importance, since it determines the amount of power that the antenna may extract from the electromagnetic field. For maximum power reception the antenna impedance and antenna termination impedance should be the complex conjugate of each other, i.e.

$$Z_L = Z^* \tag{4.1}$$

should hold for maximum power reception. Impedance Z_L is the antenna termination impedance and Z is the antenna impedance. If the load impedance Z_L is very far from Z^* a matching network may be necessary to prevent mismatch effects. Mismatch effects are usually standing wave patterns along the transmission line that connects the antenna and the termination impedance.

Until now it has been argued that the antenna efficiency is not important since the main noise source is channel noise and/or adjacent channel

d	$\lambda/64$	$\lambda/32$	$\lambda/16$	$\lambda/8$
Z	$.54 + j10.3$	$2.5 + j23.3$	$10.4 + j46.6$	$38.4 + j77.9$
$\|\Gamma\|$	0.9795	0.9211	0.8016	0.6684
d	$\lambda/4$	$\lambda/2$	∞	
Z	$96.1 + j76.1$	$85.3 + j30.5$	$79.6 + j44.1$	
$\|\Gamma\|$	0.5401	0.3364	0.3880	

TABLE 4.1: The antenna impedance Z and reflection coefficient Γ for different distances d between the active and the parasitic antenna element.

interference. Thus, a low antenna efficiency implies that the antenna receives a lower amount of both the desired signal power and noise/interference power. The signal-to-noise-interference ratio (SINR) is therefore roughly independent of the antenna efficiency. This is true only to a certain extent. If the antenna efficiency is very low, other noise sources may be become relevant as well. The thermal noise of the amplifier may in that situation contribute to the total noise.

Antenna impedances will now be computed for some of the antenna configurations presented earlier. The purpose is to give some sort of intuitive feeling on the practical implementability of these antenna configurations. The standard receiver termination used in the industry is 50Ω, where Ω represents the unit of impedance. Therefore, the further the antenna impedance is from 50Ω the more difficult it becomes to match the antenna. Table 4.1 shows the antenna impedance and the reflection coefficient for an antenna consisting of a single active and a short-circuited parasitic element. The reflection coefficient is calculated for the case when no matching circuit is present. The reflection coefficient ,Γ, is found by the following formula (Pozar [1998], Section 2.3)

$$\Gamma = \frac{Z_L - Z}{Z_L + Z}, \tag{4.2}$$

where Z is the antenna impedance seen at the input terminal of the active antenna.

When the dominant noise source is amplifier noise and not channel noise, the received signal power becomes of high interest. Equations will now be given that express the average power received by the active antenna when a parasitic element is placed close to the active element. The open-circuit voltages $v_{oc,1}$ and $v_{oc,2}$ represent the voltages or the field values that would be present if the antennas were not terminated. The open-circuit voltages therefore represent the electric field values at the antenna

positions before mutual-coupling is taken into consideration. The equation that expresses the currents on the antennas as a function of the mutual coupling parameters and the open circuit voltages is given by

$$\begin{aligned} v_{oc,1} &= (Z_{11} + Z_L) \cdot i_1 + Z_{12} \cdot i_2 \\ v_{oc,2} &= Z_{12} \cdot i_1 + Z_{11} \cdot i_2, \end{aligned} \tag{4.3}$$

where Z_{11}, Z_{12}, i_1 and i_2 are defined as in (2.10), and Z_L is the termination impedance of the active antenna element. By using the fact that the average power received by the active antenna element is given by $P_R = \mathbb{E}\{Z_L \cdot |i_1|^2\}$, the average received power may be expressed as

$$P_R = Z_L \cdot \frac{\mathbb{E}\{|v_{oc,1}|^2\}|Z_{11}|^2 - 2 \cdot \Re\{Z_{12}^* Z_{11}\} \cdot J_0(k \cdot d) + \mathbb{E}\{|v_{oc,2}|^2\}|Z_{12}|^2}{|Z_{11}|^2 \cdot |Z_{11} + Z_L|^2 - 2 \cdot \Re\{Z_{12}^2 Z_{11}^* (Z_{11}^* + Z_L^*)\} + |Z_{12}|^4}, \tag{4.4}$$

where $J_0(k \cdot d)$ is the Bessel function of first kind and zero order as in (2.11). In the derivation of (4.4) it has been assumed that the correlation between the open-circuit voltages $v_{oc,1}$ and $v_{oc,2}$ is given by $\mathbb{E}\{v_{oc,1} v_{oc,2}^*\} = J_0(k \cdot d)$. This assumption is reasonable for a rich scattering environment for which the angles of arrivals are uniformly distributed (Jakes [1974]).

The power received by an active antenna element with a parasitic element close by ($\lambda/16$ antenna spacing) will now be compared with the power received by a single antenna. Assume that in both cases the active antennas are terminated with $Z_L = 50\Omega$. By calculating the power in both cases we come to the conclusion that the power received by the single antenna is 3 dB higher than the power received by the active antenna with a parasitic close by. This is mainly due to a larger impedance mismatch for the two antenna case. That there is a larger impedance mismatch for the two antenna case can be seen from table 4.1. Note that the single antenna case is equivalent to two antennas with infinite separation. Assume now that both the active antenna for the two antenna case and the single antenna are perfectly impedance matched. The power received by both antennas will in this case be the same. In practise the matching of the active element with the parasitic element close by becomes harder than the matching of the single antenna. It is therefore expected that some powerloss will be introduced by the inclusion of the matching network.

4.2 Broadband properties

Most of the analysis in this thesis is done based on a narrow-band analysis. The capacity is mostly evaluated at a unit bandwidth around the carrier fre-

quency. A wideband analysis was however made in Section 2.4.3 where the antenna patterns were calculated over different frequencies. The capacity was then found by assuming perfect impedance match at all frequencies. This assumption is probably not realistic. A quantity that is closely related to the bandwidth of an antenna array is the quality factor, Q. The inverse of the quality factor is approximately equal to the fractional bandwidth of the antenna system. The relationship between the quality factor and the fractional bandwidth is given by (Pozar [1998], Section 6.1)

$$\frac{1}{Q} \approx \frac{\Delta f}{f_c}, \tag{4.5}$$

where Δf is the bandwidth and f_c is the center frequency. The quality factor can be decomposed into two terms, $Q = Q_t \cdot Q_e$, where Q_t is the quality factor of the antenna array and Q_e is the quality factor of the antenna elements when they are in isolation Uzsoky and Solymar [1956]. Due to the reciprocity theorem, the quality factor in transmit mode and receive mode will be the same. Hence we may assume that the array is in transmit mode.

According to Morris, Jensen, and Wallace [2005], the quality factor of the antenna array is given by

$$Q_t = \frac{\mathbf{i}^H \mathbf{i}}{\mathbf{i}^H \mathbf{A}_t \mathbf{i}}, \tag{4.6}$$

where $\mathbf{i}$ is the antenna current vector, and $\mathbf{A}_t$ is defined by

$$\mathbf{A}_t = 1/C \cdot \int_{\Omega_t} \mathbf{E}_t(\Omega_t)^H \mathbf{E}_t(\Omega_t) d\Omega_t. \tag{4.7}$$

Matrix $\mathbf{E}_t(\Omega_t)$ consists of the electric field values at transmit solid angle Ω_t. The constant C is used for normalizing matrix $\mathbf{A}_t$ such that it has unit entries along the diagonal. The electric field matrix is given by

$$\mathbf{E}_t(\Omega_t) = \begin{bmatrix} e_\theta^1(\Omega_t) & .... & e_\theta^{n_t}(\Omega_t) \\ e_\phi^1(\Omega_t) & .... & e_\phi^{n_t}(\Omega_t) \end{bmatrix}, \tag{4.8}$$

where $e_\theta^1(\Omega_t)$ and $e_\phi^1(\Omega_t)$ are the two orthogonal electric far field components due to antenna element 1. Note that the far field consists of only two orthogonal components. These components are also orthogonal to the propagation direction.

For an antenna array the currents on the antenna are given by

$$\mathbf{i} = (\mathbf{Z} + \mathbf{Z}_L)^{-1} \cdot \mathbf{v}_T, \tag{4.9}$$

d	$\lambda/64$	$\lambda/32$	$\lambda/16$	$\lambda/8$	$\lambda/4$
Q_t	21.7	13.6	5.6	2.1	1.1
$\frac{\Delta f}{f_c}$	$4.6 \cdot 10^{-3}$	$7.3 \cdot 10^{-3}$	$1.8 \cdot 10^{-2}$	$4.7 \cdot 10^{-2}$	$9.3 \cdot 10^{-2}$

TABLE 4.2: Quality factor Q_t and fractional bandwidth $\frac{\Delta f}{f_c}$ computed for various inter-element distances d between the active and parasitic antenna element. An quality factor $Q_e = 10$ of the individual antenna elements is assumed in the calculations.

where $\mathbf{Z}$ is the impedance matrix containing the mutual coupling parameters, $\mathbf{Z}_L$ is a diagonal matrix with the termination of the antenna elements on the diagonal, and $\mathbf{v_T}$ is the voltage excitation vector. If only one active antenna is present the vector $\mathbf{v_T}$ consists only of one non-zero element.

By plugging (4.9) into (4.6) the quality factor Q_t may be computed for various antenna configurations. The quality factor and an estimation of the fractional bandwidth for a few antenna configurations are given in table 4.2. An inter-element distance $\lambda/64$ between the active and the parasitic element leads to $Q_t = 21$, which means that the fractional bandwidth is less than the bandwidth of an antenna in isolation by a factor of 21.

4.3 Transient effects of the rotating antenna

The antenna patterns that we have considered are steady state antenna patterns. If a sinusoid at a single frequency is applied to antenna array there will be a certain transient period before the steady state antenna pattern occurs. To get the picture of how large this transient period is, simulations are performed. The Finite-Difference-Time-Domain (FDTD) method (Taflove [1995]) is used to calculate the electric field in the time domain.

The simulation scenario is as follows: Two antenna elements, one active antenna and one parasitic element, are placed next to each other with an inter-element distance $\lambda/8$. The parasitic element has a switch in the middle of the element which may be open or closed. The time change of the electric field at a point in space when the antenna array is in transmission mode is shown in Fig. 4.1. Is seems that steady state of the electric field is reached 7-8 periods after a switching operation of the parasitic element has occured. When more parasitic elements are involved the transient period is expected to be even longer.

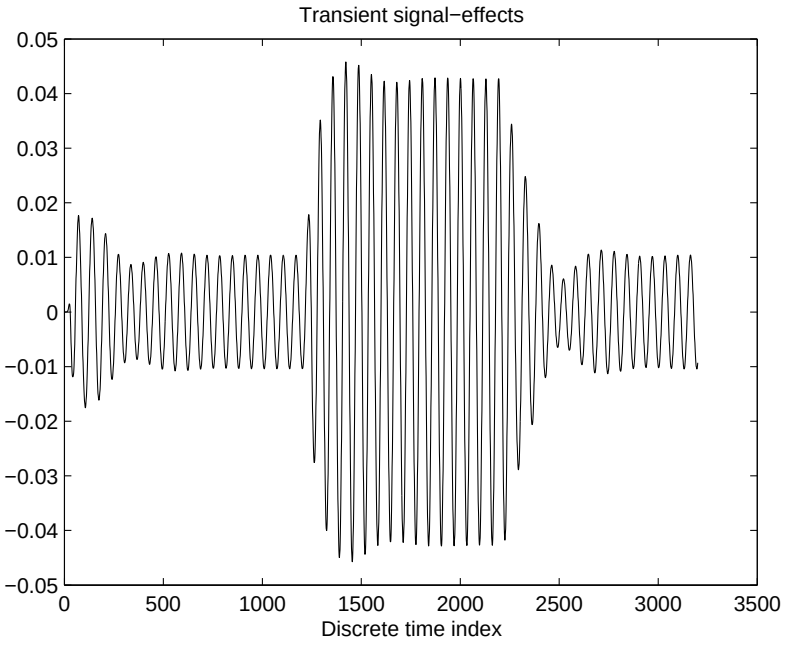

FIGURE 4.1: The transient effect of the electric field when a parasitic element switches between an open- and short-circuit state. The antennas have an inter-element distance $\lambda/8$.

Chapter 5

Comparing the rotating antenna with active antenna elements

So far the capacity of the rotating antenna has been compared with the performance of a single receive antenna. Since the rotating antenna requires a larger space than a single receive antenna, the comparison can be considered to be somewhat unfair. This chapter aims at analyzing the performance of a standard array of active dipole antennas in order to give a more fair comparison.

5.1 Performance of active dipoles antennas when channel noise and co-channel interference are the dominant signal impairments

It has been demonstrated in chapter 3 that the rotating antenna performs best when operating in unlicensed frequency bands. Let us assume that a standard array of active dipole antennas operates in the same environment. Since co-channel interference and channel noise are present, it is likely that the power levels of these two noise sources are much higher than the amplifier noise level. Assume for the present analysis that the combined co-channel interference and channel noise are described as AWGN, and assume that the amplifier noise is zero. In this section the equations are presented in a circuit analysis manner. Let the voltages at the receiver

terminations be described by

$$\mathbf{v}_R = \mathbf{Z}_{L,R} \cdot (\mathbf{Z}_R + \mathbf{Z}_{L,R})^{-1} \mathbf{H} \cdot (\mathbf{Z}_T + \mathbf{Z}_{L,T})^{-1} \cdot \mathbf{v}_T + \mathbf{Z}_{L,R} \cdot (\mathbf{Z}_R + \mathbf{Z}_{L,R})^{-1} \mathbf{n}, \tag{5.1}$$

where $\mathbf{v}_R$ represents the voltages at the receiver terminations, $\mathbf{Z}_{L,R}$ and $\mathbf{Z}_{L,T}$ are the termination impedances at the receiver and transmitter respectively, $\mathbf{Z}_R$ and $\mathbf{Z}_T$ are the mutual coupling matrices of the receiver and transmitter, $\mathbf{v}_T$ represents the voltages from the source generators at the transmitter, $\mathbf{H}$ describes the propagation for the currents on the transmit antennas to the open-circuit voltages at the receive antenna connectors and $\mathbf{n}$ represents the co-channel interference/channel-noise open-circuit voltage. Assume for the time being that the antennas are lossless which means they have zero resistance. Let us define the open circuit voltage $\mathbf{v}_{oc,R}$ at the receive antenna connectors as

$$\mathbf{v}_{oc,R} = \mathbf{H} \cdot (\mathbf{Z}_T + \mathbf{Z}_{L,T})^{-1} \cdot \mathbf{v}_T + \mathbf{n}. \tag{5.2}$$

Note that according to the data processing inequality (Cover and Thomas [1991], Section 2.8) the following property holds for mutual information

$$I(\mathbf{v}_{oc,R}; \mathbf{v}_T) = I(\mathbf{v}_R; \mathbf{v}_T) \tag{5.3}$$

as long as the linear transformation $\mathbf{Z}_{L,R} \cdot (\mathbf{Z}_R + \mathbf{Z}_{L,R})^{-1}$ is full rank. The consequence of this is that the mutual coupling does not have an impact on the channel capacity as long as the channel noise is the only noise source. This result is realized by many researchers (Gans [2006a]; Bikhazi and Jensen [2007]; Wallace and Jensen [2004a]). It is therefore sufficient to analyze the open-circuit voltages in our search for the capacity. For two closely spaced dipole antennas both the open-circuit signal and noise voltages are expected to be correlated. Let $P_n(\phi)$ denote the power distribution of the noise in the azimuth angular domain. Assume that noise from different angles, $n(\psi)$ and $n(\phi)$, are uncorrelated. In other words

$$\mathbb{E}\{n(\psi) n^*(\phi)\} = P_n(\phi) \delta(\psi - \phi). \tag{5.4}$$

The open circuit noise voltages, n_1 and n_2, at the two antenna connectors may be described by

$$\begin{aligned} n_1 &= \int_0^{2\pi} a_1(\phi) n(\phi) d\phi \\ n_2 &= \int_0^{2\pi} a_2(\phi) n(\phi) d\phi, \end{aligned} \tag{5.5}$$

where $a_1(\phi)$ and $a_2(\phi)$ are the element antenna patterns of the two dipole antennas when mutual coupling is neglected. Mutual coupling is neglected since we are considering the open-circuit noise voltages. The correlation between n_1 and n_2 may now be computed, and is given by

$$\mathbb{E}\{n_1 n_2^*\} = \int_0^{2\pi}\int_0^{2\pi} \mathbb{E}\{n(\phi)n^*(\psi)\}a_1(\phi)a_2^*(\psi)d\phi d\psi \tag{5.6}$$

$$= \int_0^{2\pi} P_n(\phi)a_1(\phi)a_2^*(\phi)d\phi. \tag{5.7}$$

By assuming uniform noise power distribution, i.e. $P_n(\phi) = \frac{1}{2\pi}\sigma_n^2$, and by assuming that one of the dipole antennas is placed at the center of the coordinate system along the z-axis, the correlation may be further expressed as

$$\mathbb{E}\{n_1 n_2^*\} = \frac{1}{2\pi}\int_0^{2\pi} \sigma_n^2 e^{j\frac{2\pi}{\lambda}d\cos(\phi)}d\phi = \sigma_n^2 \cdot \mathrm{J}_0(k \cdot d). \tag{5.8}$$

where $a_1(\phi) = 1$ and $a_2(\phi) = e^{-j\frac{2\pi}{\lambda}d\cos(\phi)}$ are the element antenna patterns when mutual coupling is neglected, d is the antenna inter-element distance, λ is the wave-length and $J_0()$ is the zeroth order Bessel function of the first kind. Equation (5.8) shows that by decreasing the antenna element distance the correlation between the open-circuit noise voltages increases. The same behaviour is also expected of the signal correlation matrix $\mathbf{K}_{v_{oc}}$ which is defined as

$$\mathbf{K}_{v_{oc}} = \mathbb{E}\{\mathbf{v}_{oc,R}\mathbf{v}_{oc,R}^H\}. \tag{5.9}$$

The noise correlation matrix is defined the same way

$$\mathbf{K}_n = \mathbb{E}\{\mathbf{n}\mathbf{n}^H\}. \tag{5.10}$$

It is now possible to find the expression for the mutual information between $\mathbf{v}_{oc,R}$ and $\mathbf{v}_T$. The mutual information is given by

$$I(\mathbf{v}_{oc,R};\mathbf{v}_T) = \log(|\mathbf{I} + \mathbf{K}_n^{-1}\mathbf{H}\cdot(\mathbf{Z}_T + \mathbf{Z}_{L,T})^{-1}\mathbf{K}_{v_T}(\mathbf{Z}_T + \mathbf{Z}_{L,T})^{-1,H}\mathbf{H}^H|)$$

$$= \log(|\mathbf{I} + \mathbf{K}_n^{-1}\mathbf{K}_{v_{oc}}|), \tag{5.11}$$

where $\mathbf{K}_{v_T}$ is the correlation matrix of the transmit signal. A quite surprising result is that the product $\mathbf{K}_n^{-1}\mathbf{K}_{v_{oc}}$ is approximately independent of the antenna spacing for a rich scattering channel. Decreasing the antenna spacing increases the correlation for both the signal and noise, but since the correlations increase in the same manner the capacity stays the

same. This was realized also by (Gans [2006a]), where it is stated that for a full 3-dimensional rich scattering channel the capacity is independent of the antenna element spacing. The spatial multiplexing gain for two dipole receive antennas becomes therefore equal to 2 no matter how small the antenna spacing is.

There is one effect that has been ignored until now. The antennas usually have some resistance, which means that the currents that run on these antennas generate thermal noise. The thermal noise on the two antennas will be independent from each other. The thermal noise will lead to a higher total noise power, but the most detrimental effect is the decorrelation of the noise. Consider the following simple case

$$\mathbf{K}_{\mathbf{v}_{\mathbf{oc}}} = \text{SNR} \cdot \mathbf{K}_n = \text{SNR} \cdot \begin{bmatrix} 1 & .96 \\ .96 & 1 \end{bmatrix}. \tag{5.12}$$

This noise correlation matrix is obtained if the correlation is calculated according to (5.8) and the antenna inter-element distance is set to $\lambda/16$. The signal correlation matrix $\mathbf{K}_{\mathbf{v}_{\mathbf{oc}}} = \text{SNR} \cdot \mathbf{K}_n$ may be obtained in a rich scattering channel. The capacity when we have SNR $= 20\ dB$ becomes 13.32 bits/s/Hz. If we add thermal noise with variance 0.1, but rescale such that the total SNR stays the same, we get the following noise correlation matrix

$$\mathbf{K}_n = \begin{bmatrix} 1 & .87 \\ .87 & 1 \end{bmatrix}. \tag{5.13}$$

The capacity in this case becomes 11.74 bits/s/Hz, which means that the capacity decreases by 1.57 bits/s/Hz due the decorrelation of the noise.

It is now appropriate to evaluate the capacity of the active antenna elements by simulations and compare with the rotating antenna. Assume a total of 7 antenna elements. Let 1 antenna element be placed at the center and let the 6 remaining elements be placed on a circle around the center antenna element. The radius of the circle is chosen to be equal to $\lambda/8$. It is now of interest to calculate the capacity when all antenna elements are active elements. The rotating antenna may be implemented with the same antenna elements but by letting the center element be an active element and the rest of the antennas parasitic elements. The parasitic elements are reactively loaded as in Section 2.3. The capacity is plotted in Fig. 5.1 as a function of SNR. When all antenna elements are active elements the capacity is calculated both by assuming correlated noise and uncorrelated noise. The correlated noise is obtained by assuming channel noise and the noise correlation is calculated in a similar manner to equation (5.8). The uncorrelated noise is included just for comparison. The capacity plot basically

shows that the rotating antenna cannot achieve as high capacity as the active antenna elements.

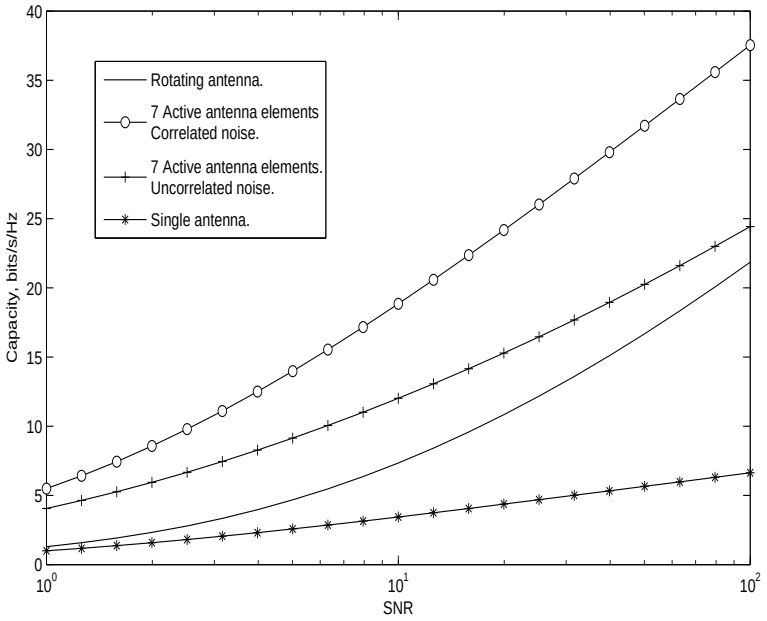

FIGURE 5.1: Capacity as a fuction of SNR. The active antenna elements and the rotating antenna occupy the same volume.

Part II

Parasitic Elements for Implementing the Transmitter

Chapter 6

Introduction

In part I of the thesis parasitic elements are used at a mobile receiver terminal for implementing rotating antenna patterns. It should be noted that the idea of the rotating antenna pattern could also be implemented at the base-station. But the goal of the rotating antenna is to achieve a compact antenna solution, and therefore the main commercial interest would be to implement it in small handheld terminals. Apart from the fact that the antenna solution is compact it should also offer some of the capacity gains which is achieved by $\lambda/2$ spaced MIMO antennas. It is assumed in Part I of the thesis that the transmitting unit is a base-station with widely spaced antennas. To some extent one can argue that the down-link capacity is more important for a mobile unit than the up-link capacity. For that case, when the mobile unit transmits to the base-station, an omni-directional antenna pattern from a single antenna might be used. The omni-directional antenna pattern is achieved by letting the parasitic elements be open-circuited. Note that an omni-directional pattern when transmitting and rotating antenna pattern when receiving cannot be achieved simultaneously. Therefore, a terminal that implements this scheme will be constrained to time division duplex communication.

The main goal of the second part of the thesis is to analyze a scheme for increasing the up-link capacity. Kalis *et al.* [2006]; Kalis, Papadias, and Kanatas [2007] have found a way of increasing the capacity of the up-link by the usage of parasitic elements. Kalis and Carras [2005] show that the entropy of a signal transmitted from an antenna array consists of two components. One component is due to the uncertainty of which antenna pattern is used, the other component is due to the uncertainty of which symbol is transmitted with the corresponding antenna pattern. It was further showed that this new way of representing information may be imple-

mented by the usage of a single active antenna and multiple parasitic antenna elements. Note, however, that the idea of using parasitic elements for creating multiple antenna patterns is not new. Several references proposed using parasitic elements for diversity (Vaughan [1999]), beam-forming (Schaer *et al.* [2005]; Sun, Hirata, and Karmakar [2004]), basestation tracking and direction of arrival estimation (Preston, Thiel, Smith, O'Keefe, and Lu [1998]; Sun and Karmakar [2004]). But it seems that no one, except Kalis, has considered using the parasitic elements for achieving a spatial multiplexing gain.

The work in this part of the thesis builds on the research done by Kalis. The contribution of the second part of the thesis is as follows:

- The ergodic capacity is analyzed for a two element array consisting of one parasitic element and one active antenna. The Arimoto-Blahut algorithm is used for finding the capacity achieving distribution. Previous research has only considered 3 and 5 element antenna arrays with one active antenna element and two and four parasitic elements respectively, and the capacity achieving distribution has not been found.

- The spectral efficiency is calculated, by assuming a uniform distribution on the signal points, for a 2 and 3 element antenna array. The spectral efficiency obtained by a 3 element antenna array is calculated for a rich scattering channel only. For the 2 element antenna array, the spectral efficiency is evaluated for both a rich scattering channel and clustered channel. The performance is compared against traditional antenna arrays and beamforming schemes.

- The performance is evaluated for schemes that use a high number of signal points.

- The antenna patterns and symbols are designed by minimizing the maximum pairwise error probability.

6.1 Power constraint considerations

An important result was found by Morris *et al.* [2005], which showed that using the average radiated power as a constraint gives different capacities than the traditional power constraint. This result explains why relatively high capacity gains can be made with compact antennas. The traditional

power constraint is that the following should hold

$$\mathbb{E}\left\{\text{tr}\left(\mathbf{i}\mathbf{i}^H\right)\right\} \leq P_T, \tag{6.1}$$

where the components of $\mathbf{i}$ are the currents on the antennas, and P_T is the power constraint. Equation (6.1) does not represent the average power radiated. The accuracy of this expression, as radiated power, becomes less with decreasing antenna spacing. The power of an electromagnetic wave is described by Poyinting vector, defined as (Balanis [1997], Section 2.3)

$$\mathbf{W} = \mathbf{H} \times \mathbf{E}, \tag{6.2}$$

where $\mathbf{W}$ is the complex power vector, $\mathbf{H}$ is the vector of the instaneous magnetic field intensity and $\mathbf{E}$ is the vector of the instaneous electric field intensity. The time averaged Poyinting vector can be written as

$$\mathbf{W}(x,y,z) = \frac{1}{2}\Re(\mathbf{H} \times \mathbf{E}), \tag{6.3}$$

where x, y and z are the rectangular position coordinates in space, and $\Re()$ is an operator that takes the real part of a variable. The radiated power is obtained by integrating $\mathbf{W}(x,y,z)$ over a sphere. Since in this thesis transmission is only evaluated in the azimuth plane, $\mathbf{W}(x,y,z)$ is only integrated in the two dimensional azimuth plane. This is the same as integrating the antenna pattern in the azimuth plane. An expression for the radiated power is derived in Appendix A. For a two element antenna array the transmitted power becomes

$$C \cdot \left(|i_1|^2 + |i_2|^2 + 2 \cdot \mathrm{J}_0(k \cdot d) \cdot \Re(i_1 i_2^*)\right), \tag{6.4}$$

where C is a constant which is derived in Appendix A, i_1 and i_2 are the currents on the two antennas, $\mathrm{J}_0()$ is the Bessel function of first kind and zero order, $k = 2\pi/\lambda$ is the wave-number, and d is inter-element distance. The term $2 \cdot \mathrm{J}_0(k \cdot d) \cdot \Re(i_1 i_2^*)$ represents either constructive or descructive interference between the fields radiating from the two antennas. Note that the electric field and magnetic field follows the super-position principle. The field from each of the antennas add together. How they add is dependent on the phase of the current on each of the antennas, i.e. it is controlled by the term $\Re(i_1 i_2^*)$. The distance between the antenna elements comes into play by the Bessel-function, $\mathrm{J}_0(k \cdot d)$. This term determines how strong the interference between the two fields are. The closer the antennas are, the larger $|\mathrm{J}_0(k \cdot d)|$ becomes. Note also that for very small antenna distances

$J_0(k \cdot d) \approx 1$. The implication of this is that currents i_1 and i_2 with 180 degrees phase shift relative to each other result in very low radiated power, since the fields from the antennas cancel out.

It should be noted, that $J_0(k \cdot d)$ also represents the correlation of the open-circuit voltages when the antennas are in receive mode, in some cases. The open circuit voltages are the voltages that are present at the antenna connectors when the antennas are not terminated. This correlation expression does therefore not take into consideration the mutual coupling between the antennas. Teal, Abhayapala, and Kennedy [2002] have shown that $J_0(k \cdot d)$ expresses the open circuit correlation for a two-dimensional omni-directional diffuse field.

The effect that the radiated power constraint has on capacity can most easily be seen by evaluating the singular value spread of the equivalent channel matrix. For a MIMO system the received signal $\mathbf{y}$ can be expressed as

$$\mathbf{y} = \mathbf{H} \cdot \mathbf{i} + \mathbf{n}, \tag{6.5}$$

where $\mathbf{H}$ is the channel matrix, $\mathbf{i}$ is the antenna current vector and $\mathbf{n}$ is the AWGN. The radiated power P_T can be expressed as

$$P_T = \mathbf{i}^H \mathbf{A_t} \mathbf{i}, \tag{6.6}$$

where $\mathbf{A_t}$ is defined as

$$\mathbf{A_t} = \begin{bmatrix} 1 & J_0(k \cdot d) \\ J_0(k \cdot d) & 1 \end{bmatrix}. \tag{6.7}$$

Note that matrix $\mathbf{A_t}$ is equivalent to matrix $\mathbf{A_t}$ in (4.7). Proceeding in a similar way as Morris *et al.* [2005], equation (6.5) may be rewritten

$$\mathbf{y} = \mathbf{H} \cdot \mathbf{A_t}^{-1/2} \mathbf{A_t}^{1/2} \mathbf{i} + \mathbf{n} = \hat{\mathbf{H}} \hat{\mathbf{i}} + \mathbf{n}, \tag{6.8}$$

where $\hat{\mathbf{H}} = \mathbf{H} \cdot \mathbf{A_t}^{-1/2}$ and $\hat{\mathbf{i}} = \mathbf{A_t}^{1/2} \cdot \mathbf{i}$. The radiated power P_T can be expressed as

$$P_T = \hat{\mathbf{i}}^H \hat{\mathbf{i}}. \tag{6.9}$$

The singular value spread of the channel matrix $\mathbf{H}$ is usually large when the inter-element distance between the antennas is small. The consequence of this is low capacity. However, because of the decorrelating effect of matrix $\mathbf{A_t}^{-1/2}$, the singular value spread of matrix $\hat{\mathbf{H}}$ is much smaller.

Note that two orthogonal current vectors $\mathbf{i_1}$ and $\mathbf{i_2}$ do not necessarily represent orthogonal antenna patterns. However, two orthogonal vectors

$\hat{\mathbf{i}}_1$ and $\hat{\mathbf{i}}_2$ do correspond to current vectors that again represent orthogonal antenna patterns. The current vectors may be found from the relationship $\mathbf{i} = \mathbf{A}_t^{-1/2} \cdot \hat{\mathbf{i}}$. The matrix $\mathbf{A}_t^{-1/2}$, which is a Hermitian positive definite matrix, may be eigenvalue decomposed

$$\mathbf{A}_t^{-1/2} = \mathbf{U}\Sigma\mathbf{U}^H, \tag{6.10}$$

where $\mathbf{U}$ is the eigenvector matrix and Σ is the singular-value matrix. Setting $\hat{\mathbf{i}}_1 = \mathbf{u}_1$ and $\hat{\mathbf{i}}_2 = \mathbf{u}_2$, with $\mathbf{u}_1$ and $\mathbf{u}_2$ being the columns of $\mathbf{U}$, leads to currents $\mathbf{i_1} = \sigma_1 \cdot \mathbf{u}_1$ and $\mathbf{i_2} = \sigma_2 \cdot \mathbf{u}_2$, where σ_1 and σ_2 are the singular values. The sigular values represent the scaling which is needed in order for the vectors $\hat{\mathbf{i}}_1$ and $\hat{\mathbf{i}}_2$ to have unit norm. As an example, consider an antenna array with inter-element distance $\lambda/16$. Then the singular values become $\sigma_1 = 5$ and $\sigma_2 = 0.71$. The magnitude of the current vector $\mathbf{i_2}$ therefore needs to be 7 times larger than $\mathbf{i_1}$ in magnitude, in order for the corresponding antenna patterns to radiate the same amount of power. The antenna patterns that correspond to $\mathbf{i}_1$ and $\mathbf{i}_2$ are shown in Fig. 6.1. Note that since $\hat{\mathbf{i}}_1\hat{\mathbf{i}}_2^H = 0$, the antenna patterns are orthogonal.

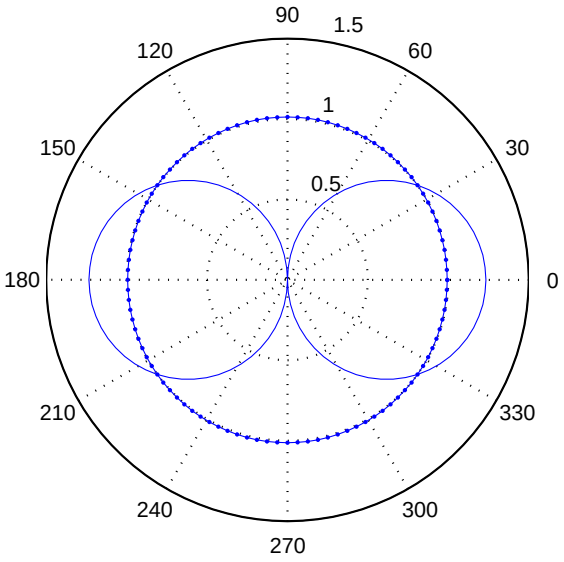

FIGURE 6.1: Orthogonal antenna patterns that correspond to the eigenvectors of $\mathbf{A}_t^{-1/2}$.

The capacity of an antenna array consisting of two $\lambda/16$ spaced active antenna elements is presented in Fig. 6.2. Both the traditional and the radiated power constraint are used in the capacity calculations. The capacity plot clearly shows that the choice of power constraint has a dramatic effect on the capacity results.

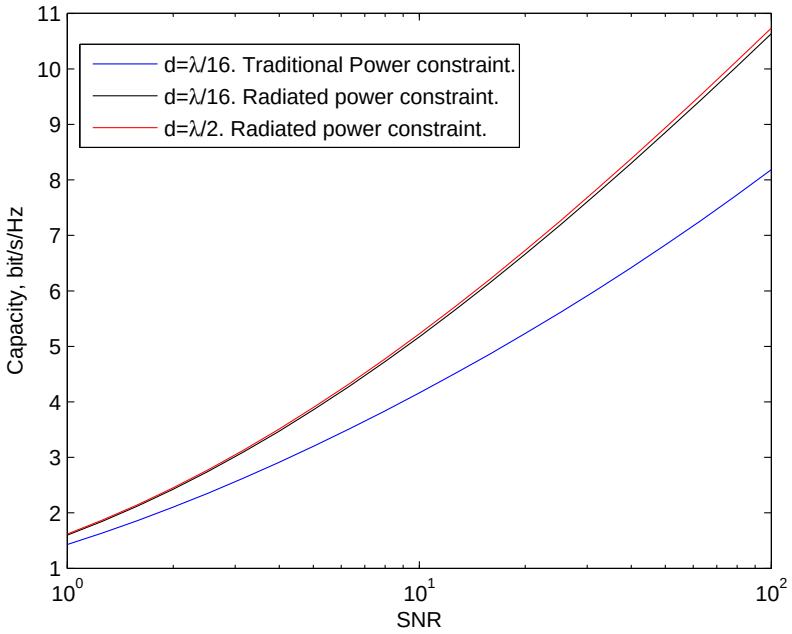

FIGURE 6.2: Comparison of the capacity achieved by two active antenna elements with inter-element distance $\lambda/2$ and $\lambda/16$. The average power is constrained according to both the traditional power constraint and the radiated power constraint for an inter-element distance $\lambda/16$.

6.2 Constructing antenna patterns by maximizing the upper bound on capacity

The material presented in the present section is included in order to give greater insight into issues regarding the channel and antenna patterns. We are in the following concerned with constructing antenna patterns for two active transmit antennas. Assume that the channel is described by $g(\phi_r, \phi_t)$, which expresses how a signal transmitted from angle ϕ_t and received from angle ϕ_r is modified in amplitude and phase. Let the channel have the

following property

$$\mathbb{E}\{g(\phi_r,\phi_t)\cdot g^*(\psi_r,\psi_t)\} = C\cdot\delta(\phi_r-\psi_r)\cdot\delta(\phi_t-\psi_t) \tag{6.11}$$

with C being a constant. Assume that the antenna patterns of the transmit antennas are described by $a_{t,1}(\phi_t)$ and $a_{t,2}(\phi_t)$ and the receive antennas by $a_{r,1}(\phi_r)$ and $a_{r,2}(\phi_r)$. The channel matrix between the transmit antennas and the received antennas may now be constructed

$$\mathbf{H} = \begin{bmatrix} \int_{\phi_t}\int_{\phi_r} a_{r,1}(\phi_r)g(\phi_r,\phi_t)a_{t,1}(\phi_t)d\phi_r\phi_t & \int_{\phi_t}\int_{\phi_r} a_{r,1}(\phi_r)g(\phi_r,\phi_t)a_{t,2}(\phi_t)d\phi_r\phi_t \\ \int_{\phi_t}\int_{\phi_r} a_{r,2}(\phi_r)g(\phi_r,\phi_t)a_{t,1}(\phi_t)d\phi_r\phi_t & \int_{\phi_t}\int_{\phi_r} a_{r,2}(\phi_r)g(\phi_r,\phi_t)a_{t,2}(\phi_t)d\phi_r\phi_t \end{bmatrix}.$$

Let the received signal $\mathbf{y}$ be written as

$$\mathbf{y} = \mathbf{H}\cdot\mathbf{x} + \mathbf{n}, \tag{6.12}$$

with $\mathbf{x}$ being the signal transmitted with antenna patterns $a_{t,1}(\phi_t)$ and $a_{t,2}(\phi_t)$, and $\mathbf{n}$ being AWGN. An upper bound the mutual information between the transmitted and received signal may be found

$$\mathbb{E}\{I(\mathbf{y};\mathbf{x})\} \leq \log_2\left(\mathbf{I} + \frac{P_t}{2N_0}\mathbb{E}\{\mathbf{H}^H\mathbf{H}\}\right), \tag{6.13}$$

where P_t is the average transmit power constraint and N_0 is the noise variance. It may be shown that the upper bound on the mutual information is maximized if $a_{t,1}(\phi_t)$ and $a_{t,2}(\phi_t)$ are orthogonal. In a similar way, by considering $\mathbb{E}\{\mathbf{H}\mathbf{H}^H\}$ instead of $\mathbb{E}\{\mathbf{H}^H\mathbf{H}\}$, it may be shown that $a_{r,1}(\phi_r)$ and $a_{r,2}(\phi_r)$ maximize an upper bound on the mutual information if they are orthogonal.

6.3 Aerial entropy

The transmission technology presented in the second part of the thesis is based on the concept of aerial entropy or angular entropy which it is also called. Kalis and Carras [2005] showed that a signal radiated from an array of electromagnetic point sources may be presented as

$$s(\phi) = i_0\cdot AF(\phi), \tag{6.14}$$

where ϕ is the azimuth angle, and $AF(\phi)$ is the array factor defined as

$$AF(\phi) = [1\ Z_1....Z_{N-1}]\cdot[1\ e^{\psi_1(\phi)}.....e^{\psi_{N-1}(\phi)}]^T, \tag{6.15}$$

where $Z_1, ..., Z_{N-1}$ describe the amplitude and phase difference between the currents on the antenna elements. The phase difference of the electromagnetic field due to different positions of the antenna elements are given by $[1\ e^{\psi_1(\phi)}.....e^{\psi_{N-1}(\phi)}]$. Kalis and Carras [2005] showed that the source entropy of the electromagnetic signal $s(\phi)$ may be written as

$$H(s(\phi)) = H(i_0 \cdot AF(\phi)) = H(i_0) + H(AF(\phi)|i_0), \tag{6.16}$$

where $H()$ is the entropy operator. Equation (6.16) shows that the information content of the radiated signal can be decomposed into two terms. The first term, $H(i_0)$, represents the uncertainty of the input signal to the antenna array, whereas the second term , $H(AF(\phi)|i_0)$, represents the uncertainty of the array factor.

Equation (6.16) is just an alternative formulation of the entropy of a signal radiated from an electromagnetic source. Note that when parasitic elements are present, the elements $Z_1, ..., Z_{N-1}$ of the array factor become the mutual coupling parameters of the antenna array.

Chapter 7

Uplink capacity

In the introductory chapter it was explained that the entropy of a signal transmitted from an antenna array may be decomposed into the entropy of the input signal and the entropy of the array-factor. In this chapter it is shown how the entropy of the array factor can be implemented by the usage of parasitic elements.

Parts of the material in this chapter are presented in (Bains, Müller, and Kalis [2007, Bains *et al.*]; Bains and Müller [b]).

7.1 Background theory

Assume for the present analysis that a transmit array consists of one active antenna element and one parasitic antenna element. Let $\mathbf{y}$ denote a signal received with an antenna array at the base-station, and let $\mathbf{i}(x, v_T)$ denote the transmit current vector. The received signal may be written as

$$\mathbf{y} = \mathbf{H} \cdot \mathbf{i}(x, v_T) + \mathbf{n}. \tag{7.1}$$

The variable $x \in \Im$ ($\Im$ represents the imaginary numbers) denotes the reactive impedance value which is used as a termination of the parasitic element, $v_T \in \mathbb{C}$ is the voltage applied to the active element. The antenna currents are defined by

$$\begin{aligned} i_1 &= \frac{(Z_{11} + x) \cdot v_T}{(Z_{11} + Z_L) \cdot (Z_{11} + x) - Z_{12}^2} \\ i_2 &= \frac{-Z_{12}}{Z_{11} + x} \cdot i_1, \end{aligned} \tag{7.2}$$

where i_1 and i_2 are the currents on the active and parasitic antenna respectively, Z_{11} and Z_{12} are defined the same way as in (2.10), and Z_L is the ter-

mination impedance of the active antenna element. Equation (7.2) shows that the currents on the antennas are dependent on both the voltage source and the reactive impedance. Each choice of the reactive impedance x corresponds to a distinct array factor $AF(\phi)$ as defined in (6.15). The voltage value v_T has a direct relation to the signal i_0 on the input of the antenna array.

Note from equation (7.2) that $|i_1| \geq |i_2|$ always holds , i.e. that the current on the parasitic element is never larger than the current on the active antenna element. This can be seen by considering the ratio $\left|\frac{i_2}{i_1}\right|$. The maximum ratio, $\left|\frac{i_2}{i_1}\right|_{max}$, is obtained when $x = -\mathrm{Im}\{Z_{11}\}$, and hence the maximum ratio between the currents becomes

$$\left|\frac{i_2}{i_1}\right| = \frac{|Z_{12}|}{\Re\{Z_{11}\}} \leq 1. \tag{7.3}$$

Because of this, the capacity by using one active and one parasitic element can never exceed the capacity of two active antenna elements. In order to see this even further, Fig. 7.1 shows the possible values of i_2 when $i_1 = 1$ and $i_1 = 10$. The curve of the possible values of i_2 becomes elliptical in the 2-D complex plane. The advantage of using parasitic elements is that only a single RF-frontend is required, and thus represents a much cheaper antenna solution.

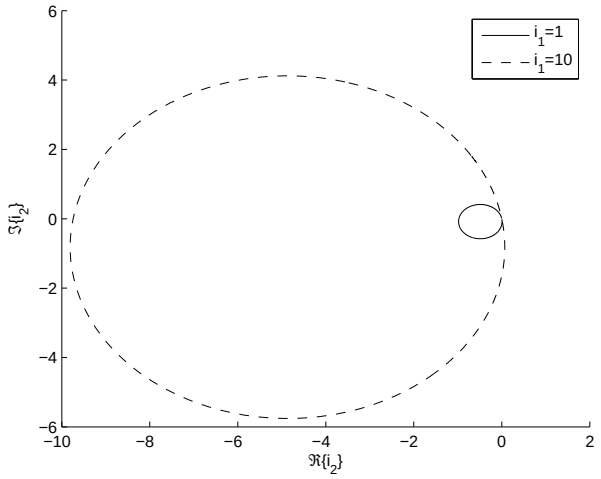

FIGURE 7.1: Possible values of i_2 when i_1 and $i_1 = 10$. Note that the operator $\Im$ (on the y-axis) takes the imaginary value of a number.

Note that the channel $\mathbf{H}$ in this chapter is normalized in the following way

$$\mathbb{E}\{\mathrm{tr}(\mathbf{H}\mathbf{H}^H)\} = n_r \cdot n_t, \tag{7.4}$$

with n_t being the number of transmit antennas, and n_r being the number of receive antennas. If we assume a single transmit antenna with average radiated power $\mathbb{E}\{|i_1|^2\} = 1$, the total received power becomes $\mathbb{E}_{\mathbf{H}}\{\mathbf{y}^H\mathbf{y}\} = n_r$. The noise per receive antenna is assumed to have unit variance,i.e. $\sigma_n^2 = 1$, which means we get $SNR = 1$ per receive antenna. Therefore when in this chapter the capacity is plotted as a function of SNR, the SNR actually refers to both the average SNR per receive antenna and average radiated power.

7.2 Capacity analysis of a $\lambda/16$ spaced two element antenna array

In this section the capacity of a two element antenna array, with an inter-element distance equal to $\lambda/16$, is searched for. The received signal is given by equation (7.1), and it is assumed that the receiver, i.e. the base station, has two antennas. In order to find the capacity an expression for the mutual information is needed. The mutual information $I(\mathbf{y}; x, v_T)$ may be expressed as

$$\begin{aligned} I(\mathbf{y}; x, v_T|\mathbf{H}) = &\int_{\mathbf{y}}\int_{x}\int_{v_T} P_{\mathbf{n}}\left(\mathbf{y} - \mathbf{H}\cdot\mathbf{i}(x, v_T)\right)\cdot P(x, v_T) \\ &\cdot \log_2\left(\frac{P_{\mathbf{n}}\left(\mathbf{y} - \mathbf{H}\cdot\mathbf{i}(x, v_T)\right)}{\int_x\int_{v_T} P_{\mathbf{n}}\left(\mathbf{y} - \mathbf{H}\cdot\mathbf{i}(x, v_T)\right)\cdot P(x, v_T)dv_T dx}\right) dv_T dx d\mathbf{y}, \end{aligned} \tag{7.5}$$

where $\mathbf{y}$ is the received signal, x and v_T are defined as in the preceding section, $P(x, v_T)$ is the joint probability density function (PDF) of the reactive impedance x and the voltage signal v_T. The distribution $P_{\mathbf{n}}()$ is the Gaussian PDF defined as

$$P_{\mathbf{n}}(\mathbf{n}) = \frac{1}{\pi^2\sigma_n^2}\cdot\exp\left(\frac{1}{\sigma_n^2}\cdot\mathbf{n}^H\mathbf{n}\right), \tag{7.6}$$

with σ_n^2 being the variance of the AWGN. An analytical solution to the integral in (7.5) has not been found. Numerical techniques are therefore needed in order to solve the integrals. A Gauss-quadrature rule is used in order to perform the integration. For integrals such as $\int_{-\infty}^{\infty}\exp(-x^2)f(x)dx$ the Gauss-Hermite polynomial quadrature rule is particularly suitable (Liu and Pierce [1994]).

The capacity analysis of the two element antenna will be conducted in two steps. First the spectral efficiency obtained by varying the array factor is explored in Section 7.2.1. The capacity when both the input signal v_T and the reactive impedance x is varied is then explored in Section 7.2.2.

7.2.1 Reactive impedance values used as a source

Since the source entropy is given by both the entropy of the input signal v_T and the reactive impedance x, it would be interesting to see how much information can be conveyed by changing the array factor, i.e. by changing the reactive impedance x. For that purpose a numerical algorithm (Arimoto [1972]; Blahut [1972]; Matz and Duhamel [2004]) is employed for finding the distribution $P_x(x)$ that maximizes the average mutual information $\mathbb{E}_{\mathbf{H}}\{I(\mathbf{y};x|\mathbf{H})\}$. The algorithm is the well known Arimoto-Blahut algorithm, which is used for finding capacity achieving distributions. Because of the numerical complexity a finite number of discrete reactive impedance values is used. The impedance values were chosen to lie between $-100\ \Omega$ and $+100\ \Omega$ with a resolution of $2\ \Omega$.

Maximizing the average mutual information $\mathbb{E}_{\mathbf{H}}\{I(\mathbf{y};x|\mathbf{H})\}$ with respect to a distribution $P_x(x)$ is relevant for the case when the receiver has channel state information and the transmitter has statistical knowledge about the channel.

The average mutual information is approximated by the empirical average

$$\mathbb{E}_{\mathbf{H}}\{I(\mathbf{y};x|\mathbf{H})\} \approx \frac{1}{N}\sum_{k=1}^{N} I(\mathbf{y};x|\mathbf{H}_k), \tag{7.7}$$

where N is the number of channel realizations, and $\mathbf{H}_k$ is a specific channel realization. The average mutual information is maximized at different SNRs. The SNR is selected by choosing the voltage level v_T.

The channel model used in the calculations is a geometrical double bounce channel as shown in Fig. 7.2. The channel represents therefore a rich scattering channel. Both the transmitter and the receiver are surrounded by a cloud of scatterers. Each new channel realization is made by picking random positions of the scatterers. The attenuation of each ray as it bounces off a scatterer is chosen to be constant, i.e. the same attenuation for all scatterers. In addition, the amplitude of the ray is attenuated as a function of distance. The electric field in free space decays proportional to $1/d$, where d is the distance, and it is this attenuation which is used in the simulations. The scatterers are assumed to introduce phase-shifts which

are uniformly distributed between 0 and 2π, and the phase shift of each scatterer is assumed to be independent. The distance between the transmitter and receiver is chosen not to be too large compared to the radius of each cloud of scatterers, since a too large distance leads to the keyhole effect (Molisch [2004]).

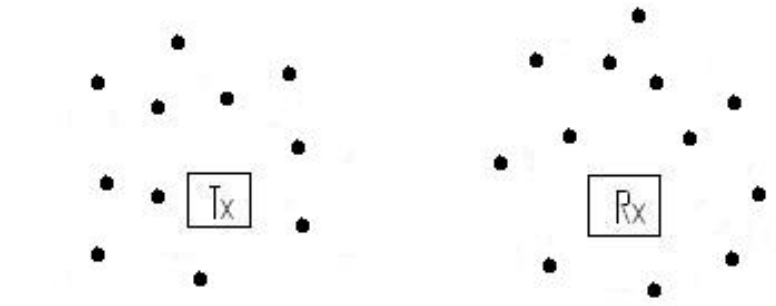

FIGURE 7.2: Geometrical double bounce channel model.

The spectral efficiency at various SNR is given in Fig. 7.3 for different inter-element distances between the active and the parasitic antenna. The smallest inter-element distance yields the highest spectral efficiency. This can be explained by the fact that the mutual coupling is higher for smaller antenna spacings. The currents on both antennas can therefore to a larger degree be controlled by the reactive impedance value.

7.2.2 Reactive impedance values and modulation

Calculating the capacity when both the voltage signal v_T and the reactive impedance value x is varied leads to much higher numerical complexity than when only the reactive impedance is varied. Because of the restriction on the numerical complexity in order for the simulations to finish within reasonable time, only 4 distinct reactive impedances are utilized. These reactive impedances correspond to 4 distinct antenna patterns, as shown in Fig 7.4. The antenna patterns were picked on an intuitive ground. Since no optimality criterion for the antenna patterns is found, a reasonable starting point might be to select patterns that are "sufficiently" different. The voltage signal v_T was chosen to be a 100 QAM symbol, which means that 400 different signals may be transmitted from the antenna array. The noise vari-

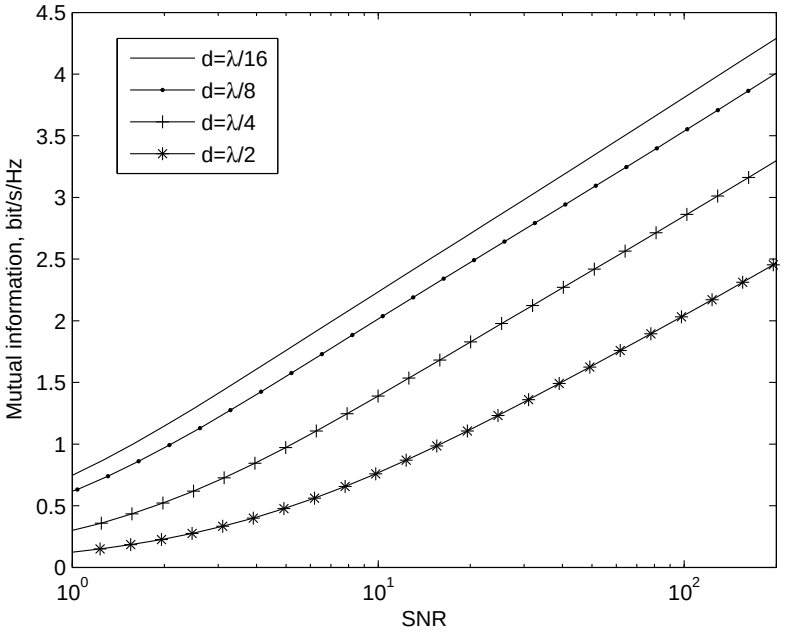

FIGURE 7.3: Spectral efficiency obtained by varying the reactive impedance value x for various inter-element distances between the active and the parasitic element.

ance was held fixed at $\sigma_n^2 = 1$ for all SNRs. In addition the signal points v_T were also held at fixed positions. The implication of this is that the capacity saturates at some SNR since there are no more signal points v_T available for increasing the capacity above a certain SNR threshold. In some sense this situation corresponds to an average power and peak power constraint scenario. The peak power P_{peak} for the proposed antenna array is expressed as

$$P_{peak} = \max_{v_T, x} \mathbf{i}(x, v_T)^H \mathbf{A}_t \mathbf{i}(x, v_T), \tag{7.8}$$

where $\mathbf{A}_t$ is defined in (6.7). In the simulations, the voltage symbols were normalized such that the peak power became equal to 81.

The capacity achieving distribution of the voltage symbols $P_{v_T}(v_T)$ is shown in 7.5 for two different SNRs. The distribution of the voltage symbols seems to be similar to the Gaussian distribution for low SNR. For higher SNR the distribution seems to deviate from the Gaussian distribution. The capacity is plotted as a function of SNR in Fig. 7.6. For com-

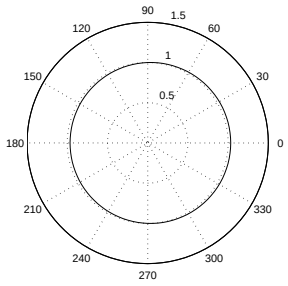

(a) Obtained with $x = -j1000\Omega$.

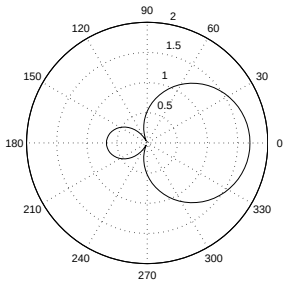

(b) Obtained with $x = -j43\Omega$.

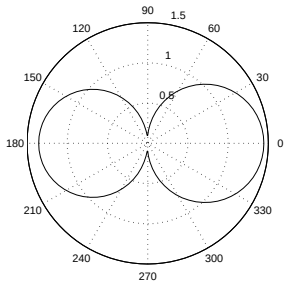

(c) Obtained with $x = -j24\Omega$.

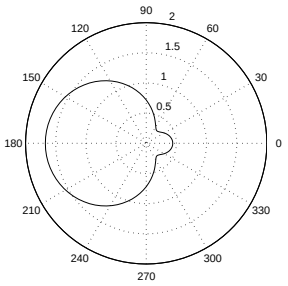

(d) Obtained with $x = 0\Omega$.

FIGURE 7.4: Antenna patterns obtained by loading the parasitic element with 4 different reactive impedances.

parison the capacity is also evaluated both for a single transmit antenna and a transmit array of two widely spaced ($\lambda/2$ spacing) active antennas. The single transmit antenna and the transmit array utilize continuous signal points with a Gaussian distribution. The capacity plot shows that the antenna system consisting of one active and one parasitic element outperforms the single transmit antenna with 0.8 bit/s/Hz for an SNR of 15 dB. The two active antenna elements beat the proposed antenna system by 0.45 bit/s/Hz. By employing even more antenna patterns the capacity of the proposed antenna system is expected to come even closer to the spectral efficiency obtained by two active antenna elements.

Note that a change in the reactive impedance value x results in a change in the antenna impedance. A too large change of the reactive impedance value x results in an impedance mismatch between the termination impedance of the active antenna and the antenna impedance. The consequence of this

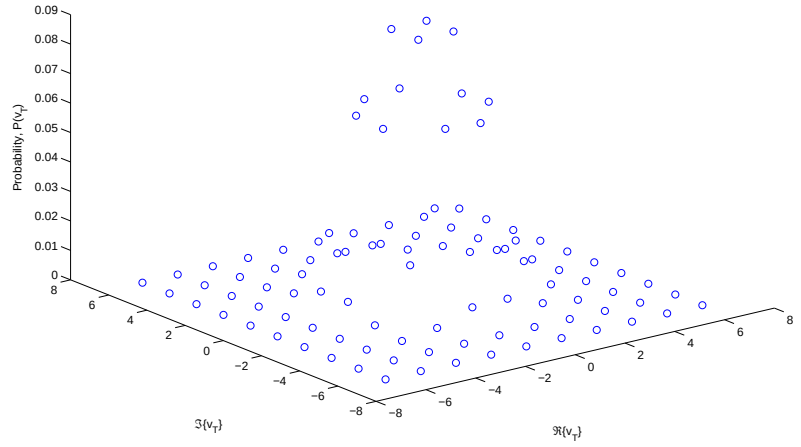

(a)

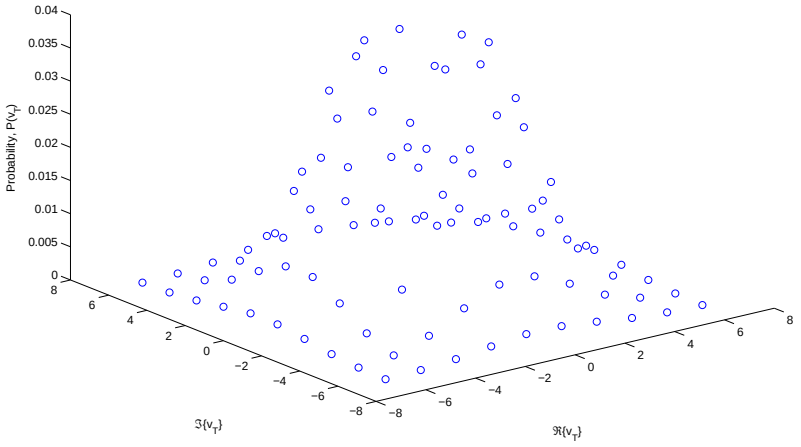

(b)

FIGURE 7.5: The capacity achieving distribution $P_{v_T}(v_T)$ for two different SNRs, a) SNR=4.5 and b) SNR=13.

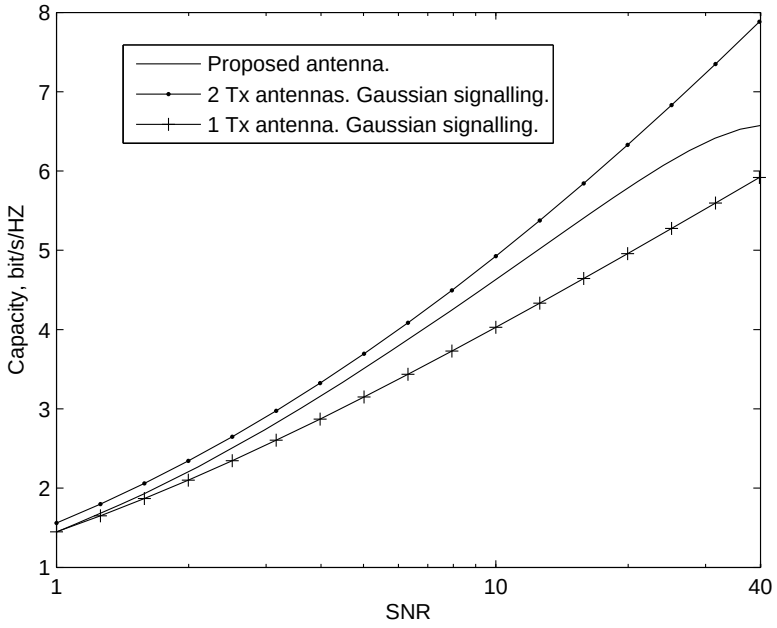

FIGURE 7.6: Capacity as function of SNR. The proposed antenna system utilizes 4 distinct antenna patterns, and transmits a 100 QAM symbol with each pattern.

is a reduced antenna efficiency. We therefore consider now that the antenna is impedance matched for a specific choice of reactive impedance value, and then only change the reactive impedance such that the voltage standing-wave-ratio is smaller than 1.5 (See Pozar [1998], Section 2.3 for the definition of voltage standing-wave ratio). With only one parasitic element and one active element, the number of patterns that are sufficiently different is not that high. With $x = -j24\Omega$, an antenna pattern that consists of two beams, one beam towards zero degrees in the azimuth plane and one beam towards 180 degrees, is created (See Fig. 7.4c). Slightly smaller reactive impedances than $-j24\Omega$ leads to antenna patterns that are directive towards 0 degrees in the azimuth plane. Reactive impedances larger than $-j24\Omega$ leads to antenna patterns that are directive towards 180 degrees. Since $x = -j24\Omega$ is the turning-point, where the antenna pattern changes its direction, it seems natural to assume that the antenna is impedance matched for $x = -j24\Omega$. We then let the reactive impedance change only such that the voltage standing-wave ratio is below 1.5.

We have performed simulations in order to determine the obtainable

spectral efficiency when it is required that the voltage standing-wave ratio is below 1.5. In the simulations, we have assumed that the reactive impedance values lie within the interval $[-j32\Omega, -j8\Omega]$, with a resolution of $j2\Omega$, which gives 13 different reactive impedances. We assumed that the voltage signal v_T is a 64 QAM symbol. This antenna array has the possibility of transmitting $13 \cdot 64 = 832$ different signals. The capacity achieved by the proposed antenna array is compared with the capacity achieved with a single omni-directional antenna. The single omni-directional antenna is assumed to transmit a 1024 QAM symbol. In order to make the comparison fair, we normalize the QAM-symbols such that the maximum radiated power becomes the same for both the single omni-directional antenna and the proposed antenna array.

The capacities achieved when $P_{peak} = 49$ and $P_{peak} = 196$ are shown in Fig. 7.7. The plot shows that the proposed antenna array achieves 1 bit/s/Hz higher capacity than the single omni-directional antenna for an SNR equal to 78 and peak power equal to 196. The capacity achieving distribution of the voltage symbols $P_{v_T}(v_T)$ and reactive impedances $P_x(x)$ are shown in Fig. 7.8 when SNR=5.5 and $P_{peak} = 49$.

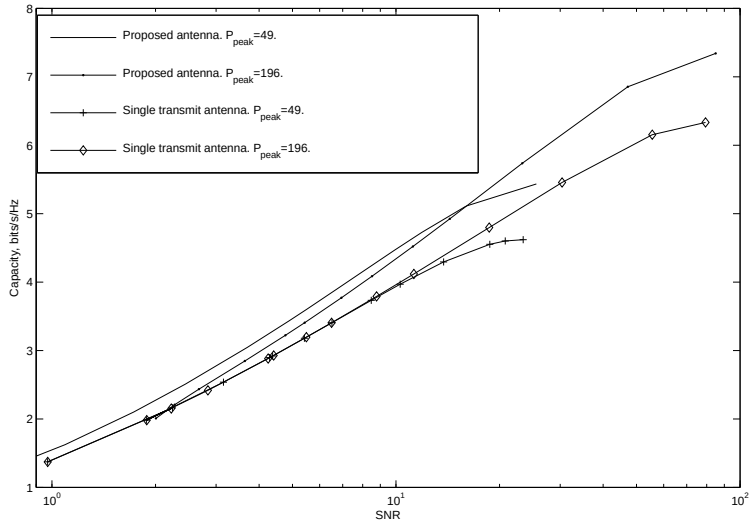

FIGURE 7.7: Capacity achieved by the proposed antenna and a single transmit antenna for two different peak power constraints. A total number of 13 different antenna patterns are utilized, and with each antenna pattern a 64 QAM symbol is transmitted.

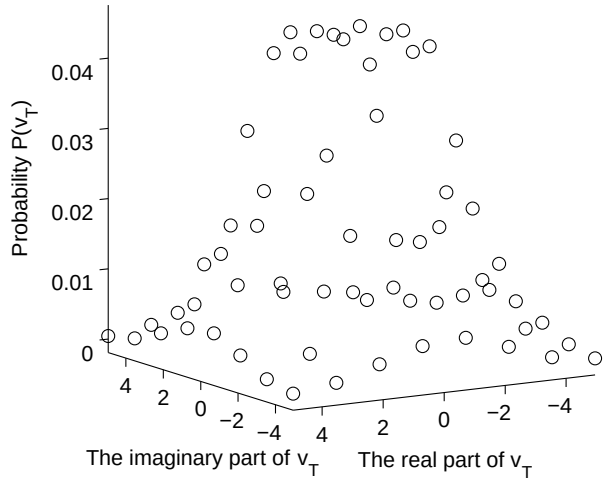

(a)

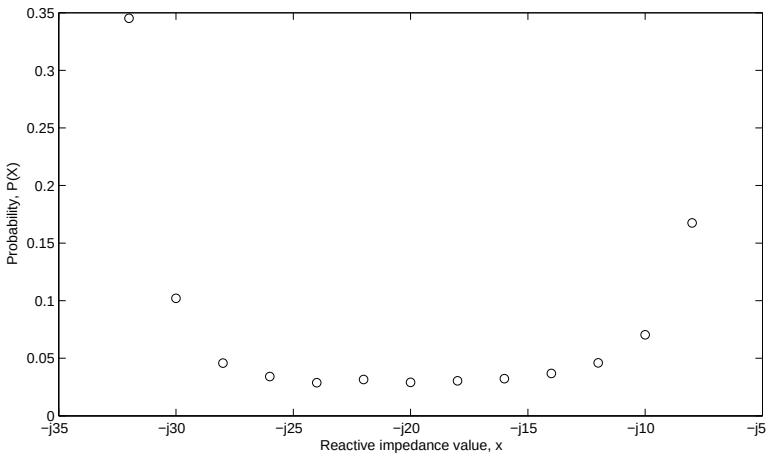

(b)

FIGURE 7.8: The capacity achieving distributions, a) $P(v_T)$ and b) $P_x(x)$, when $SNR = 5.5$ and $P_{peak} = 49$.

7.3 Spectral efficiency of a three element antenna array with inter-element distance $\lambda/8$

The antenna system which is considered in this section is shown in Fig. 7.9. The antenna array consists of one active antenna element and two parasitic elements. The distance between the elements is $\lambda/8$, which means that the total array length becomes $\lambda/4$. Since the number of antennas in this section is larger than in the previous section, a higher spectral efficiency is expected to be achievable with this antenna configuration. The transmitted signal may now be varied by changing the voltage signal supplied to the active element and the two reactive impedances within the parasitic elements. In this section 4 distinct antenna patterns are employed. The antenna patterns are shown in Fig 7.10. These antenna patterns were found by solving a non-convex optimization problem. The idea is as following: Assume that the current vector $\mathbf{i}(x_1^{(k)}, x_2^{(k)}, v_T^{(k)})$ represents the current on the antennas for a specific choice of reactive impedances $x_1^{(k)}$ and $x_2^{(k)}$ and voltage $v_T^{(k)}$. Let the noise-less received signal be denoted by $\mathbf{y}^k$, and let it be expressed by

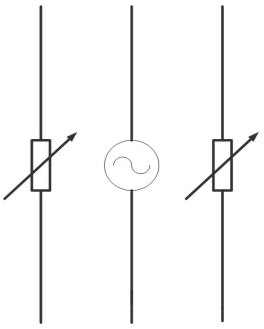

FIGURE 7.9: One active and two parasitic antenna elements.

$$\mathbf{y}^k = \mathbf{H} \cdot \mathbf{i}(x_1^{(k)}, x_2^{(k)}, v_T^{(k)}), \tag{7.9}$$

where $\mathbf{H}$ is the channel matrix as before. The antenna patterns are found by minimizing the expected inner product between $\mathbf{y}^k$ and $\mathbf{y}^l$. Vector $\mathbf{y}^k$ and $\mathbf{y}^l$ correspond to two different noise less received signals that are the result of two different antenna patterns. But minimizing this inner product may result in choosing one antenna pattern that lies in the null space of the channel. To avoid that this happens, a constraint need to be put on the minimum power of each received signal. The optimization problem may

be posed in the following way

$$\min_{x_1^k, x_2^k, v_T^k, x_1^l, x_2^l, v_T^l} \mathbb{E}_{\mathbf{H}}(|\mathbf{y}^{k,H} \cdot \mathbf{y}^l|)$$

subject to

$$\mathbb{E}_{\mathbf{H}}\{\mathbf{i}^{(k)H} \cdot \mathbf{H}^H \mathbf{H} \cdot \mathbf{i}^{(k)}\} \geq P_k$$

$$\mathbb{E}_{\mathbf{H}}\{\mathbf{i}^{(l)H} \cdot \mathbf{H}^H \mathbf{H} \cdot \mathbf{i}^{(l)}\} \geq P_l \tag{7.10}$$

$$\mathbb{E}_{\mathbf{H}}\{\mathbf{i}^{(k)H} \cdot \mathbf{A_t} \cdot \mathbf{i}^{(k)}\} = P_T$$

$$\mathbb{E}_{\mathbf{H}}\{\mathbf{i}^{(l)H} \cdot \mathbf{A_t} \cdot \mathbf{i}^{(l)}\} = P_T, \tag{7.11}$$

where $\mathbf{A_t}$ is defined in (6.7) and (4.7). The expectation $\mathbb{E}_{\mathbf{H}}$ is included to make sure that the ”patterns” which are best on average are picked and not the best patterns for a specific channel. The two first constraints make sure the powers of the received signals lie above a certain threshold, i.e. above P_l and P_k, whereas the last two constraints make sure that the radiated power is the same for both antenna patterns. Note that the posed optimization problem in equation (7.10) only specifies two antenna patterns. Multiple patterns may be found through a multi objective optimization problem, through which the ”correlation” between each pair of patterns is considered. The meaning of correlation here is the inner-product between received signals that correspond to different patterns.

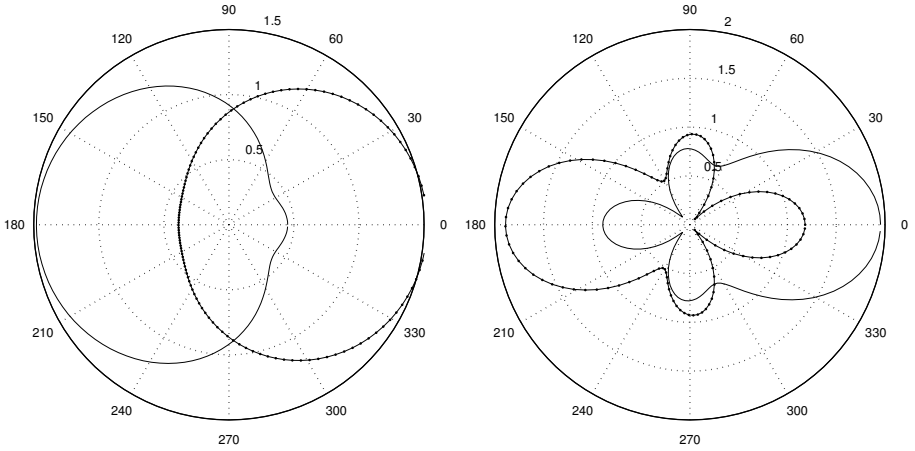

FIGURE 7.10: Antenna pattern obtained by loading two parasitic elements with 4 different reactive impedances. A varactor diode is placed in the middle of each parasitic elemenent, which makes it possible to dynamically change the reactive impedance value.

Since the optimization problem is non-convex, the solution which is found may be a local extremal point. The numerical algorithm which solves the optimization problem was run multiple times from random starting points, and the best of these solutions was picked. It should be noted, however, that there were many antenna patterns that resulted in almost the same "correlation" between the received signals.

The spectral efficiency for the three element antenna array was evaluated by employing 4 distinct patterns as shown in Fig 7.10. The voltage signal ,v_T, was chosen to be a 64 QAM symbol, which means that $4 \cdot 64 = 256$ different signals may be transmitted from the antenna array.

For the spectral efficiency evaluation, an uniform distribution was chosen for the signal points. The spectral efficiency by using such a distribution is given in Fig. 7.11 for different SNRs. The channel used in the calculations is the same rich scattering channel that was used in the previous section. A comparison is made with both a two element array of widely spaced ($\lambda/2$ spacing) active antenna elements and a single transmit antenna. The two antenna array uses a 16 QAM symbol on each antenna which results in $16 \cdot 16 = 256$ different signals, whereas the single transmit antenna transmits a 256 QAM symbol.

As can been from Fig. 7.11, the 3 element antenna array performs nearly as well as the two antenna array of widely spaced antennas. One of the advantages of the 3 element antenna array is that it is more compact, with an array width of $\lambda/4$ instead of $\lambda/2$. The other advantage is that it uses a single RF-frontend.

7.4 Spectral efficiency evaluation for rich scattering and clustered channels

The spectral efficiency has so far only been evaluated for rich scattering channels. This section aims at investigating the performance of the compact antenna array both for rich scattering and clustered channels. In addition other transmission schemes such as beamforming will be analyzed and compared against the transmission schemes presented in Section 7.2 and 7.3.

Beamforming was one of the first applications for antenna arrays consisting of parasitic elements. Beamforming is a technique that directs the antenna beam towards the angular direction that yields the highest SNR at the receiver. This technique might be implemented at both the transmitter and receiver. In this part of the thesis the focus is put on the transmitter, and therefore beamforming is considered only at the transmitter.

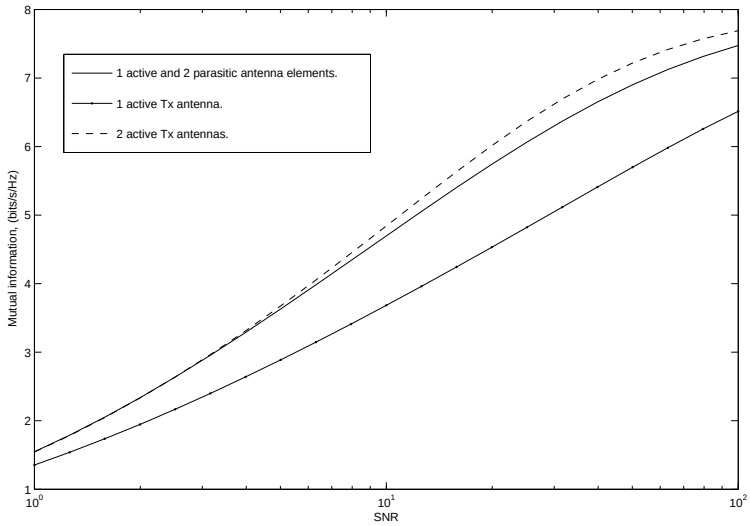

FIGURE 7.11: Average mutual information as a function of SNR for a rich scattering channel.

In order for the transmitter to know which direction it should direct its antenna beam, it needs some feedback information from the receiver. The scheme might work as follows: Assume that the transmitter has 3 antenna patterns to choose between. If the transmitter consists of one active antenna and one parasitic antenna, the current on the antennas may be expressed by

$$\mathbf{i}(x^k) \cdot v_T. \tag{7.12}$$

The reactive impedance x^k leads to a specific antenna pattern. The voltage signal v_T which is supplied to the active antenna element is then transmitted with antenna pattern k. Let the transmitter send $\mathbf{i}(x^1), \mathbf{i}(x^2)$ and $\mathbf{i}(x^3)$ onto the channel as training symbols. The receiver may use these signals to estimate the channel and detect which antenna pattern leads to the highest SNR. An index which represents the antenna pattern with the highest SNR is then fed back to the transmitter.

Beamforming will now be compared to the schemes presented in Section 7.3 and 7.2 for a rich scattering channel. From now on let the scheme presented in the previous sections be called "coding by patterns" scheme.

For the analysis the same two element array as in Section 7.2 will be considered. Let the beamforming scheme choose one out of 3 available

antenna patterns (antenna patterns a,b and d from Fig. 7.4) and let the "coding by patterns" scheme employ the four distinct patterns in Fig. 7.4. To make the comparison between the two schemes fair the same number of signal points should be considered for both cases.

The spectral efficiency will be evaluated for 4 different schemes. A summary of each of the schemes are listed below.

- Beamforming. This scheme picks the pattern that result in the highest receiver SNR. A 256 QAM symbol is transmitted with the chosen antenna pattern. This scheme requires feedback from the receiver.
- Coding by patterns. Information is coded both by the choice of antenna pattern and the choice of symbol to be transmitted with the antenna pattern. Four different antenna patterns are employed, and for each choice of antenna pattern a 64 QAM symbol is transmitted.
- Coding by patterns version 2. The transmitter selects two out of the four antenna patterns that yield the highest SNR at the receiver. A 128 QAM symbol is transmitted with the selected antenna pattern. Requires feedback from the receiver.
- Single transmit antenna which transmits a 256 QAM symbol on each symbol period.

The spectral efficiency is calculated by generating the signal points according to a uniform distribution. Fig. 7.12 shows the mutual information for the 4 different schemes. As the plot shows, the spectral efficiency is higher for the beamforming scheme than the "coding by patterns" scheme for low SNR, whereas for high SNR the opposite occurs. This transition occurs at an SNR of 4 dB. The coding by pattern scheme, that uses the two antenna patterns that yield the highest receiver SNR, seems to achieve the highest spectral efficiency for all SNR.

An analogue can be made to a regular MIMO system. When the transmitter in a MIMO system has channel state information the optimal power distribution is found according to the waterfilling principle. In the low SNR region almost all the transmit power is put into the strongest channel eigenmode. Note that beamforming has a strong connection to MIMO communication in the low SNR region, since beamforming selects the "strongest eigenmode" in some sense. In the high SNR region, for a regular MIMO system, the transmitted power is divided more equally between the channel eigenmodes . The "coding by patterns" scheme corresponds to the high SNR region of a regular MIMO system, since all antenna patterns (and all eigenmodes) are used with equal probability.

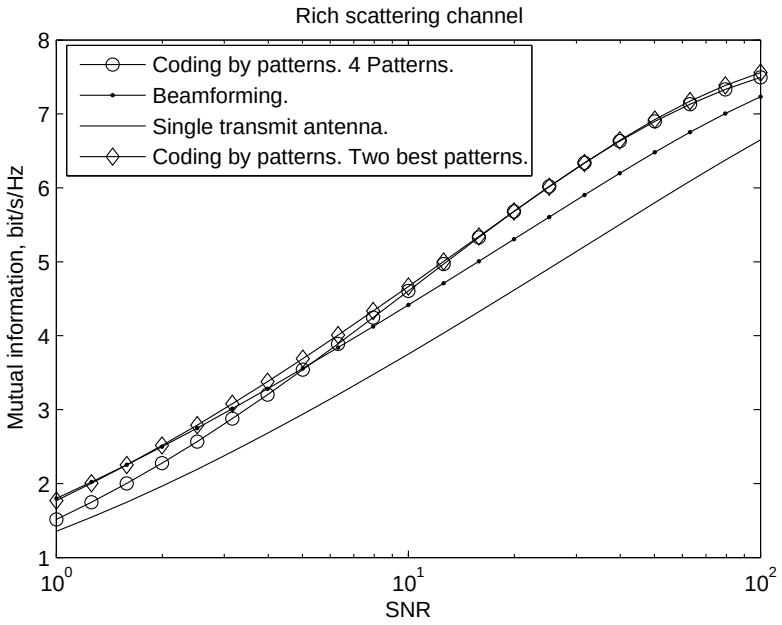

FIGURE 7.12: Average mutual information as a function of SNR for a rich scattering channel.

Next the spectral efficiency will be evaluated for clustered channels. The clustered channel model is depicted in Fig. 7.13. The transmitter is assumed to be at the center of a circle with a radius of 10 meters. A total number of 4 clusters are placed at random positions on the circle. A separation of 30 meters is chosen between the transmitter and the receiver. The clustered channel implies a channel with higher singular value spread than the rich scattering channel in Fig. 7.2. Therefore a smaller increase in mutual information is expected by using the ″coding by patterns″ scheme than was obtained for the rich scattering channel.

The spectral efficiency for the clustered channel is depicted in Fig. 7.14. As expected, the increase in mutual information by using the ″coding by patterns″ scheme is lower than for the rich scattering channel. Also ,beamforming surpasses the spectral efficiency obtained by the ″coding by patterns″ scheme at all SNRs. The coding by patterns scheme that uses the two best antenna patterns achieves a slightly higher spectral efficiency than the beamforming scheme in the high SNR-region.

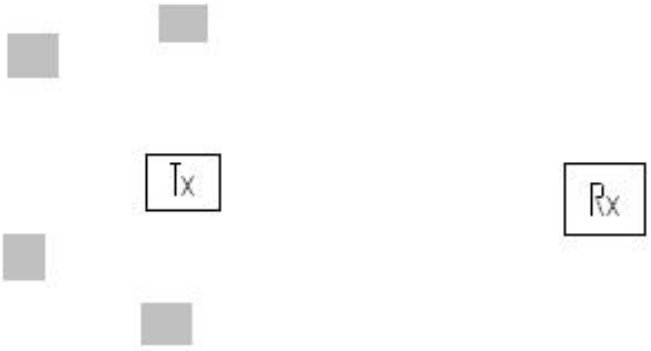

FIGURE 7.13: Clustered channel.

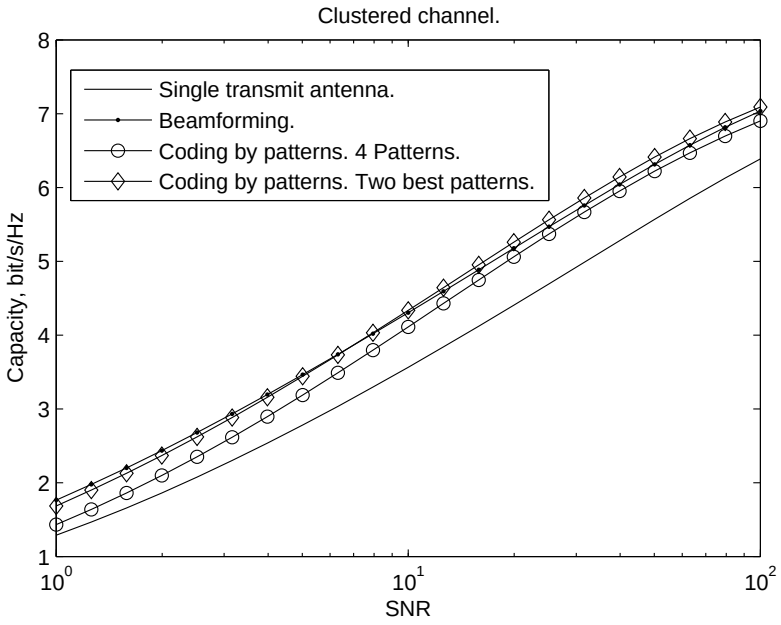

FIGURE 7.14: Average mutual information as a function of SNR for a clustered channel.

7.5 Symbol/antenna pattern design based on symbol error rate performance

This section aims at designing antenna patterns or symbols by minimizing the symbol error rate. Note that this criteria is relevant for uncoded transmission only. Symbols that are designed according to the minimum symbol error criteria do not necessarily represent symbols that yield the highest mutual information. For the present analysis there will be no distinction between antenna patterns and symbols, and these two words will be used interchangeably. A specific symbol or antenna pattern in this context simply means a distinct current vector $\mathbf{i}$.

Before presenting the criteria which is used to design the symbols, consider that the channel may be written as

$$\mathbf{H} = \mathbf{A}_r^{1/2}\hat{\mathbf{H}} \cdot \mathbf{A}_t^{1/2}, \tag{7.13}$$

where $\hat{\mathbf{H}}$ consists of i.i.d complex Gaussian entries, $\mathbf{A}_r^{1/2}$ and $\mathbf{A}_t^{1/2}$ introduce receive and transmit correlation, respectively, into the channel matrices. This channel description is the well known Kronecker channel model. Some claim that this channel model is effective in matching measured results for systems with up to four antenna elements (Yu, Bengtsson, Ottersen, McNamara, Karlsson, and Beach [2002]; Kermoal, Schumacher, Pedersen, Mogensen, and Fredriksen [2002]), whereas newer results have demonstrated key deficiencies in the model (Özcelik, Herdin, Weichselberger, Wallace, and Bonek. [2003]). Never the less, this model is well suited for finding analytical results. The channel model, as given by (7.13), describes the propagation paths for the antenna currents at the transmitter to the open-circuit voltages at the receiver array and hence does not include mutual coupling. Mutual coupling at the transmitter array is including in the calculation of the currents, as can be seen from (7.2). For the receiver array, mutual coupling is neglected since it consists of widely spaced antennas.

A common approach for designing symbols is to minimize the maximum pairwise error probability. Lee and Messerschmitt [1994] gave an approximation to the average bit error rate P_e

$$P_e \approx C \cdot \frac{1}{\sqrt{2\pi\sigma_n^2}} \int_{d_{min}/\sigma_n}^{\infty} e^{-n^2/2} dn, \tag{7.14}$$

where d_{min} is the minimum distance between any pair of signals at the receiver, C is a constant and σ_n^2 is the noise variance. This expression shows that the average probability of error is dominated by the largest pairwise error probability. The Chernoff bound on the average pairwise error for

space-time coding was found by Hochwald and Marzetta [2000]; Tarokh, Seshadri, and Calderbank [1998]. The probability that the receiver makes a decision in favour of space-time codeword $\mathbf{c}$ when in fact $\mathbf{d}$ was transmitted, for a complex Gaussian channel with i.i.d components, may be written as

$$P(\mathbf{c} \to \mathbf{d}) \leq \left(\prod_{i=1}^{r} \lambda_i\right)^{-N_t} \cdot \left(\frac{E_s}{4N_0}\right)^{-rn_t}, \tag{7.15}$$

where E_s is a scaling factor such that the average transmitted power is 1, N_0 is the noise variance, n_t is the number of transmit antennas, r and λ_i are the rank and the i-th eigenvalue of the product matrix $\mathbf{E}\mathbf{E}^H$ respectively, where $\mathbf{E}$ is the codeword difference matrix. If coding is not performed across time, as in the present section, matrix $\mathbf{E}$ becomes a vector $\mathbf{e}$ instead. If we consider the pairwise error for codewords $\mathbf{c}$ and $\mathbf{d}$, the codeword difference vector becomes $\mathbf{e} = \mathbf{c} - \mathbf{d}$ and the only eigenvalue becomes $\lambda = \mathbf{e}^H\mathbf{e}$. The pairwise error is therefore seen to depend on the Euclidean distance between the codewords $\mathbf{c}$ and $\mathbf{d}$.

In the derivations of equation (7.15) it was assumed that the channel components were i.i.d complex Gaussian. This assumption does not hold for closely spaced antennas. Assume that the receive antennas are widely spaced such that $\mathbf{A}_r^{1/2} = \mathbf{I}$. The channel is then described by

$$\mathbf{H} = \hat{\mathbf{H}}\mathbf{A}_t^{1/2}. \tag{7.16}$$

If we instead of considering a current vector $\mathbf{i}$ consider $\hat{\mathbf{i}} = \mathbf{A}_t^{1/2}\mathbf{i}$, we note that $\hat{\mathbf{i}}$ sees an i.i.d complex Gaussian channel, i.e. it sees channel $\hat{\mathbf{H}}$. The pairwise error between two vectors $\hat{\mathbf{i}}^k$ and $\hat{\mathbf{i}}^l$ may be found from equation (7.15). Minimizing the pairwise error of vectors $\hat{\mathbf{i}}^k$ and $\hat{\mathbf{i}}^l$ is then equivalent to maximizing $(\mathbf{i}^k - \mathbf{i}^l)^H\mathbf{A}_t(\mathbf{i}^k - \mathbf{i}^l)$.

Now we are able to state the design criteria for the current vectors. The current vectors should be found by minimizing the maximum pairwise error probability according to

$$\min_{x^{(k)}, v_T^{(k)}, x^{(l)}, v_T^{(l)}} \max_{l,k,l\neq k} P(\mathbf{i}^k \to \mathbf{i}^l | \mathbf{i}^k), \tag{7.17}$$

where $x^{(k)}$ and $v_T^{(k)}$ are the reactive impedance and voltage needed in order to achieve the current vector $\mathbf{i}^k$. Note that the antenna array consists of one active and one parasitic element. By inserting the Chernoff bound on the pairwise error probability the optimization problem may be rephrased as

$$\min_{x^{(k)}, v_T^{(k)}, x^{(l)}, v_T^{(l)}} \max_{l,k,l\neq k} (\mathbf{i}^k - \mathbf{i}^l)^H \cdot \mathbf{A}_t \cdot (\mathbf{i}^k - \mathbf{i}^l). \tag{7.18}$$

Note that a power constraint on the symbols should also be included. Typically an average power constraint or peak power constraint is used. The objective function in (7.18) is non-convex with respect to the optimization variables, and therefore the solution found by a numerical algorithm may not be the gobal extremal point.

The optimization problem was solved by using the fminimax function in matlab. An average power criteria was used as a constraint on the optimization problem. The algorithm was run 500 times with random starting points, and the best solution among the local minimums was chosen. The symbol design procedure was executed twice with the aim of creating 8 and 16 distinct symbols respectively. Fig.7.15 shows 8 symbols that are the output of the design procedure.

Since the symbols were designed based on an error criteria it is of high interest to evaluate the symbol error rate (SER). For comparison the SER is compared against the SER obtained by a single transmit antenna. To make the comparison fair between the two schemes an optimal symbol alphabet needs to be employed also for the single transmitt antenna. Optimal symbol alphabets for a single antenna may be found in (Foschini, Gitlin, and Weinstein [1974]), where the optimal symbols are shown to be hexagonal in shape. The SER is shown in Fig. 7.16 for the two schemes, and it is apparent that the proposed antenna achieves a lower SER than the single transmit antenna.

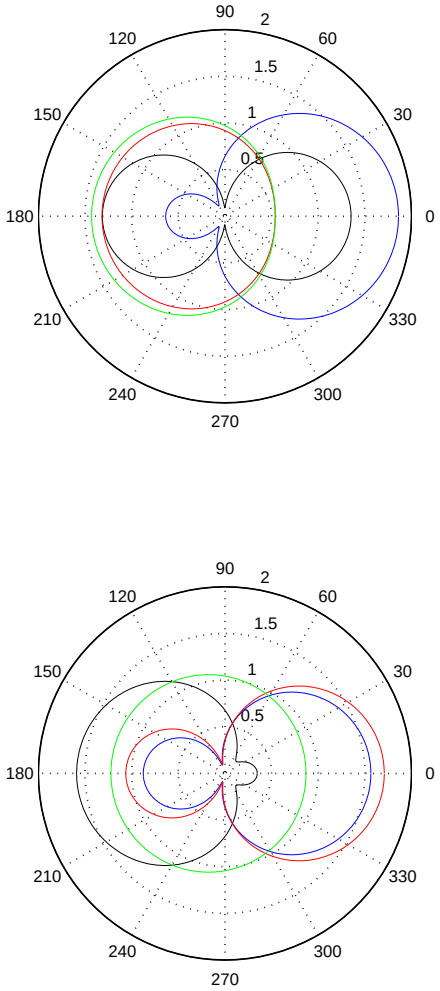

FIGURE 7.15: Eight different antenna patterns which are obtained by the solving the min-max optimization problem in (7.18).

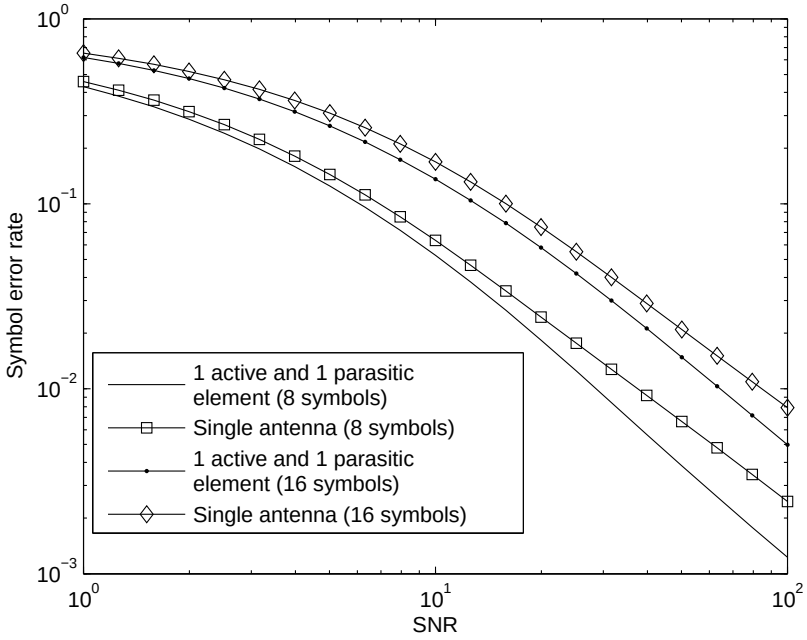

FIGURE 7.16: Symbol error rate evaluation.

Chapter 8

Conclusions

This dissertation has investigated the possibility of achieving higher spectral efficiencies by the usage of parasitic elements. The thesis is divided into two main parts. The first part considers how to implement a rotating antenna by using several parasitic elements in addition to one active antenna element. The main commercial interest for the rotating antenna is to use it as a receiver and not as a transmitter, due to the frequency bandwidth expansion. It is demonstrated by simulations that the rotating antenna is capable of achieving higher spectral efficiency than a single receive antenna in a rich scattering channel and when the power level of the co-channel and adjacent-channel interference is comparable. However, it is shown that the rotating antenna does not achieve a higher capacity than multiple active antennas that occupy the same volume as the rotating antenna. The second part of the thesis considers using parasitic elements for implementing a transmitter. It is shown that the proposed scheme is able to achieve spectral efficiencies comparable to the ones achieved by widely spaced active antenna elements. This result relies heavily on the fact that the average radiated power is used as a power constraint. The radiated power is the power radiated in the far-field, and it is not the same as the power delivered by the voltage source. If the average radiated power constraint is replaced by the average power delivered by the transmitting source, the closely spaced antenna cannot be expected to achieve the same spectral efficiency as the widely spaced antennas.

8.1 Main contributions of the thesis

A summary of the contributions of each chapter is listed as follows.

- In Chapter 2, the concept of a rotating receiver antenna is explained.

It is shown how the antenna rotation results in an expanded frequency bandwidth of the received signal. The expanded frequency band consists of frequency subbands, with each subband having the same effect as a separate antenna in MIMO communications. Practical ways of achieving the rotating antenna, by the usage of parasitic elements, are proposed. Capacity simulations are presented in order to demonstrate the performance gain relative to a single receive antenna.

- In Chapter 3, many important aspects regarding the rotating antenna are discussed. Since the rotating antenna expands the frequency bandwidth the signal power is spread across a larger frequency band. Summing the signal powers from each subband gives the same received power as would have been received by a single non-rotating antenna. But also the noise and interference are impacted by the rotating antenna. It is shown that the performance of the rotating antenna is dependent on the interference situation. If the adjacent interference power and co-channel power are approximately at the same level, then there are performance gains to be achieved by the rotating antenna. However, if the adjacent channel interference power level is much higher than the co-channel interference power level, there is not much to gain from the rotating antenna. This chapter further deals with the sampling issues of the rotating antenna. Since a practical realization of the rotating antenna would not allow for a continuous rotation, rotation by discrete angular steps would be implemented istead. Equations are presented that take into consideration that the antenna pattern rotates by discrete angular steps. These equations reveal how high sampling rate is necessary in order to achieve the same capacity as the continuous rotating antenna. The last section of the chapter considers rotation by discrete angular steps, but at the same time optimizes the time to dwell on each angular direction. The capacity improvements achieved by this optimization is shown to be rather small for a rich scattering channel.

- In Chapter 4, practical issues such as antenna efficiency, broadband properties and transient effects of the rotating antenna are discussed. The antenna impedance and the reflection coefficient are calculated for a few implementations of the rotating antenna in order to give an intuitive feeling on the practical implementability of these antenna configurations. The fractional bandwidth is evaluated by computing the quality factor for the same antenna configurations, and thus gives an indication of the achievable frequency bandwidths. One of the

limitations of the rotating antenna is the maximum speed that the parasitic elements can switch from an open-circuit state to a short-circuit state. The obtainable switching-speed is limited by both the switches themselves and also by the duration of the transient period of the electromagnetic field. A plot that shows the transient period of the electromagnetic field is therefore presented in the last section of the chapter.

- In Chapter 5, the performance of the active antenna elements are studied in more detail and compared against the performance of the rotating antenna. Previous chapters have compared the rotating antenna with a single receive antenna. Since the single receive antenna occupies a smaller volume than the rotating antenna this comparison might be considered a bit unfair. The capacity is calculated for both the active antenna elements and the rotating antenna when the antenna arrays occupy the same volume. It is shown that the capacity of the rotating antenna does not exceed the capacity achieved by the active antenna elements.

- In Chapter 7, compact and cost-effective antenna structures for transmission are considered. The results presented in this chapter are based on the research done by Kalis *et al.* [2006]. Kalis considered an antenna array consisting of one active antenna element and multiple closely spaced parasitic elements. He showed that the same spectral efficiency could be obtained with the proposed antenna structure as widely spaced antennas when finite dimensional modulation schemes such as Binary Phase-Shift Keying (BPSK) and Quadrature Phase-Shift Keying (QPSK) are used. The novelty in this chapter lies in the fact that the Arimoto-Blahut algorithm is used to find the capacity achieving distribution. In addition a higher number of signal points is used for the calculation of mutual information. Previous results have only evaluated the spectral efficiency for rich scattering channels, whereas Chapter 7 also considers clustered scattering. Finally a scheme for designing a finite number of symbols/antenna-patterns is proposed for minimizing the error-probability.

8.2 Suggestions for further research

There are some topics that were not investigated due to time-limitations. Especially issues connected to the practical implementation of the antenna arrays are not yet fully explored. In that context, a list of suggestions for

further research are presented. Possible research topics for the rotating antenna are as follows.

- The transient behaviour of the switches is a topic that should be investigated more closely. In that respect, the possible switching speeds and how the received signal behaves during the transient behaviour of the switches should be investigated. Another room for improvement is to design optimal pulses for the signals that activate the switches.
- The broadband behaviour of the rotating antenna should be adressed by designing appropriate impedance matching networks. Closely spaced antennas usually imply antenna impedances which are far from 50Ω. Therefore, matching the antenna to the 50Ω termination impedance becomes a difficult task. Broadband properties of closely spaced active antenna elements have been investigated in (Lau, Andersen, Kristensson, and Molisch [2006]). The same considerations should be made for the rotating antenna. The most directive antenna patterns usually correspond to the antenna patterns with poorest broadband properties (super-directivity). This suggests that there should be a trade-off between the highest spectral efficiency per unit bandwidth around the carrier-frequency f_c and the total obtainable frequency bandwidth Δf.
- Since closely spaced antennas usually imply low antenna efficiency, the amplifiers will in that case need to amplify the received signal even more, which again results in more amplifier noise. Then it becomes necessary to determine whether or not the amplifier noise becomes comparable to the co-channel and adjacent-channel interference.
- It has been shown that the rotating antenna leads to increased adjacent channel interference. Various equalization techniques should therefore be tested and analyzed in order to determine which one is more suited for the rotating antenna.

Possible further research directions for the proposed transmit antenna array are listed below.

- The capacity achieving distribution has been found for a finite number of signal points. Because of the numerical complexity there is a limit on how many signal points may be considered. Therefore, more effort could be invested in trying to find an analytical solution to the problem.

- A criteria should be developed for finding optimal antenna patterns for various channels.
- Practical coding schemes should be deveoped for the transmit antenna.
- The radiated power was used as a power constraint in the mutual information calculations. One possibility for further research might be to give a more complete description by including the amplifiers and the impedance matching, and then calculate the power consumed by the transmitting source. The spectral regulators care about the radiated power. However, the owners of the mobile unit usually care about the battery lifetime.
- One concern with closely antennas is that the capacity performance becomes possibly more sensitive towards channel estimation errors (Gans [2006b]). This issue should be further investigated.
- Section 4.3 showed that when the switches of the parasitic elements change state from short-circuit to open-circuit, there is a transient period before the field converges to the steady-state field. In order to prevent out-of band radiation, pulse-shaping should be considered for both the signal which activates the switches and also for the signal which is transmitted with the chosen antenna pattern. Pulse-shaping will most likely result in a lower data rate than predicted by Chapter 7.

Appendix A

Derivation of the radiated power

In this appendix the radiated power from a two element antenna array is derived. The power density is given by the time average Poynting vector $\mathbf{W}(r,\theta,\phi)$ (Pozar [1998], Section 1.6)

$$\mathbf{W}(r,\theta,\phi) = \frac{1}{2}\Re\{\mathbf{E}(r,\theta,\phi) \times \mathbf{H}^*(r,\theta,\phi)\} \quad (\text{Watts/m}^2), \tag{A.1}$$

where r,θ and ϕ are the spherical coordinates, $\mathbf{E}(r,\theta,\phi)$ is the electrical field intensity and $\mathbf{H}^*(r,\theta,\phi)$ is the magnetic field intensity. Assume that the two element antenna array is positioned in the center of the coordinate system. Let one of the antennas be directed along the z-axis. In this thesis wave propagation is evaluated in a two dimensional plane rather than the three dimensional space. This is done to simplify the calculations, and it can also be justified by the fact that most of the energy is localized over the azimuth directions (Correia [2001]). The power density is therefore evaluated in the azimuth plane only. The electric and magnetic far field components are given by

$$E_\theta(r,\theta=\pi/2,\phi) = \frac{j\eta e^{-jkr}}{2\pi r}(i_1 + i_2 e^{jkd\cos\phi}) \tag{A.2}$$

$$H_\phi(r,\theta=\pi/2,\phi) = \frac{j e^{-jkr}}{2\pi r}(i_1 + i_2 e^{jkd\cos\phi}), \tag{A.3}$$

where E_θ is the component of the electric field pointing in the same direction as the unit vector $\hat{\theta}$, H_ϕ is the component of the magnetic field pointing in the same direction as the unit vector $\hat{\phi}$, η is the intrinsic impedance of the propagation medium (air), k is the wavenumber which is defined as

$k = 2\pi/\lambda$ where λ is the wave-length, d is the inter-element distance, i_1 and i_2 are the currents on the antennas. Note that the other four field components E_r, E_ϕ, H_θ and H_r are zero in the far field region. The power in the azimuth plane is found by integrating $\mathbf{W}(r, \pi = \phi/2, \phi)$ with respect to ϕ as shown below

$$\begin{aligned}
&\int_0^{2\pi} W(r, \theta = \pi/2, \phi) d\phi \\
&= \frac{1}{2} \int_0^{2\pi} \Re\{\mathbf{E}(r, \theta = \pi/2, \phi) \times \mathbf{H}^*(r, \theta = \pi/2, \phi)\} d\phi \\
&= \frac{\eta}{8\pi^2 r^2} \int_0^{2\pi} |i_1|^2 + |i_2|^2 + i_1 i_2^* e^{-jkd\cos\phi} + i_2 i_1^* e^{jkd\cos\phi} d\phi \\
&= \frac{\eta}{4\pi r^2} (|i_1|^2 + |i_2|^2 + 2 \cdot J_0(kd) \cdot \Re\{i_1 i_2^*\}) \\
&= C \cdot (|i_1|^2 + |i_2|^2 + 2 \cdot J_0(kd) \cdot \Re\{i_1 i_2^*\}),
\end{aligned} \tag{A.4}$$

where $J_0()$ is the zeroth order Bessel function of the first kind and $C = \frac{\eta}{4\pi r^2}$.

Appendix B

Proof of the concavity of equation (3.56) with respect to τ

First note that since $\hat{\mathbf{P}}$ has orthogonal columns the product $\hat{\mathbf{P}}^H\hat{\mathbf{P}}$ becomes a diagonal matrix. When the antenna points its beam towards two angular directions only, the matrix product $\hat{\mathbf{P}}^H\hat{\mathbf{P}}$ becomes

$$\hat{\mathbf{P}}^H\hat{\mathbf{P}} = \begin{bmatrix} \frac{\tau}{T} & 0 \\ 0 & \frac{T-\tau}{T} \end{bmatrix}. \tag{B.1}$$

Showing the concavity of (3.56) with respect to τ is the same showing the concavity of (3.56) with respect to the diagonal elements of $\hat{\mathbf{P}}^H\hat{\mathbf{P}}$. Equation (3.56) may be written as

$$\log_2\left(\left|\mathbf{I} + \frac{P_T}{N_0}\mathbf{K}\hat{\mathbf{P}}^H\hat{\mathbf{P}}\right|\right) = \log_2\left(\left|\mathbf{I} + \frac{P_T}{N_0}\mathbf{K}^{1/2}\hat{\mathbf{P}}^H\hat{\mathbf{P}}\mathbf{K}^{1/2}\right|\right) \tag{B.2}$$

where $\mathbf{K} = \mathbf{A}\mathbf{H}\mathbf{H}^H\mathbf{A}^H$ is a positive semidefinite Hermitian matrix. Since $\hat{\mathbf{P}}^H\hat{\mathbf{P}}$ is a diagonal matrix with positive or zero valued elements, it is also a positive semidefinite matrix. Note that $\mathbf{I} + \frac{P_T}{N_0}\mathbf{K}^{1/2}\hat{\mathbf{P}}^H\hat{\mathbf{P}}\mathbf{K}^{1/2}$ is a linear mapping of $\hat{\mathbf{P}}^H\hat{\mathbf{P}}$, which means it preserves positive definiteness. It is shown in (Vandenberghe and Boyd [1996]; Horn [1996]) that $\log|\ |$ is a concave function on the set of positive semidefinite matrices. By using the composition rule from (Boyd and Vandenberghe [2004],Section 3.2.4) we may conclude that $\mathbf{I} + \frac{P_T}{N_0}\mathbf{K}^{1/2}\hat{\mathbf{P}}^H\hat{\mathbf{P}}\mathbf{K}^{1/2}$ is a concave function with respect to $\hat{\mathbf{P}}^H\hat{\mathbf{P}}$, and therefore a concave function with respect to variable τ. If we assume that the antenna rotates towards n different directions then we have to show that B.2 is concave with respect to $\tau_1, \tau_2, .., \tau_{n-1}$. Variables $\tau_1, \tau_2, .., \tau_{n-1}$ represent how long the antenna beam points towards the n different angles.

Since B.2 is concave with respect to $\hat{\mathbf{P}}^H\hat{\mathbf{P}}$ for an arbritary dimension of $\hat{\mathbf{P}}^H\hat{\mathbf{P}}$ it is also concave with respect to $\tau_1, \tau_2, .., \tau_{n-1}$.

Bibliography

Andersen, J. B. and B. K. Lau (2006, December).
On closely coupled dipoles in a random field.
IEEE Antennas Wireless Propagat. Lett. 5(1), 73–75.

Arimoto, S. (1972, January).
An algorithm for computing the capacity of arbitrary discrete memoryless channels.
IEEE Trans. Inform. Theory 18(1), 14–20.

Bains, R. and R. R. Müller.
Adaptive virtually rotating antennas.
Submitted to IEEE Communications Letters.

Bains, R. and R. R. Müller.
On the link performance of a proposed compact antenna system.
Submitted to IEEE Communications Letters.

Bains, R. and R. R. Müller.
Using parasitic elements for implementing the rotating antenna for MIMO receivers.
Accepted for publication in IEEE Trans. Wireless. Commun.

Bains, R. and R. R. Müller (2006a, February).
Appropriate Antenna Patterns for a Compact MIMO Receiver.
In *International Zurich Seminar on Communications (IZS)*, Zurich, Switzerland, pp. 22–25.

Bains, R. and R. R. Müller (2006b, March).
On Sampling Issues of a Virtually Rotating MIMO Antenna.
In *International ITG/IEEE Workshop on Smart Antennas (WSA)*, Reisensburg, Germany.

Bains, R., R. R. Müller, and A. Kalis.

Link Performance of an ESPAR-Antenna Array in Rich Scattering and Clustered Channels.
Accepted for publication in Wireless Personal Communications.

Bains, R., R. R. Müller, and A. Kalis (2007, October).
Link performance of an ESPAR-antenna array in rich scattering and clustered channels.
In *IEEE 4th International Symposium on Wireless Communication Systems (ISWCS).*, Trondheim, Norway, pp. 308–312.

Balanis, C. A. (1997).
Antenna theory: analysis and design (Second ed.).
John Wiley & Sons, Inc.

Bikhazi, N. W. and M. A. Jensen (2007, May).
The relationship between antenna loss and superdirectivity in MIMO systems.
IEEE Trans. Wireless Commun. 6(5), 1796–1802.

Blahut, R. E. (1972, July).
Computation of channel capacity and rate-distortion functions.
IEEE Trans. Inform. Theory 18(4), 460–473.

Boyd, S. and L. Vandenberghe (2004).
Convex Optimization.
Cambridge University Press.

Chiurtu, N., B. Rimoldi, I. E. Telatar, and V. Pauli (2003, December).
Impact of correlation and coupling on the capacity of MIMO systems.
In *Proc. IEEE International Symposium on Signal Processing and Information Technology*, pp. 154–157.

Correia, L. M. (2001).
Wireless Flexible Personalised Communications.
New York, USA: John Wiley & Sons Inc.

Cover, T. M. and J. A. Thomas (1991).
Elements of Information Theory.
John Wiley & Sons, inc.

Edwards, C. H. and D. E. Penney (1998).
Calculus with analytical geometry (Fifth ed.).
Prentice Hall International, Inc.

Foschini, G. J. and M. J. Gans (1998, March).
On the limits of wireless communications in a fading environment when using multiple antennas.
In *Wireless Personal Communications*, Volume 6, pp. 311–335.

Foschini, G. J., R. D. Gitlin, and S. B. Weinstein (1974, January).
Optimization of two-dimensional signal constellations in the presence of Gaussian noise.
IEEE Trans. Commun. 22(1), 28–38.

Gans, M. J. (2006a, September).
Channel capacity between antenna arrays - Part I: Sky noise dominates.
IEEE Trans. Commun. 54(9), 1586–1592.

Gans, M. J. (2006b, November).
Channel capacity between antenna arrays - Part II: Amplifier noise dominates.
IEEE Trans. Commun. 54(11), 1983–1992.

Gyoda, K. and T. Ohira (2000, July).
Design of electronically steerable passive array radiator (ESPAR) antennas.
In *Proc. IEEE Antennas and Propagation Society International Symposium*, Volume 2, pp. 922–925.

Hansen, R. C. (1981, February).
Fundamental limitations in antennas.
Proc. IEEE 69(2), 170–182.

Harrington, R. (1978, May).
Reactively controlled directive arrays.
IEEE Trans. Antennas Propagat. 26(3), 390–395.

Hochwald, B. M. and T. L. Marzetta (2000, March).
Unitary space-time modulation for multiple-antenna communications in Rayleigh flat fading.
IEEE Trans. Inform. Theory 46(2), 543–564.

Horn, R. A. (1996).
Matrix analysis.
Cambridge university press.

Jakes, W. C. (1974).
Microwave mobile communications.
John Wiley & Sons.

Janaswamy, R. (2002).
Effect of element mutual coupling on the capacity of fixed length linear arrays.
IEEE Antennas Wireless Propagat. Lett. 1(1), 157–160.

Kalis, A. and M. J. Carras (2005, May).
Aerial entropy and capacity of an MEA EM source.
In *26th Symposium on Information Theory in the Benelux*.

Kalis, A., A. G. Kanatas, M. Carras, and A. G. Constantinides (2006, June).
On the performance of MIMO systems in the wavevector domain.
In *15th IST Mobile and Wireless Communications Summit*.

Kalis, A., C. Papadias, and A. G. Kanatas (2007, June).
An ESPAR antenna for beamspace-MIMO systems using PSK modulation schemes.
In *IEEE International Symposium on Wireless Communication Systems (ISWCS)*, pp. 5348–5353.

Kermoal, J. P., L. Schumacher, K. I. Pedersen, P. E. Mogensen, and F. Fredriksen (2002, August).
A stochastic MIMO radio channel model with experimental validation.
IEEE J. Select. Areas Commun. 20, 1211–1226.

Kildal, P. S. and K. Rosengren (2003).
Electromagnetic analysis of effective and apparent diversity gain of two parallel dipoles.
IEEE Antennas Wireless Propagat. Lett. 2(1), 9–13.

Kildal, P. S. and K. Rosengren (2004, December).
Correlation and capacity of MIMO systems and mutual coupling, radiation efficiency, and diversity gain of their antennas: simulations and measurements in a reverberation chamber.
IEEE Commun. Mag. 42(12), 104–112.

Kirkpatrick, S., C. D. Gelatt, and M. P. Vecchi (1983, May).
Optimization by simulated annealing.
Science 220, 671–680.

Kolundž, B. M., J. S. Ognjanoveć, and T. K. Sarkar (2000).
WIPL-D Electromagnetic modeling of composite metallic and dielectric structures.
Boston, MA: Artech House.

Lau, B. K., J. B. Andersen, G. Kristensson, and A. F. Molisch (2006, November).
Impact of matching network on bandwidth of compact antenna arrays.
IEEE Trans. Antennas Propagat. 54(11), 3225–3238.

Lee, E. A. and D. G. Messerschmitt (1994).
Digital Communication (Second ed.).
Kluwer Academic Publishers.

Liu, Q. and D. A. Pierce (1994).
A note on Gauss-Hermite Quadrature.
Biometrika 81(3), 624–629.

Marcenko, V. A. and L. A. Pastur (1967).
Distribution of eigenvalues for some sets of random matrices.
USSR-Sbornik 1(4), 457–483.

Matz, G. and P. Duhamel (2004, October).
Information Geometric Formulation and Interpretation of Accelerated Blahut-Arimoto-Type Algorithms.
In *IEEE Information Theory Workshop (ITW)*, Texas,USA, pp. 66–70.

Migliore, M. D. (2006, February).
On the role of the number of degrees of freedom of the field in MIMO channels.
IEEE Trans. Antennas Propagat. 54(2), 620–628.

Migliore, M. D., D. Pinchera, and F. Schettino (2006, November).
Improving Channel Capacity Using Adaptive MIMO antennas.
IEEE Trans. Antennas Propagat. 54(11), 3481–3488.

Molisch, A. F. (2004).
A Generic Model for MIMO Wireless Propagation Channel in Macro- and Microcells.
IEEE Trans. Signal Processing 52(1), 61–71.

Morris, M. L. and M. A. Jensen (2005, July).
Improved network analysis of coupled antenna diversity performance.
IEEE Trans. Wireless Commun. 4(4), 1928–1934.

Morris, M. L., M. A. Jensen, and J. W. Wallace (2005, September).
Superdirectivity in MIMO systems.
IEEE Trans. Antennas Propagat. 53(9), 2850–2857.

Müller, R., R. Bains, and J. A. Aas (2005, September).
A compact MIMO receiver antenna.
In *Proc. 43rd Annual Allerton Conference on Communications, Control and Computing.*, Monticello, IL, USA.

Müller, R. R. (2002, September).
A random matrix model for communication via antenna arrays.
IEEE Trans. Inform. Theory 48(9), 2495–2506.

Nakane, Y., T. Noguchi, and Y. Kuwahara (2005, October).
Trial model of adaptive antenna equipped with switched loads on parasitic elements.
IEEE Trans. Antennas Propagat. 53(10), 3398–3402.

Ngamjanyaporn, R. and A. Krairiksh (2002, January).
Switched-beam single patch antenna.
Electron. Lett. 38(1), 7–8.

Orfanidis., S. J.
Electromagnetic Waves and Antennas.
http://www.ece.rutgers.edu/ orfanidi/ewa/.

Özcelik, H., M. Herdin, W. Weichselberger, J. Wallace, and E. Bonek. (2003).
Deficiencies of the Kronecker MIMO radio channel model.
Electron. Lett. 39, 1209–1210.

Packard, H. (1999, October).
Fast switching PIN diodes.
In *Application note 929*, http://www.home.agilent.com/agilent/home.jspx.

Pollock, T. S., M. I. Y. Williams, and T. D. Abhayapala (2005, March).
Spatial limits to mutual information scaling in multi-antenna systems.
In *Proc. IEEE Iinternational Conference on Acoustics, Speech, and Signal Processing*, Volume 3, pp. 389–392.

Poon, A. S. Y., R. W. Brodersen, and D. N. C. Tse (2005, February).
Degrees of freedom in multiple-antenna channels: a signal space approach.
IEEE Trans. Inform. Theory 51(2), 523–536.

Poon, A. S. Y., D. N. C. Tse, and R. W. Brodersen (2006, March).
Impact of scattering on the capacity, diversity, and propagation range of multiple-antenna channels.
IEEE Trans. Inform. Theory 52(3), 1087–1100.

Pozar, D. M. (1998).
Microwave Engineering (Second ed.).
John Wiley & Sons, Inc.

Preston, S. L., D. V. Thiel, T. A. Smith, S. G. O'Keefe, and J. W. Lu (1998, June).
Base-station tracking in mobile communications using a switched parasitic antenna array.
IEEE Trans. Antennas Propagat. 46(6), 841–844.

Schaer, B., K. Rambabu, J. Borneman, and R. Vahldieck (2005, June).
Design of reactive parasitic elements in electronic beam steering arrays.
IEEE Trans. Antennas Propagat. 53(6), 1998–2003.

Schlub, R., D. V. Thiel, and J. W. Lu (2000, March).
Dual band switched-parasitic wire antennas for communications and direction finding.
In *Microwave Conference, Asia-Pacific*, pp. 74–78.

Scott, N. L., M. O. Leonard-Taylor, and R. G. Vaughan (1999, June).
Diversity gain from a single-port adaptive antenna using switched parasitic elements illustrated with a wire and monopole prototype.
IEEE Trans. Antennas Propagat. 47(6), 1066–1070.

Shiu, D. S., G. J. Foschini, M. J. Gans, and J. M. Kahn (2000, March).
Fading correlation and its effect on the capacity of multielement antenna systems.
IEEE Trans. Commun. 48(3), 502–513.

Sun, C., A. Hirata, and T. O. N. C. Karmakar (2004, July).
Fast beamforming of electronically steerable parasitic array radiator antennas: Theory and experiment.
IEEE Trans. Antennas Propagat. 52(7), 1819–1831.

Sun, C. and N. C. Karmakar (2004, January).
Direction of arrival estimation with a novel single-port smart antenna.
EURASIP Journal on applied signal processing 2004(1), 1364–1375.

Svantesson, T. and A. Ranheim (2001, May).
Mutual coupling effects on the capacity of multielement antenna systems.
In *Proc. IEEE Iinternational Conference on Acoustics, Speech, and Signal Processing*, Volume 4, Salt Lake City, UT, pp. 2485–2488.

Taflove, A. (1995).
Computational Electrodynamics: The Finite-Difference Time-Domain Method.
Norwood, MA: Artech House.

Tarokh, V., N. Seshadri, and A. R. Calderbank (1998, March).
Space-time codes for high data rate wireless communication: Performance criterion and code construction.
IEEE Trans. Inform. Theory 44(2), 744–765.

Teal, P. D., T. D. Abhayapala, and R. A. Kennedy (2002, October).
Spatial correlation for general distributions of scatterers.
IEEE Signal Processing Letters 10, 305–308.

Telatar, I. E. (1999, December).
Capacity of multi-antenna Gaussian channels.
European Trans. on Telecomm. 10(6), 585–595.

Thiel, D. V. and S. Smith (2002).
Switched parasitic antennas for cellular communications.
Boston, MA: Artech House.

Uzsoky, M. and L. Solymar (1956).
Theory of super-directive linear antennas.
Acta Phys 6, 185–204.

Vandenberghe, L. and S. Boyd (1996, March).
Semidefinite programming.
SIAM Review 38, 49–95.

Vaughan, R. (1999, February).
Switched parasitic elements for antenna diversity.
IEEE Trans. Antennas Propagat. 47(2), 399–405.

Wallace, J. W. and M. A. Jensen (2004a, July).
Mutual coupling in MIMO wireless systems: a rigorous network theory analysis.
IEEE Trans. Wireless Commun. 3(4), 1317–1325.

Wallace, J. W. and M. A. Jensen (2004b, January).
Termination-dependent diversity performance of coupled antennas: network theory analysis.
IEEE Trans. Antennas Propagat. 52(1), 98–105.

Wennstrom, M. and T. Svantesson (2001, September).
An antenna solution for MIMO channels: the switched parasitic antenna.
In *Proc. IEEE International Symposium on Personal, Indoor and Mobile Radio Communications*, Volume 1, pp. A–159–A–163.

Yu, K., M. Bengtsson, B. Ottersen, D. McNamara, P. Karlsson, and M. Beach (2002, May).
A wideband statistical model for NLOS indoor MIMO channels.
In *Proc. IEEE 55th Veh. Technol. Conf.*, Volume 6, Birmingham,AL, pp. 370–374.

Zekavat, S. A. and C. R. Nassar (2002, October).
Smart antenna arrays with oscillating beam patterns: characterization of transmit diversity in semi-elliptic coverage.
IEEE Trans. Commun. 50(10), 1549–1556.